

Resource-efficient shadow tomography using equatorial stabilizer measurements

Guedong Park, Yong Siah Teo, and Hyunseok Jeong

Department of Physics and Astronomy, Seoul National University, Seoul, 08826, Republic of Korea

We propose a resource-efficient shadow-tomography scheme using equatorial-stabilizer measurements generated from subsets of Clifford unitaries. For n -qubit systems, equatorial-stabilizer-based shadow-tomography schemes can estimate M observables (up to an additive error ε) using $\mathcal{O}(\log(M), \text{poly}(n), 1/\varepsilon^2)$ sampling copies for a large class of observables, including those with traceless parts possessing polynomially-bounded Frobenius norms. For arbitrary quantum-state observables, sampling complexity becomes n -independent. Our scheme only requires an n -depth controlled- Z (CZ) circuit [$\mathcal{O}(n^2)$ CZ gates] and Pauli measurements per sampling copy, exhibiting a smaller maximal gate count relative to previously-known randomized-Clifford-based proposals. Implementation-wise, the maximal circuit depth is reduced to $\frac{n}{2} + \mathcal{O}(\log(n))$ with controlled-NOT (CNOT) gates. Alternatively, our scheme is realizable with $2n$ -depth circuits comprising $\mathcal{O}(n^2)$ nearest-neighboring CNOT gates, with possible further gate-count improvements. We numerically confirm our theoretically-derived shadow-tomographic sampling complexities with random pure states and multiqubit graph states. Finally, we demonstrate that equatorial-stabilizer-based shadow tomography is more noise-tolerant than randomized-Clifford-based schemes in terms of average gate fidelity and fidelity estimation for Greenberger–Horne–Zeilinger (GHZ) state and W state.

Contents

1	Introduction	2
2	Preliminaries	3
2.1	Clifford group and equatorial stabilizer POVM	3
2.2	Random Clifford tomography and classical shadows	4
3	Results	5
3.1	Equatorial-stabilizer shadow tomography	5
3.2	Sampling-copy complexity of equatorial stabilizer POVMs	8
3.3	Low gate count and depth for implementing (R)ESPOVM shadow tomography	10
3.4	Noise tolerance of (R)ESPOVM shadow tomography	11
4	Discussion	13

Yong Siah Teo: ys_teo@snu.ac.kr

Hyunseok Jeong: jeongh@snu.ac.kr

5	Technical aspects of (R)ESPOVM shadow tomography	14
5.1	Procedures and algorithm for equatorial-stabilizer shadow tomography	14
5.2	Estimation-variance analysis of equatorial-stabilizer shadow tomography	17
5.3	Gate, depth, and time complexity for circuit implementation	22
5.4	Average gate fidelity	24
5.5	Survey of recent CZ-gate implementation schemes	26
6	Acknowledgements	26
A	Variance of sum of independent estimators	32
B	Proofs of Lemmas	32
B.1	Proof of Lemma 1	32
B.2	Proof of Lemma 2	34
B.3	Proof of Lemma 3	35
B.4	Proof of Lemma 4	37
B.5	Proof of Lemma 5	40
C	Informational completeness of ESPOVM+computational basis	44
D	CNOT—CZ—CNOT decomposition of a CZ circuit	45
E	Linear nearest-neighboring (LNN) architecture of CZ circuits [1]	46

1 Introduction

Quantum algorithms, which are algorithms based on quantum-mechanical principles, have been shown to outperform classical algorithms for many computational tasks [2–4]. For these purposes, certifying the quality of the prepared (noisy) quantum state is an important prerequisite. Quantum tomography [5–8] is a general method to reconstruct a typically unknown noisy n -qubit quantum state ρ (or a channel). This, however, requires exponentially many copies of ρ in n for an accurate reconstruction.

On the other hand, if we are to estimate certain classes of physical properties of unknown states, *shadow tomography* [9] enables us to do so with a polynomially-large number of samples. The well-known randomized Pauli tomography, or “six-Paulis” tomography [10, 11], is useful for estimating the expectation values of Hamiltonians with low locality, learning quantum channels [12] and measuring non-stabilizerness (or magic) [13, 14]. This procedure uses a simple single-layer circuit structure, and is therefore ineffective in estimating highly-entangled properties of large quantum systems [10]. The second protocol, randomized-Clifford shadow tomography [10], is better for estimating the fidelity between the unknown input and entangled target states for large qubit number n . This advantage originates from the fact that Clifford operations are unitary 3-designs [15–18]. However, for large n , this protocol utilizes at most $\frac{7n^2}{2}$ neighboring CNOT gates [19, 20]. Therefore, shadow tomography with arbitrary Clifford gates could lead to noisy measurement results in real experiments as the large number of noisy gates accumulate physical noise.

To cope with such problems, recent works showed that target observables with low bond dimension possess good shadow norms even with neighboring gates of shallow depths [21, 22]. Furthermore, for arbitrary pure-state observables, it is uncertain whether randomized-Clifford tomography is indeed the most optimal for achieving a given estimation accuracy from the perspective of gate count, circuit depth, and input-state copy number. It is known

that generalized measurements [11, 24, 25] can reduce the gate count or sampling complexity. However, noise-tolerant implementation of such non-Clifford measurements is believed to be challenging [26–28]. There exist alternatives with reduced Clifford-gate resources [29, 30]. Nevertheless, applicable input states and target observables that lead to poly(n)-shadow norms are restrictive. Hence, a complete analysis of an optimal tomography scheme for broad classes of observables remains an open problem.

In this work, we introduce resource-efficient schemes for shadow tomography, catered to observable-expectation-value estimations, that offer a lower gate count and circuit depth while still being applicable to a large observable class. The key point is that it is not necessary to utilize the entire set of stabilizer states [31, 32] comprising all Clifford-rotated bases. Instead, our proposed schemes employ a smaller stabilizer subset, namely the *equatorial stabilizer positive operator-valued measure* (ESPOVM) [33] together with the computational basis. Additionally, it is sufficient to perform shadow tomography with an even smaller subset, namely the *real ESPOVM* or RESPOVM, when the target observable is real with respect to the computational basis. Our scheme only involves a uniform sampling of commuting CZ gates as the only two-qubit gate resources.

Next, we theoretically prove shadow-tomographic capabilities for (R)ESPOVM schemes by deriving upper bounds of sampling-copy complexity for the observable-expectation-value estimation, which is directly related to *shadow norm* [10, 21]. Specifically, we note that a sampling complexity of $\mathcal{O}(\log(M), \text{poly}(n), 1/\varepsilon^2)$ suffices to simultaneously estimate (up to an additive error ε) M complex observables belonging to a broad class, which *sufficiently* include observables possessing polynomially-bounded Frobenius norms for their traceless parts. For arbitrary *quantum-state* observables (*fidelity estimation*), the sampling complexity is reduced to simply $\mathcal{O}(\log(M), 1/\varepsilon^2)$, which is constant in n and on par with randomized-Clifford tomography [10]. These results are promising when compared with a recent result [34] which utilizes smaller subsets of CZ-circuit-based measurements consisting of mutually-unbiased bases (MUB) [35], for estimation of observable expectation values, but has an exponentially large bound of sampling copies to estimate arbitrary state observables. As a side, we argue that $\mathcal{O}(\text{poly}(n))$ single-layer Pauli measurement copies suffice to estimate expectation values of $\mathcal{O}(\text{poly}(n))$ -Pauli-term Heisenberg Hamiltonians [36, 37].

Furthermore, we shall show that our scheme can be implemented by a more simplified circuit structure, and attain improved noise tolerance. These results are derived from the fact that it involves a uniform sampling of commuting CZ gates as the only two-qubit gate resources. This enables our scheme to require with only $2n$ -depth, hence at most $n^2 < \frac{7n^2}{2}$ nearest neighboring (NN) CNOT gates [1], and to become more robust to gate noise. For these reasons, we provide numerical evidence of noise-robustness in the context of average gate fidelity. Moreover, following fidelity estimation results of Greenberger–Horne–Zeilinger (GHZ) state [38] and W states [39] manifest that the mathematical structure of RESPOVM enables our scheme to tolerate a broad spectrum of measurement errors. There also exists a study on post-processing classical shadows to adapt to random and noisy Clifford gate operations [40]. On the other hand, this work presents a hardware-based alternative to achieve better gate-noise tolerance by reducing gate resources.

2 Preliminaries

2.1 Clifford group and equatorial stabilizer POVM

Before presenting our main results, we define and explain several concepts and terminologies that shall be used throughout the article. We consider a source that allows one to

prepare multiple copies of an n -qubit quantum state ρ . The corresponding observable O shall be a Hermitian operator and is therefore symmetric whenever its matrix elements in the computational basis are all real, at which we call O is *real*. We define the *Clifford group* Cl_n as the set of operators [41, 31],

$$\text{Cl}_n = \left\{ U \mid \forall E \in \mathcal{P}_n, U E U^\dagger \in \mathcal{P}_n \right\}, \quad (1)$$

where \mathcal{P}_n is the *Pauli group* generated by tensor products of the standard Pauli operators X, Y, Z and the identity I . Next, we define the *pure stabilizer state set* \mathcal{S}_n as the following set of quantum states:

$$\mathcal{S}_n = \{ |\psi\rangle \mid |\psi\rangle = U |0^{\otimes n}\rangle \text{ for some } U \in \text{Cl}_n \}, \quad (2)$$

Then we say the element $|\psi\rangle \in \mathcal{S}_n$ as (*pure*) *stabilizer state*.

We are now ready to look into subclasses of the stabilizer set \mathcal{S}_n . Specifically, the complex *pure equatorial stabilizer state set* [33] $\mathcal{S}_n^{\text{eq}}$ and its real counterpart $\mathcal{S}_n^{\text{req}}$ are respectively given by

$$\mathcal{S}_n^{\text{eq}} = \left\{ |\phi_{\mathbf{A}}^{\text{eq}}\rangle \equiv \frac{1}{\sqrt{2^n}} \sum_{\mathbf{x} \in \mathbb{Z}_2^n} i^{\mathbf{x}^\top \mathbf{A} \mathbf{x}} |\mathbf{x}\rangle \mid \mathbf{A} = (a_{ij})_{i,j \in [n]} \text{ where } a_{ij} = a_{ji}, a_{ij} \in \begin{cases} \mathbb{Z}_4 & \text{if } i = j \\ \mathbb{Z}_2 & \text{if } i > j \end{cases} \right\}, \quad (3)$$

$$\mathcal{S}_n^{\text{req}} = \left\{ |\phi_{\mathbf{A}}^{\text{req}}\rangle \equiv \frac{1}{\sqrt{2^n}} \sum_{\mathbf{x} \in \mathbb{Z}_2^n} (-1)^{\mathbf{x}^\top \mathbf{A} \mathbf{x}} |\mathbf{x}\rangle \mid \mathbf{A} = (a_{ij})_{i,j \in [n]} \text{ where } a_{ij} \in \begin{cases} \mathbb{Z}_2 & \text{if } i \leq j \\ \{0\} & \text{if } i > j \end{cases} \right\}. \quad (4)$$

We may define (*real*) *equatorial stabilizer states* in the same manner based on $\mathcal{S}_n^{\text{eq}}$ and $\mathcal{S}_n^{\text{req}}$. From Eqs. (3) and (4), we know that the number of complex equatorial stabilizer states is $|\mathcal{S}_n^{\text{eq}}| = 2^{\frac{n^2+3n}{2}}$, and that of real equatorial stabilizer states is $|\mathcal{S}_n^{\text{req}}| = 2^{\frac{n^2+n}{2}}$. As the names suggest, these are subsets of \mathcal{S}_n . The $\mathcal{S}_n^{\text{eq}}$ was originally used for a faster classical simulation [33, 32]; more explicitly, a faster norm estimation of a given state with a large stabilizer rank.

In this work, we shall turn these two stabilizer subclasses into POVMs for shadow tomography, and consequently reveal the key advantages that are related to the exploitation of their smaller set sizes relative to \mathcal{S}_n . That $\mathcal{S}_n^{\text{eq}}$ and $\mathcal{S}_n^{\text{req}}$ may be readily transformed into POVMs is straightforward [42], as the corresponding sets of positive operators $\left\{ \frac{2^n}{|\mathcal{S}_n^{\text{eq}}|} |\phi_{\mathbf{A}}^{\text{eq}}\rangle \langle \phi_{\mathbf{A}}^{\text{eq}}| \right\}$ and $\left\{ \frac{2^n}{|\mathcal{S}_n^{\text{req}}|} |\phi_{\mathbf{A}}^{\text{req}}\rangle \langle \phi_{\mathbf{A}}^{\text{req}}| \right\}$ house elements that sum to the identity. We coin them (*real*) *equatorial stabilizer POVMs*, or (R)ESPOVMs for short.

2.2 Random Clifford tomography and classical shadows

The typical methods for fidelity estimation (with pure target states) are the direct fidelity-estimation scheme [29] and randomized-Clifford shadow tomography [10]. While the first method invokes a lower gate count and circuit depth than our schemes, the estimable region of observables is more restricted than both the randomized-Clifford and our (R)ESPOVM schemes. As such, only the latter two schemes shall be of interest *in our work*.

We briefly explain how the random Clifford operation may be used to estimate $\widehat{\langle O \rangle} = \text{tr}(\rho O)$ (see Ref. [10] for details). For this purpose, the algorithm using N sampling-copy number is stated below:

1. Take ρ as an input and uniformly choose a Clifford unitary U from Cl_n .
2. Take $\rho \leftarrow U\rho U^\dagger$.
3. Measure in the Z basis and obtain the outcome $\mathbf{p} \in \mathbb{Z}_2^n$.
4. Compute $\widehat{O} = \text{tr}\left(\mathcal{M}^{-1}(U^\dagger |\mathbf{p}\rangle\langle\mathbf{p}| U)\right) = (2^n + 1) \langle\mathbf{p}| U O U^\dagger |\mathbf{p}\rangle - \text{tr}(O)$.

Repeat the aforementioned steps N times and take the average of N \widehat{O} 's to obtain the estimator $\widehat{\langle O \rangle}$ for $\langle O \rangle$.

Here, $\mathcal{M}^{-1}(O) \equiv (2^n + 1)O - \text{tr}(O)I$ for an arbitrary operator O is known as the *classical shadow* [10]. Reference [10] showed that such randomized-Clifford tomography achieves ε -accurate fidelity estimation between an unknown quantum state and target pure state with the sampling-complexity upper bound $\mathcal{O}(3\text{tr}(O^2)/\varepsilon^2)$. Hence, this scheme is efficient when O is a target pure state of which $\text{tr}(O^2)$ is a constant, albeit with the assumption that every \widehat{O} is efficiently computable. Reference [20] showed that we can efficiently sample a Clifford unitary U from Cl_n in $\mathcal{O}(n^2)$ -time. In addition, the sampled form contains the HF'—SW—H—HF sections (where small uppercase letters here refer to gate layers as opposed to the regular uppercase ones that denote gate labels, and HF and HF' are *Hadamard-free sections*) where HF-section is a circuit containing layers of CNOT^\dagger —CZ—S—PAULI. Here, H, SW, CNOT^\dagger , CZ and S respectively refer to *pure layers* of Hadamard gates, SWAP gates, CNOT gates with control qubits higher than the target ones when visualized in a standard circuit diagram, CZ gates and S gates. Naturally, SW contains many CNOT gates.

Reference [43] showed that a random Clifford circuit can be implemented in $2n$ -depth by compressing the depths of CNOT and CZ sections to n . Furthermore, if only neighboring gates are available, a recent result [19] showed that $7n$ -depth is needed. In the next section, we show that shadow tomography with the (R)ESPOVM attains a similar scaling of sampling-copy complexity, but with a reduced circuit depth and gate count.

3 Results

3.1 Equatorial-stabilizer shadow tomography

We now introduce the shadow tomography scheme that uses (real) equatorial stabilizer POVMs. Figure 1 illustrates its schematic implementation, which is used to estimate the expectation value $\text{tr}(\rho O)$ for an unknown state ρ and a known observable O within an additive error ε . This is carried out with a given total number of input-state copies N .

The complete systematic procedure for (R)ESPOVM shadow tomography is shown in Algo. 1. Let us summarize the main steps, starting from the ESPOVM scheme. After preparing the input state ρ , the observer operates uniformly chosen CZ gates to the input and then measures in Pauli X or Y -basis, to obtain the measurement outcome $|\phi_{\mathbf{A}}^{\text{eq}}\rangle\langle\phi_{\mathbf{A}}^{\text{eq}}|$. The ESPOVM, all by itself, is *not* informationally complete (IC), whereas the union of the ESPOVM and computational basis is IC [42, 44] and indeed capable of reconstructing an arbitrary ρ and, thus, general observable expectation values. Therefore, to perform the complete shadow tomography scheme, the observer additionally measures ρ with the Z -basis measurement. So, two copies of ρ are required for a single measurement trial, which would give us a bit-string column \mathbf{p} from the ESPOVM and another bit-string column \mathbf{p}' from the computational basis. However, in Sec. 3.2, we shall see that only a single copy of the input state is necessary for each trial if O is a cluster state.

Algorithm 1 (R)ESPOVM shadow tomography algorithm

Require: n -qubit unknown quantum state ρ , total input-state copies $N \in \mathbb{N}$ (even), observable O and the (R)ESPOVM scheme.

Ensure: m .

```
1:  $m \leftarrow 0$ 
2: for  $k \in [N/2]$  do
3:   Prepare  $\rho$  as the input state.
4:   Randomly choose  $|\phi_{\mathbf{A}}^{(r)\text{eq}}\rangle$  uniformly in  $\mathcal{S}_n^{(r)\text{eq}}$ . Denote  $\mathbf{A} = (a_{ij})$ .
5:   for  $i < j \in [n]$  do
6:     if  $a_{ij} = 1$  then
7:        $\rho \leftarrow \text{CZ}_{ij} \rho \text{CZ}_{ij}$ ,  $\text{CZ}_{ij}$  is the CZ operator acting on the  $i$ -th and  $j$ -th qubits.
8:     end if
9:   end for
10:  for  $i \in [n]$  do
11:    if ESPOVM is used then
12:      if  $a_{ii} = 0 \pmod{2}$  then
13:        Perform a Pauli  $X$  measurement on the  $i$ -th qubit.
14:      else
15:        Perform a Pauli  $Y$  measurement on the  $i$ -th qubit.
16:      end if
17:    else
18:      Perform a Pauli  $X$  measurement on the  $i$ -th qubit.
19:    end if
20:  end for
21:  Obtain the measurement bit-string outcome  $\mathbf{p} \in \mathbb{Z}_2^n$ .
22:  for  $i \in [n]$  do
23:    if ESPOVM is used then
24:       $a_{ii} \leftarrow a_{ii} + 2p_i \pmod{4}$ .
25:    else if RESPOVM is used then
26:       $a_{ii} \leftarrow a_{ii} + p_i \pmod{2}$ .
27:    end if
28:  end for
29:  Prepare  $\rho$  as an input state.
30:  Perform a Pauli  $Z$  measurement on  $\rho$  to obtain the bit-string outcome  $\mathbf{p}' \in \mathbb{Z}_2^n$ .
31:  if ESPOVM is used then
32:     $m \leftarrow m + 2^n \langle \phi_{\mathbf{A}}^{\text{eq}} | O | \phi_{\mathbf{A}}^{\text{eq}} \rangle + \langle \mathbf{p}' | O | \mathbf{p}' \rangle - \text{tr}(O)$ .
33:  else if RESPOVM is used then
34:     $m \leftarrow m + 2^{n-1} \langle \phi_{\mathbf{A}}^{\text{req}} | O | \phi_{\mathbf{A}}^{\text{req}} \rangle + \langle \mathbf{p}' | O | \mathbf{p}' \rangle - \frac{1}{2} \text{tr}(O)$ .
35:  end if
36: end for
37:  $m \leftarrow \frac{m}{(N/2)}$ .
```

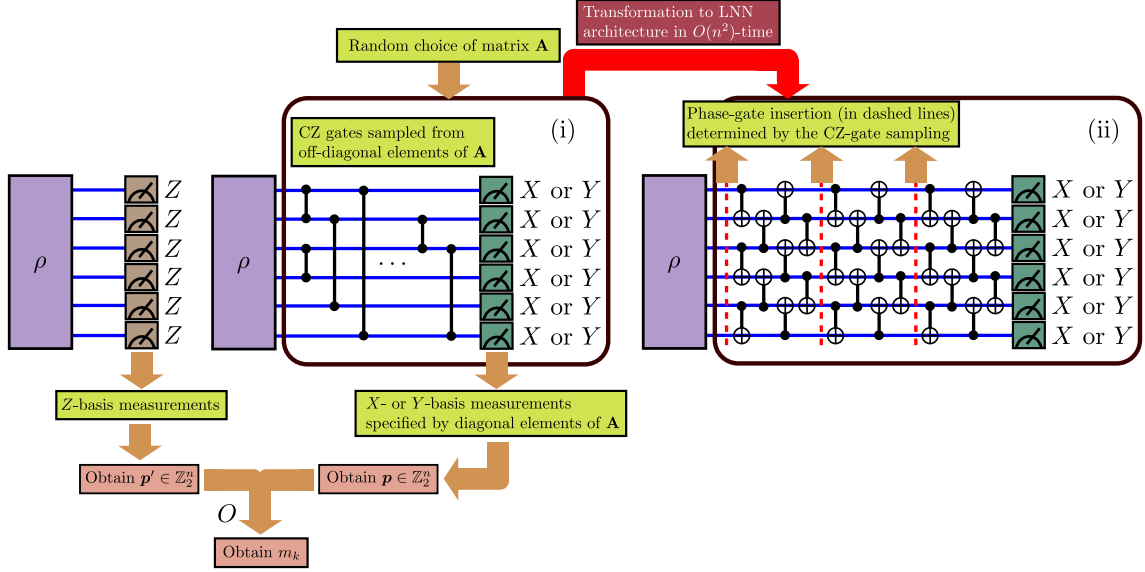


Figure 1: Schematic for 6-qubit (R)ESPOVM shadow tomography to estimate $\langle O \rangle = \text{tr}(\rho O)$ of an unknown state ρ and target observable O . Sampled CZ circuits can be transformed to a linear nearest-neighbor (LNN) architecture [1] [circuit (ii)]. Also in (ii), the inserted phase gates are single-qubit gates and the measurement is done in the same manner as in (i). Any one of the two architectures (i) and (ii) can be executed to obtain the measurement bit-string column $\mathbf{p} \in \mathbb{Z}_2^n$. Together with the bit-string column \mathbf{p}' acquired from the computational-basis measurement, the observable expectation value can be reconstructed after repeating N rounds of $(\mathbf{p}, \mathbf{p}')$ collection.

The RESPOVM shadow tomography scheme, which is applicable to estimating expectation values of real target observables, takes on a simpler structure in that the observer does not need to perform the Y -basis measurement. This scheme may be implemented with Algo. 1 with a slight modification in step 4, where in the RESPOVM measurement part the observer now measures only with X -basis to obtain the outcome $|\phi_{\mathbf{A}}^{\text{req}}\rangle \langle \phi_{\mathbf{A}}^{\text{req}}|$. In Sec. 3.2, we shall see that in many cases, the RESPOVM requires much fewer sampling-copy numbers than ESPOVM to achieve the same estimation accuracy.

This sampling procedure is repeated for $N/2$ measurement trials, with a total of N sampling copies (where N should then be even). For each sampling, our (R)ESPOVM tomography scheme outputs following respective classical shadows. (inverted channel map \mathcal{M}^{-1} [10]):

$$\mathcal{M}^{-1}(O) = \begin{cases} 2^n O - \text{tr}(O) I & \text{(ESPOVM)}, \\ 2^{n-1} O - \text{tr}(O) \frac{I}{2} & \text{(RESPOVM)}, \\ O & \text{(Computational basis)}. \end{cases} \quad (5)$$

We summarize the requirements for implementing Algo. 1 for (R)ESPOVM shadow tomography in

Theorem 1. [(R)ESPOVM implementation] *On an n -qubit state ρ , the implementation of n -qubit ESPOVM shadow tomography requires CZ-gate circuits of depths of at most n by Vizing's theorem [43], and n single-qubit Pauli (X, Y, Z) measurements. For RESPOVM shadow tomography, the Y -basis measurement is not needed.*

3.2 Sampling-copy complexity of equatorial stabilizer POVMs

Shadow tomography aims to estimate state properties with a sampling complexity that grows at most polynomially quickly with the qubit number n . To be more precise, let us specify that a single property estimator is accurate up to a maximal additive error of $\varepsilon > 0$. Then, the number of sampling copies should scale as $\mathcal{O}(\text{poly}(n)/\varepsilon^2)$. We shall prove that our (R)ESPOVM algorithms also possess upper bounds of similar scaling behaviors with randomized-Clifford tomography. To do so, we can apply the median of means (MOM) estimation technique [45–47] by simply repeating the scheme. Hence, from now on, let us assume that the sampling-copy number be total number of copies after such MOM estimation routine when applied. The following theorem shown as below specifies our statements.

Theorem 2. [Sampling-complexity efficiency of (R)ESPOVM shadow tomography] *Suppose that one is able to prepare multiple copies of an unknown input quantum state ρ , and that one is given $M \geq 1$ observables O_1, O_2, \dots, O_M (for RESPOVM shadow tomography, all O_j s are real).*

(i) *With (R)ESPOVM shadow-tomography scheme and MOM estimation technique, we can estimate each $\text{tr}(\rho O_j)$ to within an additive ε -error margin with a success probability $1 - \delta$ if we repeat this scheme over $N \leq \mathcal{O}\left(\frac{\max_{1 \leq j \leq M} \{\text{tr}(O_{j0}^2)\}}{\varepsilon^2} \log\left(\frac{2M}{\delta}\right)\right)$ copies, where*

O_{j0} is the traceless part, $O_j - \frac{1}{2^n} \text{tr}(O_j)$.

(ii) *If $2^n \gg 1$, the averaged sampling-copy number, to achieve the estimation within an additive ε -error margin and a success probability $1 - \delta$, over uniformly-distributed complex pure states ρ and real pure states σ approaches at most $\frac{136 \text{ (68 resp.)}}{\varepsilon^2} \log\left(\frac{2M}{\delta}\right)$ for (R)ESPOVM.*

(iii) *If $2^n \gg 1$, the averaged sampling-copy number, to achieve the estimation within an additive ε -error margin and a success probability $1 - \delta$, over uniformly-distributed complex pure states ρ and σ approaches at most $\frac{136}{\varepsilon^2} \log\left(\frac{2M}{\delta}\right)$ for ESPOVM.*

Theorem 2 (i) suggests that the sampling-copy complexity grows at most polynomially with the qubit number n in many cases. Most notably, if O is also a quantum state σ , then $\text{tr}(O^2)$ becomes constant, hence the required sampling-copy number N is independent of n . Since only an upper bound which has a constant factor of thousands is known, its exact value may be much lower than this bound. Indeed, Theorem 2 (ii) and (iii) imply that one can observe much lower sampling complexity bounds for many cases in state-fidelity estimation. This is especially so when the target state is real, in which case the average sampling-copy bound of RESPOVM is half of one of ESPOVM. The reason is that [42] the average of the *estimation variance* (see the Sec. 5.2 for the definition), which determines the estimation accuracy, of RESPOVM is exactly half of one of ESPOVM, and even the half of one of randomized Clifford tomography. Hence, we can expect RESPOVM shadow tomography to be more useful for real observable estimation.

To showcase the performance of (R)ESPOVM shadow tomography, we examine scenarios in observable-expectation value estimation between arbitrary quantum states. Figure 2(a–c) illustrate three exemplifying cases: ESPOVM shadow tomography for uniformly-chosen random complex input and target states, ESPOVM shadow tomography for uniformly-chosen complex input and real target states, and RESPOVM shadow tomography for the same types of random states as in the second case. We observe that within $N = 2000$, averaged squared error over randomly chosen states becomes inversely proportional to N . These results are consistent with the points of Thm. 2. Moreover, the saturated sam-

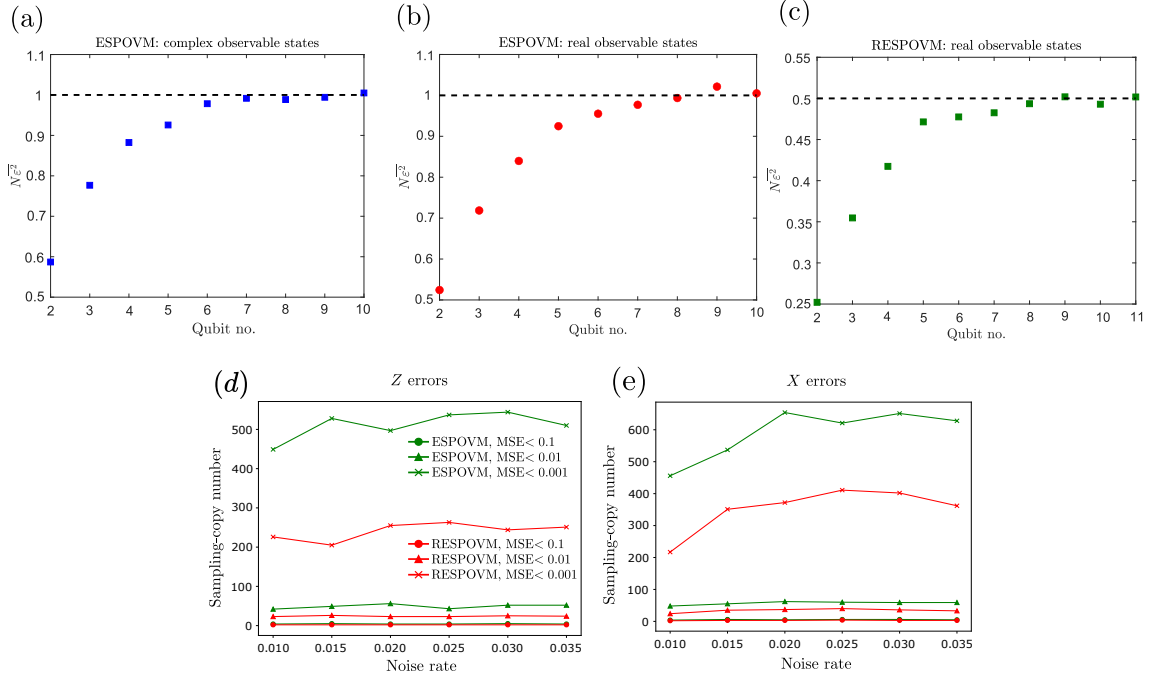


Figure 2: (a–c) Sampling-copy numbers N multiplied with squared error $\overline{\epsilon^2}$ averaged on 200 experiments of different n -qubit (pure) input and target state observables. We set $N = 2000$ for (a,b) and $N = 1000$ for (c), also for each experiment, we put 50 copies with given N to obtain the ϵ^2 which is an averaged value of squared errors between the ideal expectation value of target and estimation, for one experiment. For (a), we averaged the ϵ^2 over uniform distributions of complex input and target states. For (b) and (c), the average is over uniform distributions of complex input and real target states. The horizontal dashed lines represent theoretically asymptotic values [42] of $N\overline{\epsilon^2}$. (d,e) Sampling-copy numbers N required to achieve the respective mean squared error thresholds (averaged over 400 experiments) for the fidelity estimation between a 50-qubit noisily-prepared GHZ state and pure GHZ state. We consider the i.i.d. (d) Z - and (e) X -error channels acting on every qubit with an error probability η_{prep} .

pling copy number to achieve $\overline{\epsilon^2} \leq 0.001$ is much lower than the upper bound shown in Thm. 2 (ii,iii), even without MOM. Furthermore, for real target states, the saturated value of N for RESPOVM is exactly half of that for ESPOVM. Figure 2(d,e) demonstrates the success of (R)ESPOVM shadow tomography in estimating the fidelity between 50-qubit noisily-prepared GHZ states [48] and pure GHZ states with reasonable N values, where one also observes that RESPOVM needs significantly fewer sampling copies than ESPOVM to achieve the same accuracy. Figure 3 brings (R)ESPOVM shadow tomography to the test through estimation of fidelity between noisy 7×7 graph states [49] and its pure counterparts that has CZ-gate connections to all neighboring qubits. Here, N is also the number of measurement trials because every binary measurement outcome gives the same $\hat{O}_{\mathbf{x}}^{\text{bin}} \equiv \langle \mathbf{x} | O | \mathbf{x} \rangle = \frac{1}{2^n}$, so that binary measurements may be omitted. Note that as the preparation error rate $\eta_{\text{prep}} \rightarrow 0$, all estimated fidelities approach the desired value of unity. Even when the observable is approximately a cluster state in the sense that $|\langle \mathbf{x} | O | \mathbf{x} \rangle| < \frac{1}{2^{\alpha n}}$ for $\forall \mathbf{x} \in \mathbb{Z}_2^n$, $\alpha > 0$ and a large $n \in \mathbb{N}$, if our objective is to reduce the additive error precision, the binary measurement part may also be neglected.

Alternatively, fidelity estimations of stabilizer states may be carried out using simpler specialized quantum circuits reported in Ref. [29]. Nevertheless, we emphasize that *all* target states achieve the same asymptotic sampling-complexity bound that is constant in n with (R)ESPOVM shadow-tomography. This means that our technique clearly applies to many other interesting states, including the Dicke states [50], for which $N = \mathcal{O}(n^{2k})$ using

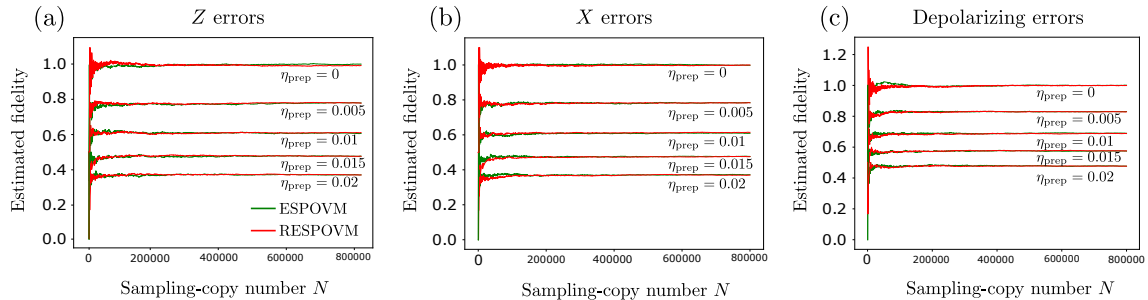


Figure 3: The estimated fidelity with the sampling-copy number N in fidelity estimation between noisily-prepared 7×7 -qubit graph states and their noiseless counterparts. The (a) Z , (b) X and (c) depolarizing preparation-noise channels are i.i.d. to the individual qubits. Each estimated value of a given N is obtained from the median of all $\langle |\widehat{7 \times 7 \text{ graph}} \rangle \langle \widehat{7 \times 7 \text{ graph}} | \rangle$ estimated using the (R)ESPOVM scheme over 400 experiments ($N/400$ copies for each experiment).

the method in Ref. [29].

Another important class of physical observables are n -qubit Heisenberg-type Hamiltonians taking the general form $O = \sum_{\mathbf{p}} J_{\mathbf{p}} \mathbf{Z}^{\mathbf{p}} + \sum_{\mathbf{q}} J'_{\mathbf{q}} \mathbf{X}^{\mathbf{q}} + \sum_{\mathbf{k}} J''_{\mathbf{k}} \mathbf{Y}^{\mathbf{k}}$ for all real $J_{\mathbf{p}}$, $J'_{\mathbf{q}}$ and $J''_{\mathbf{k}}$, where every summation has $\mathcal{O}(\text{poly}(n))$ terms. They are crucial to the study of spin systems and many other aspects of condensed-matter physics [36, 37]. While more elaborative discussions shall be presented in Sec. 5.2, we remark here that expectation values of any such Hamiltonian can be estimated with $\text{poly}(n)$ sampling complexities *via* only Pauli measurements.

3.3 Low gate count and depth for implementing (R)ESPOVM shadow tomography

For both the ESPOVM and RESPOVM shadow-tomography algorithms, we note that the intermediate Clifford operation requires only CZ gates and hence the implementation of randomly chosen CZ gates needs at most $\mathcal{O}(n^2)$ -time. In the language of quantum circuits, Vizing's theorem [51, 52, 43] states that an arbitrary CZ circuit requires a circuit depth of at most n when only CZ gates are employed.

With the aid of CNOT gates, we can reduce the depth to $\frac{n}{2} + \mathcal{O}(\log(n))$ [43]. Furthermore, with just NN two-qubit gates, only a circuit depth of $2n$ is needed [53, 42] with CNOT and S gates, which is lower than the worst-case circuit depth of $7n$ for the implementation of randomized-Clifford tomography [10, 20, 19, 42]. In Sec. 5.3, we further reduced the depth of randomized Clifford tomography to $3n$. This is possible since we are using only non-adaptive Clifford circuits. These arguments are gathered into the following statements:

Theorem 3. [Gate-count and depth efficiency of (R)ESPOVM shadow tomography] [43, 1] *Both ESPOVM and RESPOVM shadow-tomography algorithms can be implemented by circuits of depth $\frac{n}{2} + \mathcal{O}(\log(n))$ (for $n \geq 39$) comprising long-ranged Clifford gates, or those of depth of at most $2n$ using neighboring Clifford gates, while randomized Clifford needs at most $3n$ -depth neighboring Clifford gates. The implementation of linear nearest-neighboring (LNN) architecture takes $\mathcal{O}(n^2)$ -time for each sampling copy.*

This fact, along with Thm. 1 and 2, argues that (R)ESPOVM algorithm is not a simple trade-off of Clifford circuit depth and sampling-copy number. Because scale-factor reduction of depth while preserving sampling copy scale gives significant improvement of

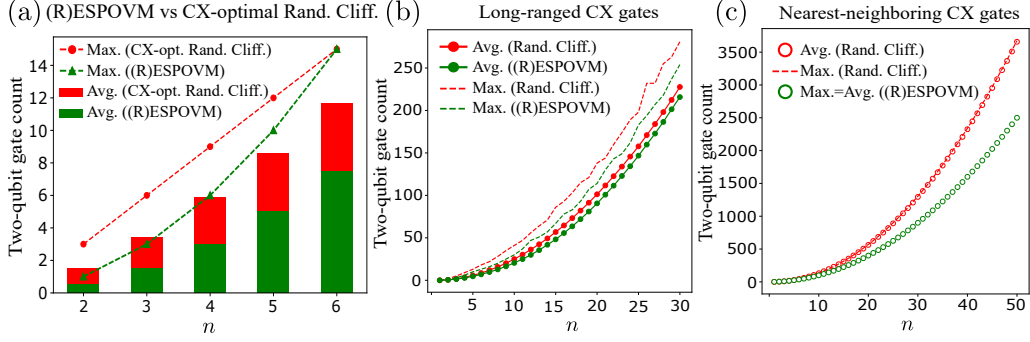


Figure 4: (a) The optimal analytical maximum and average number of long-ranged CNOT gates to implement (R)ESPOVM and randomized-Clifford circuit for low-qubit systems. The latter one is obtained via Tab. 6. of Ref. [54], and is the average gate count over all equivalence classes. (b) The average number of CNOT gates (over 4000 gate samples) to implement intermediate-sized (R)ESPOVMs and single Hadamard-free (HF) sections of randomized-Clifford circuits [20]. For (R)ESPOVMs, we further contracted the gate count *via* the Patel–Markov–Hayes construction [55]. (c) The maximum and average numbers of NN CNOT gates (over 4000 gate samples) to implement a $2n$ -depth large-qubit (R)ESPOVM and $3n$ -depth neighboring implementation of randomized-Clifford circuits [19]. Refer to Sec. 5.3 for a detailed elaboration of these graphs.

gate noise threshold and error mitigation capability [56], also it is more compatible with noisy intermediate-scale quantum (NISQ) algorithms [57].

In Fig. 4 (a,b), we can observe that even before the $\frac{n}{2}$ -depth contraction, randomized CZ-circuit implementation requires a lower gate count than what is required in randomized-Clifford tomography. In particular, Fig. 4(c) shows that the gate counts between LNN architectures differ with a more significant multiplicative factor. Although more optimistic proposals to realize unitary 2-designs with log-depth Clifford circuits exist [58, 10], it is not known how many the sampling-copy number is needed and what the actual feasible gate count would be when these proposals are transformed into LNN architectures.

The CZ-circuit-based architecture of our (R)ESPOVM schemes also presents an attractive feature for experimental implementation, especially with the soaring entangling-gate fidelities recently achieved in various quantum-computing platforms. While a more comprehensive survey shall be given in Sec. 5.5, we quote some recent experimental fidelities achieved in some of these platforms: 99.5% two-qubit gate fidelity in Rydberg-atom quantum computing [59], over 99.5% for semiconductor-spin-based systems [60], and up to 99.93% with superconducting qubits [61].

3.4 Noise tolerance of (R)ESPOVM shadow tomography

The presence of multiple two-qubit gates in a circuit-based quantum-algorithm implementation, be it randomized-Clifford or (R)ESPOVM shadow tomography, enforces a restriction on the individual gate-noise threshold if one is to achieve a given total error rate of the output state before the observable measurement is performed. From Fig. 4(a,b), we observed that our (R)ESPOVM scheme requires a lower long-ranged gate count than randomized-Clifford sampling. Therefore, we note that the required noise threshold for each two-qubit gate is affordably larger for (R)ESPOVMs. Figure. 4(c) shows that in an LNN architecture, the required number of CNOT gates is reduced more effectively and better noise improvements can be expected.

As a testament to the higher noise tolerances (R)ESPOVM shadow-tomography protocols can achieve, we firstly compare the average gate fidelity [62] of the random CZ-based

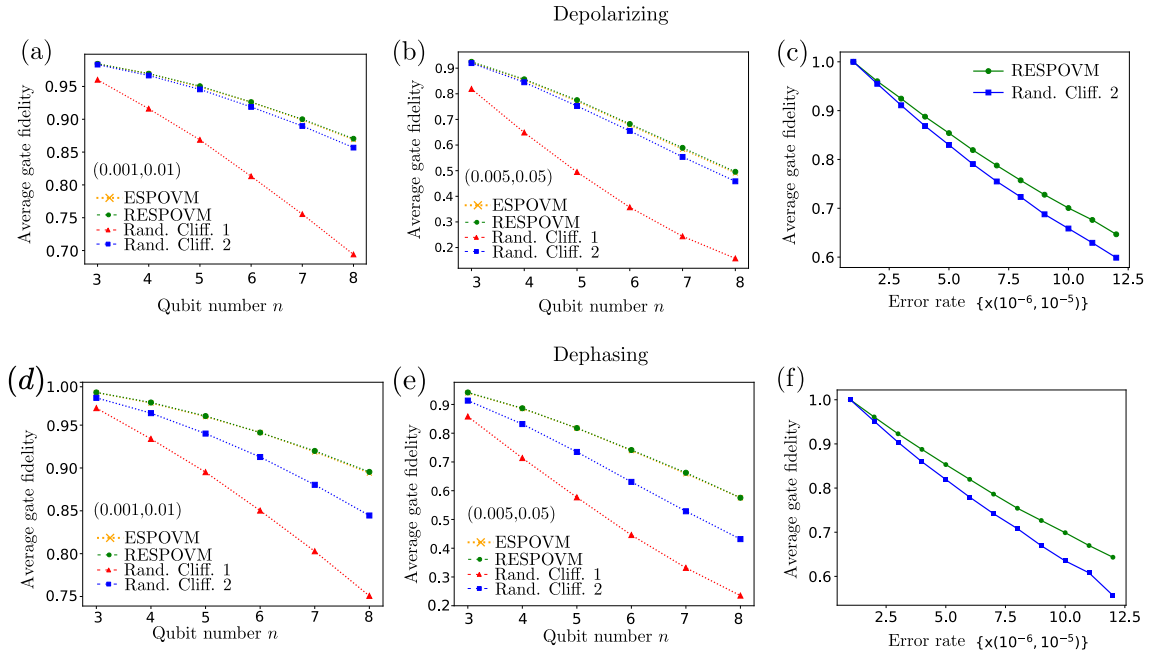


Figure 5: Averaged gate fidelity comparison between noisy (R)ESPOVM and randomized-Clifford circuit. Two randomized-Clifford circuits are considered here: Rand. Cliff. 1 indicates the sampling and decomposition scheme *via* Ref. [31] (or [54] for 3-qubit circuits), and Rand. Cliff. 2 refers to the sampling method in Ref. [20] in which noise is attributed only to the single HF-section. In (a,b) and (d,e), we employed long-range implementation, also (R)ESPOVM is implemented with arbitrary CZ gates. In (c,f), we used their 20-qubit LNN architecture. In (a–c) [(d–f) resp.], we added depolarization (Z-phase) noise to each gate with given error rates. The legends (η_1, η_2) indicate the respective depolarizing (phase) error rates for (η_1) single-qubit (H, S, Pauli) and (η_2) two-qubit gates (CNOT, CZ). Note that if a noisy CNOT gate is positioned in the circuit such that it corresponds to some linear transformation of the measurement outcomes right a perfect CNOT gate, then we need not assign noise for this gate in principle. This is because classically post-processing of the measurement outcomes is sufficient to implement such a gate operation. For (a,b) and (d,e), averaged gate fidelity is computed via the Monte Carlo method with 300 random pure states input and 2000 random long-ranged circuit samples. For (c,f), averaged gate fidelity is computed with 100 random pure states input and 2000 random NN circuit samples. Detailed explanation of noise simulation can be found in the Sec. 5.3 and 5.4.

(R)ESPOVM circuits and random Clifford circuits. The significant gap between Rand. Cliff. 1 and Rand. Cliff. 2 is derived by the fact that in Rand. Cliff. 2, we can only give the noise to the lower half of CNOT gates, while we could not in Rand. Cliff. 1. The expression and computation of the average gate fidelity are presented in Sec. 5.4. Fig. 5 manifests that gate fidelity estimation yields higher rates than one of random Clifford sampling, closer to 1 which is the desired value for pure circuits.

Second, we investigate their performances on fidelity estimations for GHZ [$|\text{GHZ}_n\rangle \equiv \frac{1}{\sqrt{2}}(|0\rangle^{\otimes n} + |1\rangle^{\otimes n})$] [38] and W states [$|\text{W}_n\rangle \equiv \frac{1}{\sqrt{n}}(|0\rangle^{\otimes(n-1)}|1\rangle + |0\rangle^{\otimes(n-2)}|1,0\rangle + \dots + |1\rangle|0\rangle^{\otimes(n-1)})$] for $n = 3, 4$ and 8 in the presence of depolarizing-noise channels. Clearly, a good estimated value should be close to unity. From the graphs presented in Fig. 6, for the same depolarizing error rates, we can observe that RESPOVM shadow tomography provides larger fidelity estimates than randomized-Clifford methods. It should be noted that the gap is much larger than the gap between previously obtained average gate fidelities. The underlying reason behind the significant estimation-quality gap has to do with the sparsity of the input GHZ state in the computational basis that results in a large room for

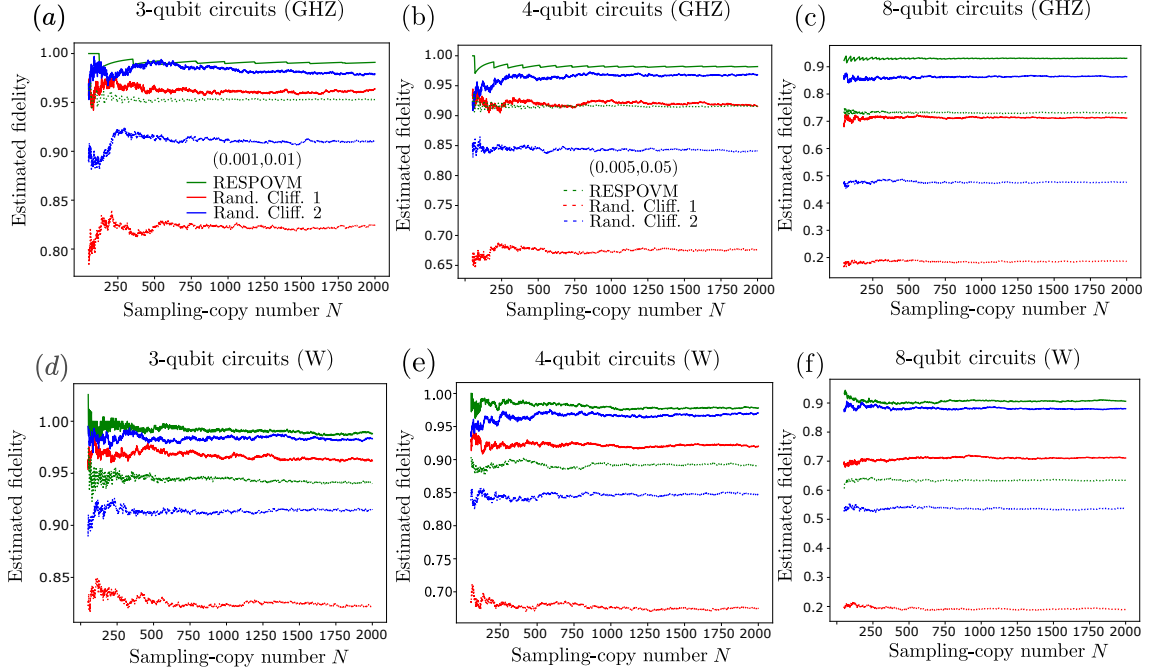


Figure 6: RESPOVM shadow-tomography performances in estimation of fidelity between noisy (a–c) GHZ [(d–f) W states resp.] and pure GHZ states (W states) with increasing number of input-state copies N . Here, we give the depolarizing noise to long-ranged implementation. Also, the method and notations of noise endowment are the same as one of Fig. 5. The estimated fidelity is obtained by taking the median of 200 estimated values for a given number of input states.

obtaining a very good estimated fidelity so long as the bit strings measured by RESPOVM are of the correct parity. One may also expect W states to behave similarly. We expect that this resource-efficient shadow tomography will offer similar estimation-accuracy advantages in many other cases, such as the fidelity estimation of large non-stabilizer quantum states, at which available schemes are more restrictive. Furthermore, since we did not use any circuit contraction technique in long-ranged CZ-gates, further gap improvement for Fig. 5 and 6 after the contraction is to be anticipated.

4 Discussion

In this article, we propose resource-efficient methods to carry out quantum shadow tomography using equatorial-stabilizer measurements that are derived from smaller subsets of the full set of stabilizer states. We first prove that these equatorial-stabilizer measurements, together with the computational-basis measurements are indeed informationally complete and possess desirable sampling complexity that grows, in many cases, at most polynomially in the number of qubits n and reciprocally in the square of the target additive estimation error. In typical scenarios, such as rank-one observable estimation, the sampling complexity of equatorial-stabilizer shadow tomography is independent of n .

Furthermore, we showed that these economic shadow-tomography algorithms utilize long-ranged Clifford bases with circuit depths of $\frac{n}{2} + \mathcal{O}(\log(n))$. When restricted to only LNN architectures, our algorithms are considerably efficient to implement, requiring only $2n$ -depth NN CNOT gates, owing to their simpler circuit geometry. We demonstrated that our methods require fewer Clifford basis count than randomized-Clifford tomography for both long-ranged and LNN implementations, while still preserving the classes of ap-

plicable observables for many cases in terms of the shadow-norm or estimation variance criterion. Our depth- (or gate-)efficient shadow-tomography schemes become practically important for performing realistic quantum-computation tasks as they permit larger gate-error thresholds. This is also crucial to certain auxiliary quantum tasks, such as those in quantum error mitigation for instance, where it is recently known [56] that such tasks would require sampling-copy numbers that increase exponentially with the circuit depth.

Thus far, the (R)ESPOVM schemes we have found to have good shadow-tomographic properties require both computational-basis and CZ-circuit measurements that involve very different circuit depths, with the former being single-layered while the latter grows linearly with n in depth. One possible future would be to investigate if there exist other such pairs of measurement circuits of comparable depths that can reduce the maximum circuit depth employed whilst maintaining the same estimation quality. Here, MUB subsets of the CZ-circuit measurements [34] could serve as an instructive starting point. Yet another desirable observation is the rather large error-threshold advantages in using equatorial-stabilizer shadow tomography on GHZ or W state-verification tasks in contrast to randomized-Clifford shadow tomography, which are far beyond what we expected from the average-gate-fidelity comparison. This readily sets another research direction on identifying important classes of target quantum states that could lead to highly-effective gate-error threshold improvements.

Clifford circuits are well-known quantum circuits [63, 64] whose noise-tolerant properties could be realizable in the near future. Therefore, we expect our work to establish practical research directions on gate-efficient observable-expectation-value estimations for noisy intermediate-scale quantum computation.

5 Technical aspects of (R)ESPOVM shadow tomography

In this section, we elaborate on our key results with discussions concerning the (R)ESPOVM shadow-tomography algorithm, calculations leading to the estimation accuracies and systematic approaches to counting the gate complexities needed to implement (R)ESPOVM schemes. Along the way, we shall sketch the proofs for Theorems 1 to 3 and include their details that are appropriate and coherent to the general discussions in this section without diving into other required technical lemmas and miscellaneous statements to complete the proofs. The reader is invited to refer to the Appendix [42] for all remaining arguments not covered here. Further, we introduce the notion of average gate fidelity and detailed expression of the recent status of Clifford gates implementation in reality.

5.1 Procedures and algorithm for equatorial-stabilizer shadow tomography

Before we present the details of (R)ESPOVM shadow tomography, we first introduce the notation $\mathbb{E}_{\sigma \sim \mathcal{D}(A)} f(\sigma)$ that refers to the expected value of the function $f(\sigma)$ of a random variable $\sigma \in A$ that follows a uniformly random distribution $\mathcal{D}(A)$ with domain A . In particular, we call $\mathbb{E}_{\sigma \sim \mathcal{D}(A)} \sigma^{\otimes t}$ as the t -th moment of A . With this, we have the following lemma [42].

Lemma 1. For the n -qubit system,

$$(i) \text{ [33]} \mathbb{E}_{|\phi_{\mathbf{A}}^{\text{eq}}\rangle \sim \mathcal{D}(\mathcal{S}_n^{\text{eq}})} |\phi_{\mathbf{A}}^{\text{eq}}\rangle \langle \phi_{\mathbf{A}}^{\text{eq}}| = \mathbb{E}_{|\phi_{\mathbf{A}}^{\text{req}}\rangle \sim \mathcal{D}(\mathcal{S}_n^{\text{req}})} |\phi_{\mathbf{A}}^{\text{req}}\rangle \langle \phi_{\mathbf{A}}^{\text{req}}| = \frac{I}{2^n}, \quad (6)$$

$$(ii) \text{ [33]} \mathbb{E}_{|\phi_{\mathbf{A}}^{\text{eq}}\rangle \sim \mathcal{D}(\mathcal{S}_n^{\text{eq}})} |\phi_{\mathbf{A}}^{\text{eq}}\rangle \langle \phi_{\mathbf{A}}^{\text{eq}}|^{\otimes 2} = \frac{1}{4^n} \left(I + \sum_{\mathbf{x}, \mathbf{y} \in \mathbb{Z}_2^n} |\mathbf{x}\mathbf{y}\rangle \langle \mathbf{y}\mathbf{x}| - \sum_{\mathbf{x} \in \mathbb{Z}_2^n} |\mathbf{x}\mathbf{x}\rangle \langle \mathbf{x}\mathbf{x}| \right), \quad (7)$$

$$(iii) \mathbb{E}_{|\phi_{\mathbf{A}}^{\text{req}}\rangle \sim \mathcal{D}(\mathcal{S}_n^{\text{req}})} |\phi_{\mathbf{A}}^{\text{req}}\rangle \langle \phi_{\mathbf{A}}^{\text{req}}|^{\otimes 2} = \quad (8)$$

$$\frac{1}{4^n} \left(I + \sum_{\mathbf{x}, \mathbf{y} \in \mathbb{Z}_2^n} |\mathbf{x}\mathbf{y}\rangle \langle \mathbf{y}\mathbf{x}| + \sum_{\mathbf{x}, \mathbf{y} \in \mathbb{Z}_2^n} |\mathbf{x}\mathbf{x}\rangle \langle \mathbf{y}\mathbf{y}| - 2 \sum_{\mathbf{x} \in \mathbb{Z}_2^n} |\mathbf{x}\mathbf{x}\rangle \langle \mathbf{x}\mathbf{x}| \right). \quad (9)$$

We note that from Lem. 1 (i), all elements from the respective sets $\left\{ \frac{2^n}{|\mathcal{S}_n^{\text{eq}}|} |\phi_{\mathbf{A}}^{\text{eq}}\rangle \langle \phi_{\mathbf{A}}^{\text{eq}}| \right\}$ and $\left\{ \frac{2^n}{|\mathcal{S}_n^{\text{req}}|} |\phi_{\mathbf{A}}^{\text{req}}\rangle \langle \phi_{\mathbf{A}}^{\text{req}}| \right\}$ form a POVM. Using Lem. 1 (ii) and (iii), we can obtain the following formulas which are directly related to our tomography schemes [42]:

Lemma 2. For an unknown n -qubit quantum state ρ and Hermitian operator O ,

$$\text{tr}(\rho O) = \sum_{|\phi_{\mathbf{A}}^{\text{eq}}\rangle \in \mathcal{S}_n^{\text{eq}}} \frac{2^{2n}}{|\mathcal{S}_n^{\text{eq}}|} \langle \phi_{\mathbf{A}}^{\text{eq}} | \rho | \phi_{\mathbf{A}}^{\text{eq}} \rangle \langle \phi_{\mathbf{A}}^{\text{eq}} | O | \phi_{\mathbf{A}}^{\text{eq}} \rangle + \sum_{\mathbf{x} \in \mathbb{Z}_2^n} \langle \mathbf{x} | \rho | \mathbf{x} \rangle \langle \mathbf{x} | O | \mathbf{x} \rangle - \text{tr}(O). \quad (10)$$

If O is a real matrix with respect to the computational basis,

$$\text{tr}(\rho O) = \sum_{|\phi_{\mathbf{A}}^{\text{req}}\rangle \in \mathcal{S}_n^{\text{req}}} \frac{2^{2n-1}}{|\mathcal{S}_n^{\text{req}}|} \langle \phi_{\mathbf{A}}^{\text{req}} | \rho | \phi_{\mathbf{A}}^{\text{req}} \rangle \langle \phi_{\mathbf{A}}^{\text{req}} | O | \phi_{\mathbf{A}}^{\text{req}} \rangle + \sum_{\mathbf{x} \in \mathbb{Z}_2^n} \langle \mathbf{x} | \rho | \mathbf{x} \rangle \langle \mathbf{x} | O | \mathbf{x} \rangle - \frac{1}{2} \text{tr}(O). \quad (11)$$

From the Lem. 1 and 2, the following estimators (denoted with a caret) are constructed:

$$\widehat{\langle O \rangle} = \begin{cases} \left(\frac{2^n}{(N/2)} \sum_{\substack{\text{sampled } \mathbf{A} \\ \text{over } N/2 \text{ copies}}} \langle \phi_{\mathbf{A}}^{\text{eq}} | O | \phi_{\mathbf{A}}^{\text{eq}} \rangle + \frac{1}{(N/2)} \sum_{\substack{\text{measured } \mathbf{p}' \\ \text{over } N/2 \text{ copies}}} \langle \mathbf{p}' | O | \mathbf{p}' \rangle - \text{tr}(O) \right) \\ \text{(ESPOVM and comp. basis),} \\ \\ \left(\frac{2^{n-1}}{(N/2)} \sum_{\substack{\text{sampled } \mathbf{A} \\ \text{over } N/2 \text{ copies}}} \langle \phi_{\mathbf{A}}^{\text{req}} | O | \phi_{\mathbf{A}}^{\text{req}} \rangle + \frac{1}{(N/2)} \sum_{\substack{\text{measured } \mathbf{p}' \\ \text{over } N/2 \text{ copies}}} \langle \mathbf{p}' | O | \mathbf{p}' \rangle - \frac{1}{2} \text{tr}(O) \right) \\ \text{(RESPOVM and comp. basis),} \end{cases} \quad (12)$$

where \mathbf{A} and \mathbf{p}' are sampled from the distribution of $\left\{ \frac{2^n}{|\mathcal{S}_n^{(\text{r})\text{eq}}|} \langle \phi_{\mathbf{A}}^{(\text{r})\text{eq}} | \rho | \phi_{\mathbf{A}}^{(\text{r})\text{eq}} \rangle \right\}$ and $\{ \langle \mathbf{p}' | \rho | \mathbf{p}' \rangle \}$ respectively. Note that these estimators are unbiased, i.e. data-average $\mathbb{E}(\widehat{\langle O \rangle}) = \langle O \rangle$.

We are ready to provide more details concerning the (R)ESPOVM shadow-tomography procedure, thereby explaining the validity of Algo. 1. We shall only discuss matters related to the ESPOVM, as the dissertation for RESPOVM follows similarly. Let us assume an

input state $\rho = \sum_{\mathbf{z}, \mathbf{w} \in \mathbb{Z}_2^n} |\mathbf{z}\rangle \langle \mathbf{w}| \langle \mathbf{z} | \rho | \mathbf{w}\rangle$. The procedure begins by a random selection of $|\phi_{\mathbf{A}}^{\text{eq}}\rangle \in \mathcal{S}_n^{\text{eq}}$, that is the matrix \mathbf{A} from uniformly distributed elements in the set

$$\mathcal{A} \equiv \left\{ \mathbf{A} \left| \mathbf{A} = (a_{ij})_{i,j \in [n]} \text{ where } a_{ij} = a_{ji}, a_{ii} \in \mathbb{Z}_4, a_{ij} \in \mathbb{Z}_2 \text{ if } i \neq j \right. \right\}. \quad (13)$$

Operationally, this is akin to flipping a coin $\frac{n^2-n}{2}$ times to determine all symmetric off-diagonal elements and flipping a uniform 4-sided die n times to determine all diagonal elements of \mathbf{A} . Now, given a single-qubit (two-qubit resp.) operation K , we define K_i (K_{ij}) as K acting on the i -th (i -th and j -th) qubit. After choosing a random \mathbf{A} , we perform CZ_{ij} gate operations whenever $a_{ij} = 1$ and $i < j$, followed by single-qubit operations U_i such that

$$U_i \equiv \begin{cases} I_i & \text{if } a_{ii} = 0, \\ S^\dagger & \text{if } a_{ii} = 1, \\ Z_i & \text{if } a_{ii} = 2, \\ S_i & \text{if } a_{ii} = 3, \end{cases} \quad \text{or simply, } U_i \equiv (S^\dagger)^i. \quad (14)$$

Next, we apply Hadamard gates $H \equiv \bigotimes_{i=1}^n H_i$. The subsequent evolved state ρ' is written as

$$\rho \leftarrow \rho' = \frac{1}{2^n} \sum_{\mathbf{z}, \mathbf{w}, \mathbf{s}, \mathbf{t} \in \mathbb{Z}_2^n} i^{3\mathbf{z}^\top \mathbf{A} \mathbf{z} + \mathbf{w}^\top \mathbf{A} \mathbf{w}} (-1)^{\mathbf{z} \cdot \mathbf{s} + \mathbf{w} \cdot \mathbf{t}} |\mathbf{s}\rangle \langle \mathbf{t}| \langle \mathbf{z} | \rho | \mathbf{w}\rangle. \quad (15)$$

Here, $\mathbf{a} \cdot \mathbf{b}$ refers to the binary inner product between \mathbf{a} and \mathbf{b} . We shall now perform the Pauli Z -basis measurement independently on all the qubits. The probability $\text{prob}(\mathbf{p} | \mathbf{A})$ to obtain a specific binary string $\mathbf{p} \in \mathbb{Z}_2^n$ is

$$\begin{aligned} \text{prob}(\mathbf{p} | \mathbf{A}) &\equiv \langle \mathbf{p} | \rho' | \mathbf{p}\rangle = \frac{1}{2^n} \sum_{\mathbf{z}, \mathbf{w}, \mathbf{s}, \mathbf{t} \in \mathbb{Z}_2^n} i^{3\mathbf{z}^\top \mathbf{A} \mathbf{z} + \mathbf{w}^\top \mathbf{A} \mathbf{w}} (-1)^{\mathbf{z} \cdot \mathbf{s} + \mathbf{w} \cdot \mathbf{t}} \langle \mathbf{p} | \mathbf{s}\rangle \langle \mathbf{t} | \mathbf{p}\rangle \langle \mathbf{z} | \sigma | \mathbf{w}\rangle, \\ &= \frac{1}{2^n} \sum_{\mathbf{z}, \mathbf{w} \in \mathbb{Z}_2^n} i^{3\mathbf{z}^\top \mathbf{A} \mathbf{z} + \mathbf{w}^\top \mathbf{A} \mathbf{w}} (-1)^{\mathbf{z} \cdot \mathbf{p} + \mathbf{w} \cdot \mathbf{p}} \langle \mathbf{z} | \sigma | \mathbf{w}\rangle, \\ &= \frac{1}{2^n} \sum_{\mathbf{z}, \mathbf{w} \in \mathbb{Z}_2^n} (-i)^{\mathbf{z}^\top \mathbf{A} \mathbf{z} - 2\mathbf{z} \cdot \mathbf{p}} i^{\mathbf{w}^\top \mathbf{A} \mathbf{w} - 2\mathbf{w} \cdot \mathbf{p}} \langle \mathbf{z} | \sigma | \mathbf{w}\rangle, \end{aligned} \quad (16)$$

$$= \langle \phi_{\mathbf{A}'}^{\text{eq}} | \rho | \phi_{\mathbf{A}'}^{\text{eq}} \rangle, \quad (17)$$

where \mathbf{A}' is an $n \times n$ matrix such that $a'_{ij} = a_{ij}$ for $i \neq j$, and $a'_{ii} = a_{ii} + 2p_i \pmod{4}$. The last equation can be obtained by following the definition of Eq. (3). Now, we define $\mathbf{D}(\mathbf{p})$ as the $n \times n$ diagonal matrix whose i -th diagonal element is equal to p_i , and also note, from Eq. (3), that

$$\frac{2^n}{|\mathcal{S}_n^{\text{eq}}|} \langle \phi_{\mathbf{A}}^{\text{eq}} | \rho | \phi_{\mathbf{A}}^{\text{eq}} \rangle = \frac{1}{|\mathcal{S}_n^{\text{eq}}|} \sum_{\mathbf{z}, \mathbf{w} \in \mathbb{Z}_2^n} (-i)^{\mathbf{z}^\top \mathbf{A} \mathbf{z}} i^{\mathbf{w}^\top \mathbf{A} \mathbf{w}} \langle \mathbf{z} | \rho | \mathbf{w}\rangle \quad (18)$$

$$= \sum_{\mathbf{p} \in \mathbb{Z}_2^n} \frac{1}{|\mathcal{S}_n^{\text{eq}}|} \text{prob}(\mathbf{p} | \mathbf{A} - 2\mathbf{D}(\mathbf{p})), \quad (19)$$

where the final equality is a result of Eq. (16).

The left-hand side of Eq. (19) corresponds to the probability distribution of \mathbf{A} we want to sample from. Also, given a $\mathbf{p} \in \mathbb{Z}_2^n$, the probability to sample the matrix $\mathbf{A} - 2\mathbf{D}(\mathbf{p})$ is

constant $\left(\frac{1}{|\mathcal{S}_n^{\text{eq}}|}\right)$. Hence, we can interpret the right-most side of Eq. (19) as the probability to get the matrix \mathbf{A} after we uniformly sampled the matrix \mathbf{A}' and add $2\mathbf{D}(\mathbf{p})$ (see steps 22 through 28 in Algo. 1). In this way, the desired sample of \mathbf{A} is obtained.

Furthermore, we note that one can propagate the measurement section to the left-over Hadamard gates and phase gates. In that case, the CZ gates are the only remaining intermediate gates, and Vizing's theorem states that only at most n layers of CZ gates are needed to realize an arbitrary n -qubit CZ circuit, which settles part of Thm. 1. One must still carry out either the Pauli X or Y measurement depending on the phase gate acting on that qubit. However, the phase gate implementation is unnecessary and we simply perform an X or Y -basis measurement. The reason is that Z (S resp.) just flips the measurement outcome of X (Y) measurement. For example, implementing Z and obtaining the X -measurement outcome 0 is equivalent to just measuring in the X -basis, obtaining the outcome 1, which gives the same diagonal value of the sampled \mathbf{A} . That is why we can transform above procedure to take X or Y -measurement depending on only the mod 2 features of sampled a_{ii} ($i \in [n]$), not using single qubit phase gates, and add $2\mathbf{D}(\mathbf{p})$ to \mathbf{A}' . This closes the proof of Thm. 1 for the ESPOVM scheme, and also justifies steps 22 through 28 in Algo. 1.

Harking back to Eq. (2), in order to complete the shadow tomography protocol, one also acquires $\mathbf{p}' \in \mathbb{Z}_2^n$ following the distribution $\langle \mathbf{p}' | \rho | \mathbf{p}' \rangle$, which can be done easily by measuring ρ in the Pauli Z basis. Hence, the algorithm for an unbiased estimation of $\text{tr}(O\rho)$ can be summarized as follows:

1. Measure one copy of ρ with the projector $|\phi_{\mathbf{A}}^{\text{eq}}\rangle \langle \phi_{\mathbf{A}}^{\text{eq}}|$ defined by a uniformly-chosen \mathbf{A} from the set \mathcal{A} in (13). This is done by (i) uniformly choosing an $\mathbf{A}' \in \mathcal{A}$, (ii) obtain a $\mathbf{p} \in \mathbb{Z}_2^n$ from measuring this ρ copy with $|\phi_{\mathbf{A}'}^{\text{eq}}\rangle \langle \phi_{\mathbf{A}'}^{\text{eq}}|$, (iii) and take $\mathbf{A} = \mathbf{A}' + 2\mathbf{D}(\mathbf{p})$. The measurement outcome \mathbf{p} would then follow the distribution $\frac{2^n}{|\mathcal{S}_n^{\text{eq}}|} \langle \phi_{\mathbf{A}}^{\text{eq}} | \rho | \phi_{\mathbf{A}}^{\text{eq}} \rangle$.
2. Measure one copy of ρ and obtain $\mathbf{p}' \in \mathbb{Z}_2^n$ following the distribution $\langle \mathbf{p}' | \rho | \mathbf{p}' \rangle$.
3. Calculate $\widehat{O}_{\mathbf{A},\mathbf{x}} \equiv 2^n \langle \phi_{\mathbf{A}}^{\text{eq}} | O | \phi_{\mathbf{A}}^{\text{eq}} \rangle + \langle \mathbf{p}' | O | \mathbf{p}' \rangle - \text{tr}(O)$.

Algorithm 1 is the pseudocode encapsulation of all the arguments we made thus far.

5.2 Estimation-variance analysis of equatorial-stabilizer shadow tomography

We shall now sketch the proof of Thm. 2 (i).

For this purpose, we denote $\widehat{O}_{\mathbf{A}}^{\text{eq}} \equiv 2^n \langle \phi_{\mathbf{A}}^{\text{eq}} | O | \phi_{\mathbf{A}}^{\text{eq}} \rangle$, $\widehat{O}_{\mathbf{A}}^{\text{req}} \equiv 2^{n-1} \langle \phi_{\mathbf{A}}^{\text{req}} | O | \phi_{\mathbf{A}}^{\text{req}} \rangle$, and $\widehat{O}_{\mathbf{x}}^{\text{bin}} \equiv \langle \mathbf{x} | O | \mathbf{x} \rangle$ for one observable O that are measured and obtained in each step of the shadow-tomography procedure, where the matrix \mathbf{A} and bit string \mathbf{x} are random in accordance with Algo. 1. The first two random numbers $\widehat{O}_{\mathbf{A}}^{\text{eq}}$ and $\widehat{O}_{\mathbf{A}}^{\text{req}}$ refer to the respective outcome estimators for ESPOVM and RESPOVM, and $\widehat{O}_{\mathbf{x}}^{\text{bin}}$ is the outcome of a Z -basis measurement. Upon defining $\mathbb{E}(\widehat{O}_{\mathbf{A},\mathbf{x}})$ as the data-average value of $\widehat{O}_{\mathbf{A},\mathbf{x}}$, which is defined as

$$\widehat{O}_{\mathbf{A},\mathbf{x}} \equiv \begin{cases} \widehat{O}_{\mathbf{A}}^{\text{eq}} + \widehat{O}_{\mathbf{x}}^{\text{bin}} - \text{tr}(O) & \text{(ESPOVM)} \\ \widehat{O}_{\mathbf{A}}^{\text{req}} + \widehat{O}_{\mathbf{x}}^{\text{bin}} - \frac{1}{2}\text{tr}(O) & \text{(RESPOVM)}, \end{cases} \quad (20)$$

the estimation variance $\text{Var}(\widehat{O}_{\mathbf{A},\mathbf{x}}) \equiv \mathbb{E}(\widehat{O}_{\mathbf{A},\mathbf{x}}^2) - (\mathbb{E}(\widehat{O}_{\mathbf{A},\mathbf{x}}))^2$ of our two shadow-tomography schemes is given as,

$$\text{Var}^{(\text{r})\text{eq}}(\widehat{O}_{\mathbf{A},\mathbf{x}}) = \text{Var}(\widehat{O}_{\mathbf{A}}^{(\text{r})\text{eq}}) + \text{Var}(\widehat{O}_{\mathbf{x}}^{\text{bin}}), \quad (21)$$

because \mathbf{A}, \mathbf{x} sampling is independent of each other [42]. The variance terms on the right side, after maximizing over the input state ρ , are equivalent to the respective squared shadow norms [10] of the (R)ESPOVM and Z -basis measurement. With Eq. (21), the complete variance of $\langle \widehat{O} \rangle$ for estimating a single property $\langle O \rangle$ is given by

$$\text{Var}(\langle \widehat{O} \rangle) = \begin{cases} \frac{1}{N/2} \text{Var}^{\text{eq}}(\widehat{O}_{\mathbf{A}, \mathbf{x}}) & \text{(ESPOVM and comp. basis)}, \\ \frac{1}{N/2} \text{Var}^{\text{req}}(\widehat{O}_{\mathbf{A}, \mathbf{x}}) & \text{(RESPOVM and comp. basis)}. \end{cases} \quad (22)$$

Note that since $\langle \widehat{O} \rangle$ is unbiased, $\text{Var}(\langle \widehat{O} \rangle)$ is identical to the mean-squared error of $\langle \widehat{O} \rangle$ that measures the estimation accuracy of $\langle \widehat{O} \rangle$ with respect to $\langle O \rangle$:

$$\text{Var}(\langle \widehat{O} \rangle) = \mathbb{E} \left((\langle \widehat{O} \rangle - \langle O \rangle)^2 \right). \quad (23)$$

Now, we scrutinize Eq. (21). We note that

$$\begin{aligned} \text{Var}(\widehat{O}_{\mathbf{A}}^{\text{eq}}) &= \mathbb{E} \left(\{2^n \langle \phi_{\mathbf{A}}^{\text{eq}} | O | \phi_{\mathbf{A}}^{\text{eq}} \rangle - \mathbb{E}(2^n \langle \phi_{\mathbf{A}}^{\text{eq}} | O | \phi_{\mathbf{A}}^{\text{eq}} \rangle)\}^2 \right) \\ &= \mathbb{E} \left(\left\{ 2^n \langle \phi_{\mathbf{A}}^{\text{eq}} | (O_0 + \frac{I}{2^n} \text{tr}(O)) | \phi_{\mathbf{A}}^{\text{eq}} \rangle - \mathbb{E} \left(2^n \langle \phi_{\mathbf{A}}^{\text{eq}} | (O_0 + \frac{I}{2^n} \text{tr}(O)) | \phi_{\mathbf{A}}^{\text{eq}} \rangle \right) \right\}^2 \right) \\ &= \mathbb{E} \left(\{2^n \langle \phi_{\mathbf{A}}^{\text{eq}} | O_0 | \phi_{\mathbf{A}}^{\text{eq}} \rangle - \mathbb{E}(2^n \langle \phi_{\mathbf{A}}^{\text{eq}} | O_0 | \phi_{\mathbf{A}}^{\text{eq}} \rangle)\}^2 \right) \\ &= \text{Var}(\widehat{O}_{0\mathbf{A}}^{\text{eq}}) \end{aligned} \quad (24)$$

where the second line is easily derived noting that O_0 is *traceless part*, $O - \frac{I}{2^n} \text{tr}(O)$, hence $\text{tr}(O_0) = 0$. Since we can follow the same reasoning to $\text{Var}(\widehat{O}_{\mathbf{A}}^{\text{req}})$ and $\text{Var}(\widehat{O}_{\mathbf{x}}^{\text{bin}})$, we only need to consider the variance of the O_0 . In other words, we obtain that

$$\text{Var}^{(r)\text{eq}}(\widehat{O}_{\mathbf{A}}^{(r)\text{eq}}) = \text{Var}^{(r)\text{eq}}(\widehat{O}_{0\mathbf{A}}^{(r)\text{eq}}) = \mathbb{E}((\widehat{O}_{\mathbf{A}}^{(r)\text{eq}})^2) - \mathbb{E}(\widehat{O}_{0\mathbf{A}}^{(r)\text{eq}})^2 \leq \mathbb{E}((\widehat{O}_{0\mathbf{A}}^{(r)\text{eq}})^2), \quad (25)$$

where \mathbb{E} is the expected value of $\widehat{O}_{0\mathbf{A}} \equiv 2^n \langle \phi_{\mathbf{A}}^{(r)\text{eq}} | O_0 | \phi_{\mathbf{A}}^{(r)\text{eq}} \rangle$. Hence, to obtain the upper bound of the estimation variance of $\widehat{O}_{0\mathbf{A}}^{(r)\text{eq}}$, all we need to do is to bound $\mathbb{E}((\widehat{O}_{0\mathbf{A}}^{(r)\text{eq}})^2)$ from above. Let us first rewrite

$$\begin{aligned} \mathbb{E}((\widehat{O}_{0\mathbf{A}}^{(r)\text{eq}})^2) &= \frac{2^\gamma}{|\mathcal{S}_n^{(r)\text{eq}}|} \sum_{|\phi_{\mathbf{A}}^{(r)\text{eq}} \rangle \in \mathcal{S}_n^{(r)\text{eq}}} \langle \phi_{\mathbf{A}}^{(r)\text{eq}} | \rho | \phi_{\mathbf{A}}^{(r)\text{eq}} \rangle \langle \phi_{\mathbf{A}}^{(r)\text{eq}} | O_0 | \phi_{\mathbf{A}}^{(r)\text{eq}} \rangle \langle \phi_{\mathbf{A}}^{(r)\text{eq}} | O_0 | \phi_{\mathbf{A}}^{(r)\text{eq}} \rangle \\ &= 2^\gamma \text{tr} \left(\mathbb{E}_{|\phi_{\mathbf{A}}^{(r)\text{eq}} \rangle \sim \mathcal{D}(\mathcal{S}_n^{(r)\text{eq}})} |\phi_{\mathbf{A}}^{(r)\text{eq}} \rangle \langle \phi_{\mathbf{A}}^{(r)\text{eq}} |^{\otimes 3} (\rho \otimes O_0 \otimes O_0) \right), \\ \gamma &= \begin{cases} 3n & \text{for eq,} \\ 3n - 2 & \text{for req.} \end{cases} \end{aligned} \quad (26)$$

Therefore, we need the third moment $\mathbb{E}_{|\phi_{\mathbf{A}}^{(r)\text{eq}} \rangle \sim \mathcal{D}(\mathcal{S}_n^{(r)\text{eq}})} |\phi_{\mathbf{A}}^{(r)\text{eq}} \rangle \langle \phi_{\mathbf{A}}^{(r)\text{eq}} |^{\otimes 3}$, and for this, let

us first define the following two sets:

$$\begin{aligned} \mathcal{K}_1(\mathbb{Z}_2^n) &\equiv \{\mathbf{P} = (\mathbf{x}, \mathbf{y}, \mathbf{z}, \mathbf{w}, \mathbf{s}, \mathbf{t}) | \mathbf{x}, \mathbf{y}, \mathbf{z}, \mathbf{w}, \mathbf{s}, \mathbf{t} \in \mathbb{Z}_2^n, \text{ all } p_i\text{'s are pairwise equal}\}, \quad (27) \\ \mathcal{K}_2(\mathbb{Z}_2^n) &\equiv \{\mathbf{P} = (\mathbf{x}, \mathbf{y}, \mathbf{z}, \mathbf{w}, \mathbf{s}, \mathbf{t}) | \mathbf{P} \in \mathcal{K}_1(\mathbb{Z}_2^n) \text{ and if } \{\mathbf{x}, \mathbf{y}, \mathbf{z}\} \text{ and } \{\mathbf{w}, \mathbf{s}, \mathbf{t}\} \text{ have a same} \\ &\quad \text{common element, say } \mathbf{v}, \text{ and the other 2 variables in } \{\mathbf{x}, \mathbf{y}, \mathbf{z}\} \setminus \{\mathbf{v}\} \text{ or} \\ &\quad \{\mathbf{w}, \mathbf{s}, \mathbf{t}\} \setminus \{\mathbf{v}\} \text{ are equal, say } \mathbf{v}', \text{ then remaining 2 variables are equal to } \mathbf{v}'\}. \end{aligned} \quad (28)$$

For example, $\{(1, 0, 0, 1, 0, 0), (1, 1, 0, 1, 1, 0), (1, 0, 0, 1, 1, 1)\} \subset \mathcal{K}_1(\mathbb{Z}_2)$, and $\{(1, 0, 0, 1, 0, 0), (1, 1, 0, 1, 1, 0)\} \subset \mathcal{K}_2(\mathbb{Z}_2)$ but $(1, 0, 0, 1, 1, 1) \notin \mathcal{K}_2(\mathbb{Z}_2)$. With these notations, we obtain another lemma:

Lemma 3.

$$(i) \mathbb{E}_{|\phi_{\mathbf{A}}^{\text{req}}\rangle \sim \mathcal{D}(S_n^{\text{req}})} |\phi_{\mathbf{A}}^{\text{req}}\rangle \langle \phi_{\mathbf{A}}^{\text{req}}|^{\otimes 3} = \frac{1}{8^n} \sum_{(\mathbf{x}, \mathbf{y}, \mathbf{z}, \mathbf{w}, \mathbf{s}, \mathbf{t}) \in \mathcal{K}_1(\mathbb{Z}_2^n)} |\mathbf{x}\mathbf{y}\mathbf{z}\rangle \langle \mathbf{w}\mathbf{s}\mathbf{t}|. \quad (29)$$

$$(ii) \mathbb{E}_{|\phi_{\mathbf{A}}^{\text{eq}}\rangle \sim \mathcal{D}(S_n^{\text{eq}})} |\phi_{\mathbf{A}}^{\text{eq}}\rangle \langle \phi_{\mathbf{A}}^{\text{eq}}|^{\otimes 3} = \frac{1}{8^n} \sum_{(\mathbf{x}, \mathbf{y}, \mathbf{z}, \mathbf{w}, \mathbf{s}, \mathbf{t}) \in \mathcal{K}_2(\mathbb{Z}_2^n)} |\mathbf{x}\mathbf{y}\mathbf{z}\rangle \langle \mathbf{w}\mathbf{s}\mathbf{t}|. \quad (30)$$

Now, we define five more finite series, $\mathcal{C}^{(i)} \equiv \sum_{\mathbf{x} \in \mathbb{Z}_2^n} |\mathbf{x}\mathbf{x}\mathbf{x}\rangle \langle \mathbf{x}\mathbf{x}\mathbf{x}|$, and,

$$\begin{aligned} \mathcal{C}^{(ii)} &\equiv \sum_{\mathbf{x}, \mathbf{y} \in \mathbb{Z}_2^n} (|\mathbf{y}\mathbf{x}\mathbf{x}\rangle \langle \mathbf{y}\mathbf{x}\mathbf{x}| + |\mathbf{x}\mathbf{y}\mathbf{x}\rangle \langle \mathbf{y}\mathbf{x}\mathbf{x}| + |\mathbf{x}\mathbf{x}\mathbf{y}\rangle \langle \mathbf{y}\mathbf{x}\mathbf{x}| + |\mathbf{y}\mathbf{x}\mathbf{x}\rangle \langle \mathbf{x}\mathbf{y}\mathbf{x}| + |\mathbf{x}\mathbf{y}\mathbf{x}\rangle \langle \mathbf{x}\mathbf{y}\mathbf{x}| \\ &\quad + |\mathbf{x}\mathbf{x}\mathbf{y}\rangle \langle \mathbf{x}\mathbf{y}\mathbf{x}| + |\mathbf{y}\mathbf{x}\mathbf{x}\rangle \langle \mathbf{x}\mathbf{x}\mathbf{y}| + |\mathbf{x}\mathbf{y}\mathbf{x}\rangle \langle \mathbf{x}\mathbf{x}\mathbf{y}| + |\mathbf{x}\mathbf{x}\mathbf{y}\rangle \langle \mathbf{x}\mathbf{x}\mathbf{y}|), \end{aligned} \quad (31)$$

$$\begin{aligned} \mathcal{C}^{(iii)} &\equiv \sum_{\mathbf{x}, \mathbf{y} \in \mathbb{Z}_2^n} (|\mathbf{y}\mathbf{x}\mathbf{x}\rangle \langle \mathbf{y}\mathbf{y}\mathbf{y}| + |\mathbf{x}\mathbf{y}\mathbf{x}\rangle \langle \mathbf{y}\mathbf{y}\mathbf{y}| + |\mathbf{x}\mathbf{x}\mathbf{y}\rangle \langle \mathbf{y}\mathbf{y}\mathbf{y}| + |\mathbf{y}\mathbf{y}\mathbf{y}\rangle \langle \mathbf{y}\mathbf{x}\mathbf{x}| + |\mathbf{y}\mathbf{y}\mathbf{y}\rangle \langle \mathbf{x}\mathbf{y}\mathbf{x}| \\ &\quad + |\mathbf{y}\mathbf{y}\mathbf{y}\rangle \langle \mathbf{x}\mathbf{x}\mathbf{y}|), \end{aligned} \quad (32)$$

$$\begin{aligned} \mathcal{C}^{(iv)} &\equiv \sum_{\mathbf{x}, \mathbf{y}, \mathbf{z} \in \mathbb{Z}_2^n} (|\mathbf{x}\mathbf{y}\mathbf{z}\rangle \langle \mathbf{x}\mathbf{y}\mathbf{z}| + |\mathbf{x}\mathbf{y}\mathbf{z}\rangle \langle \mathbf{z}\mathbf{x}\mathbf{y}| + |\mathbf{x}\mathbf{y}\mathbf{z}\rangle \langle \mathbf{y}\mathbf{z}\mathbf{x}| + |\mathbf{x}\mathbf{y}\mathbf{z}\rangle \langle \mathbf{y}\mathbf{x}\mathbf{z}| + |\mathbf{x}\mathbf{y}\mathbf{z}\rangle \langle \mathbf{x}\mathbf{z}\mathbf{y}| \\ &\quad + |\mathbf{x}\mathbf{y}\mathbf{z}\rangle \langle \mathbf{z}\mathbf{y}\mathbf{x}|), \end{aligned} \quad (33)$$

$$\begin{aligned} \mathcal{C}^{(v)} &\equiv \sum_{\mathbf{x}, \mathbf{y}, \mathbf{z} \in \mathbb{Z}_2^n} (|\mathbf{x}\mathbf{x}\mathbf{z}\rangle \langle \mathbf{y}\mathbf{y}\mathbf{z}| + |\mathbf{x}\mathbf{x}\mathbf{z}\rangle \langle \mathbf{y}\mathbf{z}\mathbf{y}| + |\mathbf{x}\mathbf{x}\mathbf{z}\rangle \langle \mathbf{z}\mathbf{y}\mathbf{y}| + |\mathbf{x}\mathbf{z}\mathbf{x}\rangle \langle \mathbf{y}\mathbf{y}\mathbf{z}| + |\mathbf{x}\mathbf{z}\mathbf{x}\rangle \langle \mathbf{y}\mathbf{z}\mathbf{y}| \\ &\quad + |\mathbf{x}\mathbf{z}\mathbf{x}\rangle \langle \mathbf{z}\mathbf{y}\mathbf{y}| + |\mathbf{z}\mathbf{x}\mathbf{x}\rangle \langle \mathbf{y}\mathbf{y}\mathbf{z}| + |\mathbf{z}\mathbf{x}\mathbf{x}\rangle \langle \mathbf{y}\mathbf{z}\mathbf{y}| + |\mathbf{z}\mathbf{x}\mathbf{x}\rangle \langle \mathbf{z}\mathbf{y}\mathbf{y}|). \end{aligned} \quad (34)$$

Then, the result for ESPOVMs can be rewritten as,

$$\begin{aligned} \mathbb{E}_{|\phi_{\mathbf{A}}^{\text{eq}}\rangle \sim \mathcal{D}(S_n^{\text{eq}})} |\phi_{\mathbf{A}}^{\text{eq}}\rangle \langle \phi_{\mathbf{A}}^{\text{eq}}|^{\otimes 3} &= \frac{1}{8^n} \sum_{(\mathbf{x}, \mathbf{y}, \mathbf{z}, \mathbf{w}, \mathbf{s}, \mathbf{t}) \in \mathcal{K}_2(\mathbb{Z}_2^n)} |\mathbf{x}\mathbf{y}\mathbf{z}\rangle \langle \mathbf{w}\mathbf{s}\mathbf{t}| \\ &= \frac{1}{8^n} \left\{ \mathcal{C}^i + (\mathcal{C}^{(ii)} - 9\mathcal{C}^{(i)}) + [\mathcal{C}^{(iv)} - 6\mathcal{C}^{(i)} - 2(\mathcal{C}^{(ii)} - 9\mathcal{C}^{(i)})] \right\} \\ &= \frac{1}{8^n} (4\mathcal{C}^{(i)} - \mathcal{C}^{(ii)} + \mathcal{C}^{(iv)}). \end{aligned} \quad (35)$$

Also, for RESPOVMs,

$$\begin{aligned}
& \mathbb{E}_{|\phi_{\mathbf{A}}^{\text{req}}\rangle \sim \mathcal{D}(\mathcal{S}_n^{\text{req}})} |\phi_{\mathbf{A}}^{\text{req}}\rangle \langle \phi_{\mathbf{A}}^{\text{req}}|^{\otimes 3} \\
&= \frac{1}{8^n} \sum_{(\mathbf{x}, \mathbf{y}, \mathbf{z}, \mathbf{w}, \mathbf{s}, \mathbf{t}) \in \mathcal{K}_1(\mathbb{Z}_2^n)} |\mathbf{x}\mathbf{y}\mathbf{z}\rangle \langle \mathbf{w}\mathbf{s}\mathbf{t}| \\
&= \frac{1}{8^n} \left\{ \mathcal{C}^{(i)} + (\mathcal{C}^{(ii)} - 9\mathcal{C}^{(i)}) + (\mathcal{C}^{(iii)} - 6\mathcal{C}^{(i)}) + [\mathcal{C}^{(iv)} - 6\mathcal{C}^{(i)} - 2(\mathcal{C}^{(ii)} - 9\mathcal{C}^{(i)})] \right. \\
&\quad \left. + [\mathcal{C}^{(v)} - 9\mathcal{C}^{(i)} - 3(\mathcal{C}^{(iii)} - 6\mathcal{C}^{(i)}) - (\mathcal{C}^{(ii)} - 9\mathcal{C}^{(i)})] \right\} \\
&= \frac{1}{8^n} (16\mathcal{C}^{(i)} - 2\mathcal{C}^{(ii)} - 2\mathcal{C}^{(iii)} + \mathcal{C}^{(iv)} + \mathcal{C}^{(v)}).
\end{aligned} \tag{36}$$

Upon recalling Eq. (26),

$$\mathbb{E}((\widehat{O}_{0\mathbf{A}}^{\text{eq}})^2) = 2^{3n} \text{tr} \left(\mathbb{E}_{|\phi_{\mathbf{A}}^{\text{eq}}\rangle \sim \mathcal{D}(\mathcal{S}_n^{\text{eq}})} |\phi_{\mathbf{A}}^{\text{eq}}\rangle \langle \phi_{\mathbf{A}}^{\text{eq}}|^{\otimes 3} (\rho \otimes O_0 \otimes O_0) \right). \tag{38}$$

For ESPOVMs, by Eq. (35), we can rewrite this as

$$\mathbb{E}((\widehat{O}_{0\mathbf{A}}^{\text{eq}})^2) = \text{tr} \left((4\mathcal{C}^{(i)} - \mathcal{C}^{(ii)} + \mathcal{C}^{(iv)}) (\rho \otimes O_0 \otimes O_0) \right). \tag{39}$$

Similarly, we can show that from Eqs. (26) and (36),

$$\mathbb{E}((\widehat{O}_{0\mathbf{A}}^{\text{req}})^2) = \frac{1}{4} \text{tr} \left((16\mathcal{C}^{(i)} - 2\mathcal{C}^{(ii)} - 2\mathcal{C}^{(iii)} + \mathcal{C}^{(iv)} + \mathcal{C}^{(v)}) (\rho \otimes O_0 \otimes O_0) \right). \tag{40}$$

We are now ready to provide an upper bound for $\mathbb{E}((\widehat{O}_{0\mathbf{A}}^{\text{req}})^2)$ by utilizing

Lemma 4. [42] *Given the above definitions, for arbitrary state ρ and hermitian operator O_0 ,*

$$\left| \text{tr} \left(\mathcal{C}^{(i)} (\rho \otimes O_0 \otimes O_0) \right) \right| \leq \text{tr} \left(O_0^2 \right), \tag{41}$$

$$\left| \text{tr} \left(\mathcal{C}^{(ii)} (\rho \otimes O_0 \otimes O_0) \right) \right| \leq 7 \text{tr} \left(O_0^2 \right), \tag{42}$$

$$\left| \text{tr} \left(\mathcal{C}^{(iii)} (\rho \otimes O_0 \otimes O_0) \right) \right| \leq 6 \text{tr} \left(O_0^2 \right), \tag{43}$$

$$\left| \text{tr} \left(\mathcal{C}^{(iv)} (\rho \otimes O_0 \otimes O_0) \right) \right| \leq 3 \text{tr} \left(O_0^2 \right), \tag{44}$$

$$\left| \text{tr} \left(\mathcal{C}^{(v)} (\rho \otimes O_0 \otimes O_0) \right) \right| \leq 7 \text{tr} \left(O_0^2 \right), \tag{45}$$

Therefore,

$$\begin{aligned}
& \mathbb{E}((\widehat{O}_{0\mathbf{A}}^{\text{eq}})^2) \\
& \leq 4 \left| \text{tr} \left(\mathcal{C}^{(i)} (\rho \otimes O_0 \otimes O_0) \right) \right| + \left| \text{tr} \left(\mathcal{C}^{(ii)} (\rho \otimes O_0 \otimes O_0) \right) \right| + \left| \text{tr} \left(\mathcal{C}^{(iv)} (\rho \otimes O_0 \otimes O_0) \right) \right| \\
& \leq 14 \text{tr} \left(O_0^2 \right).
\end{aligned} \tag{46}$$

Similarly, we can show that $E_{\rho}((\widehat{O}_{0\mathbf{A}}^{\text{req}})^2) \leq 13 \text{tr} \left(O_0^2 \right)$.

Furthermore, for $\mathbb{E}((\widehat{O}_{0\mathbf{A}}^{\text{bin}})^2)$,

$$\begin{aligned}
\mathbb{E}((\widehat{O}_{0\mathbf{A}}^{\text{bin}})^2) &= \sum_{\mathbf{x} \in \mathbb{Z}_2^n} \langle \mathbf{x} | \rho | \mathbf{x} \rangle \langle \mathbf{x} | O_0 | \mathbf{x} \rangle \langle \mathbf{x} | O_0 | \mathbf{x} \rangle \leq \sum_{\mathbf{x}, \mathbf{y} \in \mathbb{Z}_2^n} \langle \mathbf{x} | \rho | \mathbf{x} \rangle \langle \mathbf{x} | O_0 | \mathbf{y} \rangle \langle \mathbf{y} | O_0 | \mathbf{x} \rangle \\
&\leq \text{tr} \left(O_0^2 \right).
\end{aligned} \tag{47}$$

With this, and the arguments leading to Eq. (24) and Eq. (21), Thm. 2 (i) is proven. The upper bound of the sampling-copy number, that is $\frac{(68 \times 2) \text{Var}_{\rho}^{(r)\text{eq}}(\widehat{O}_{0\mathbf{A},j})}{\varepsilon^2} \log\left(\frac{2M}{\delta}\right)$ for M observables, follows from the statistical benefits of using the median-of-means estimation method [10, 45–47].

Suppose that the single observable O of interest is a quantum state σ . Then $\text{tr}(O_0^2) = \text{tr}\left(\left(\sigma - \frac{I}{2^n}\right)^2\right) = \text{tr}(\sigma^2) - \frac{\text{tr}(\sigma)}{2^{n-1}} + \frac{1}{2^n} \leq \text{tr}(\sigma^2) \leq 1$. Hence, *any quantum-state observable σ possesses a constant estimation variance and demonstrates shadow-tomographic advantage with (R)ESPOVM, provided that the trace inner-product between σ and equatorial stabilizer state is computable efficiently.*

The proofs of Thm. 2 (ii) and (iii) only need an average of estimation variance over uniformly chosen input and target state. The result is shown below.

Lemma 5. (i) *If $2^n \gg 1$, the averaged value $\overline{\text{Var}^{(r)\text{eq}}(\hat{\sigma})}^{\rho,\sigma}$ over uniformly-distributed complex pure states ρ and real pure states σ approaches 1 for eq and $\frac{1}{2}$ for req. In randomized-Clifford tomography, this average variance approaches 1.*

(ii) *If $2^n \gg 1$, the averaged value $\overline{\text{Var}^{\text{eq}}(\hat{\sigma})}^{\rho,\sigma}$ over uniformly-distributed complex pure states ρ and σ approaches 1. In randomized-Clifford tomography, this average variance approaches 1.*

Assisted by previous arguments, the proof of the above lemma naturally leads to Thm. 2 (ii) and (iii). However, it contains more technical elements that are more suitably located in the Appendix.

Furthermore, we can see that the average estimation variance of RESPOVM is exactly half of one of ESPOVM and even one of randomized Clifford tomography. Even though RESPOVM requires two copies of input states for a single sampling trial, the total number of gates used with the same number of sampling copies is, on average, half of what is required in randomized-Clifford shadow tomography.

We shall next consider the scenario in which O is a Hamiltonian. Let A , B and C be subsets of $\mathbb{Z}_2^n \setminus \{\mathbf{0}\}$, each of $\text{poly}(n)$ size. We restrict the form of the Hamiltonian to $O = \sum_{\mathbf{p} \in A} J_{\mathbf{p}} Z^{\mathbf{p}} + \sum_{\mathbf{q} \in B} J'_{\mathbf{q}} X^{\mathbf{q}} + \sum_{\mathbf{k} \in C} J''_{\mathbf{k}} Y^{\mathbf{k}}$ in terms of the Pauli operators $P = X$, Y and Z , where $P^{\mathbf{k}}$ for $\mathbf{k} \in \mathbb{Z}_2^n$ means $\otimes_{i=1}^n P^{k_i}$, and $J_{\mathbf{p}}$, $J'_{\mathbf{q}}$, and $J''_{\mathbf{k}}$ are real-valued functions. Such a *Heisenberg model* is a sufficiently representative model for explaining popular strongly-correlated systems in statistical mechanics [36, 37]. First, observe that the expectation value of the first term, $\sum_{\mathbf{p} \in A} J_{\mathbf{p}} Z^{\mathbf{p}}$, can be rewritten as

$$\begin{aligned} \text{tr}\left(\rho \sum_{\mathbf{p} \in A} J_{\mathbf{p}} Z^{\mathbf{p}}\right) &= \sum_{\substack{\mathbf{p} \in A \\ \mathbf{x}, \mathbf{y} \in \mathbb{Z}_2^n}} J_{\mathbf{p}} \langle \mathbf{x} | \rho | \mathbf{y} \rangle \langle \mathbf{y} | Z^{\mathbf{p}} | \mathbf{x} \rangle = \sum_{\substack{\mathbf{p} \in A \\ \mathbf{x}, \mathbf{y} \in \mathbb{Z}_2^n}} J_{\mathbf{p}} \langle \mathbf{x} | \rho | \mathbf{y} \rangle (-1)^{\mathbf{p} \cdot \mathbf{x}} \delta_{\mathbf{x}, \mathbf{y}} \\ &= \sum_{\substack{\mathbf{p} \in A \\ \mathbf{x} \in \mathbb{Z}_2^n}} \langle \mathbf{x} | \rho | \mathbf{x} \rangle (-1)^{\mathbf{p} \cdot \mathbf{x}} J_{\mathbf{p}}. \end{aligned} \quad (48)$$

From the above result, the corresponding estimation algorithm is straightforward. We first measure the input ρ with the Z basis, obtain the binary outcome $\mathbf{x} \in \mathbb{Z}_2^n$, and then take the estimator to be $\sum_{\mathbf{p} \in A} (-1)^{\mathbf{p} \cdot \mathbf{x}} J_{\mathbf{p}}$. Since A has $\text{poly}(n)$ size, we can calculate this efficiently. Moreover, we easily note that the *estimation variance* of this estimator is bounded by $\text{poly}(n)$, hence by the Hoeffding inequality, it only takes $N = \mathcal{O}(\text{poly}(n)/\varepsilon^2)$ sampling copies within ε additive precision. The other terms, $\sum_{\mathbf{q} \in B} J'_{\mathbf{q}} X^{\mathbf{q}}$ and $\sum_{\mathbf{k} \in C} J''_{\mathbf{k}} Y^{\mathbf{k}}$, can be estimated in a similar manner but with an additional rotation of the input with $H^{\otimes n}$

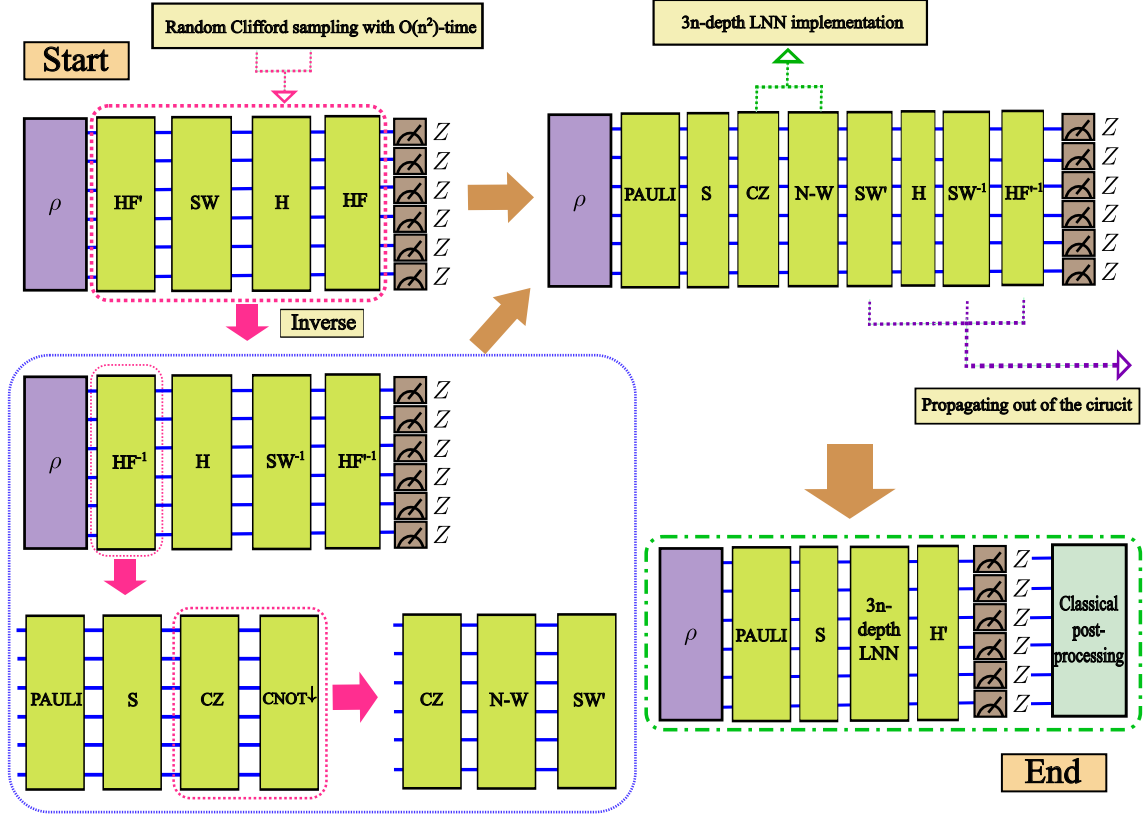


Figure 7: The schematic diagram of uniform sampling of a $3n$ -depth Clifford-circuit measurement in the LNN-architecture. Here, the N-W section is a CNOT circuit expressing the $n \times n$ north-western matrix [19] for the binary strings. The final classical post-processing step multiplies an $n \times n$ binary matrix to the measured outcome bit string, which takes $\mathcal{O}(n^2)$ -time.

or $S^{\dagger \otimes n}$ gates before the binary measurement. Even when the Hamiltonian has a general form, $O = \sum_{P \in \mathcal{P}} \alpha(P)P$, where \mathcal{P} is a poly-sized subset of the n -qubit Pauli group and α is a real-valued function, we can assert that similar scale of the sampling-copy number is needed, by rotating via single qubit gates for each Pauli term. With this, we may now conclude that our tomography methods serve as efficient hybrid-circuit platforms for both fidelity estimation and Heisenberg-type Hamiltonian estimation, in the sense that one may flexibly turn the (R)ESPOVM section on or off and employ suitable single-qubit Clifford gates before the binary-measurement section depending on the observable types measured. Therefore, this opens an avenue for more applications of our scheme in variational quantum algorithms (VQA) [65, 66].

5.3 Gate, depth, and time complexity for circuit implementation

We now discuss the architectural requirements of (R)ESPOVM shadow tomography, which cover the main ideas of the proof for Thm. 3. In particular, this discussion focuses on the implementation of an (LNN) architecture for (R)ESPOVM tomography and compares its circuit-depth and time-complexity resources with those of randomized-Clifford shadow tomography.

We recall [20] that we can efficiently and uniformly sample a Clifford unitary U from Cl_n in $\mathcal{O}(n^2)$ -time. In addition, the sampled form contains the $\text{HF}'\text{—SW—H—HF}$ sections. Each small upper case letters are explained in the Sec. 2.2. Here, we can further reduce

the depth of circuit lower than previously known results [43, 19]. We note that the $\text{HF}'\text{---SW}$ sections are not needed for randomized-Clifford shadow tomography. The reason is that the measurement outcome of a uniform-Clifford measurement can be obtained from the following procedure: One first uniformly samples a Clifford unitary operator in the above form and takes its inverse, which possesses the form $\text{HF}^{-1}\text{---H}\text{---SW}^{-1}\text{---HF}'^{-1}$. Then one just measures in the Z basis after the $\text{HF}^{-1}\text{---H}$ sections and linearly transform this intermediate bit-string outcome with the subsequent CNOT and Pauli transformations in $\text{SW}^{-1}\text{---HF}'^{-1}$ to arrive at the final bitstring outcome. In $\mathcal{O}(n^3)$ -time, one can optimize the maximal depth of $\text{HF}^{-1}\text{---H}$ sections with long-range gates to $n + \mathcal{O}(\log(n))$ if $n \geq 70$ [43]. Even though the corresponding asymptotic gate-count upper bound is $\mathcal{O}(\frac{n}{\log(n)})$ [67, 68], it has a large constant factor [43] and hence will not improve the former limit for circuits holding hundreds of qubits. If only NN gates are available, we can express the CNOT gate layers inside the HF -section in terms of a northwestern matrix [69] and SWAP gates. Here, we do not need to implement the swapping operations, since one can simply propagate all swapping operations out of the circuit. The CNOT circuit of a northwestern-matrix form after the CZ circuits can be further decomposed into $3n$ -depth NN CNOT circuits and phase-gate insertion layers [19, 69] in $\mathcal{O}(n^3)$ -time. A schematic illustration is presented in Fig. 7.

Having discussed uniform Clifford sampling, starting from random CZ-gate implementation, we shall now discuss how one can further contract the gate count for (R)ESPOVM shadow tomography. For this purpose, we make use of the Patel-Markov-Hayes (PMH) construction [55]. First, we transform Y measurements as X -basis measurements after phase gates and drag all S , S^\dagger and Z gates to the left of all the CZ gates, i.e very first of the circuit. This is possible because these gates commute with CZ gates. Next, we may decompose the CZ circuit into $\text{CNOT}\text{---CZ}\text{---CNOT}$ [42], where CZ contains only $\mathcal{O}(n)$ CZ gates. After which, we implement the left CNOT section with $\mathcal{O}(\frac{n^2}{\log(n)})$ CNOT gates [31, 55]. The right CNOT section can be ignored because we now only measure in the X basis, and so this amounts to only a linear transformation of the measurement outcome. If we return to the randomized-Clifford scheme discussed previously, one may also reduce the gate count if some CNOT gates are simplified to just linear transformations of the measured outcome. For instance, if we acted the $\text{CNOT}_{1\rightarrow 2}$ gate on first and second qubit and took X -basis measurements to both qubits and then obtained the outcome $|+-\rangle$, it is equivalent to measure in X -basis without CNOT gate and obtain the outcome $|--\rangle$. In Fig. 4(b), we applied both reductions and saw that there is still gate count improvement with (R)ESPOVM.

As we saw in Thm. 1, there is an alternative depth reduction technique for CZ circuits. (R)ESPOVM shadow tomography can be implemented with at most n -depth long-ranged CZ gates (or with CNOT and H gates). This maximal depth can be reduced to $\frac{n}{2} + \mathcal{O}(\log(n))$ given that $n \geq 39$ according to Ref. [43], which is half the gate complexity in contrast to randomized-Clifford implementation. Furthermore, with only neighboring CNOT gates and S gates, we can implement (R)ESPOVM with $2n$ -depth LNN architecture in $\mathcal{O}(n^2)$ -time. To show this time-complexity bound, we may use the strategy employed in Ref. [1]. We first construct a $2n$ -depth circuit consisting of NN CNOT gates in advance following the designated rules dictated by Thm. 6 in [1]. With this, the main task for the time-complexity-bound proof is as follows: Given a CZ circuit that performs the map $|\mathbf{x}\rangle \mapsto (-1)^{Q(\mathbf{x})} |\mathbf{x}\rangle$, where $\mathbf{x} \in \mathbb{Z}_2^n$ and Q is a quadratic binary-valued polynomial, find the values $u_j, u_{j,k}$ in \mathbb{Z}_4 ($j \in [n], k \in \{j+1, j+2, \dots, n\}$) such that

$$(-1)^{Q(\mathbf{x})} = i^{\sum_{j=1}^n u_j y_j + \sum_{j=1}^n \sum_{k=j+1}^n u_{j,k} (y_j \oplus y_k)}. \quad (49)$$

Here, \oplus and $+$ respectively refer to modulo-2 and modulo-4 additions. The y_i 's ($i \in [n]$)

are defined by,

$$y_i = x_1 \oplus x_2 \oplus x_3 \oplus \cdots \oplus x_i. \quad (50)$$

After inserting the phase gates $S^{u_{j,k}}$ and S^{u_l} following the manual in Ref. [1], we finally realize the LNN architecture of CZ circuit. To analyze the time-complexity, we rewrite Eq. (50) as

$$\begin{cases} x_1 = y_1 \\ x_i = y_i \oplus y_{i-1} \quad (i \in \{2, 3, \dots, n\}). \end{cases} \quad (51)$$

Now, consider one off-diagonal component of $(-1)^{Q(x)}$. We have simple identity $(-1)^{x_\mu x_\nu} = i^{3x_\mu + 3x_\nu + (x_\mu \oplus x_\nu)}$. Then by Eq. (51),

$$(-1)^{x_\mu x_\nu} = i^{3(y_\mu \oplus y_{\mu-1}) + 3(y_\nu \oplus y_{\nu-1}) + (y_\mu \oplus y_{\mu-1} \oplus y_\nu \oplus y_{\nu-1})}, \quad y_0 \equiv 0. \quad (52)$$

Using the equality $i^{a \oplus b \oplus c} = i^{3a + 3b + 3c + 3(a \oplus b) + 3(a \oplus c) + 3(b \oplus c)}$ ($a, b, c \in \mathbb{Z}_2$) and setting $a = y_\mu, b = y_{\mu-1}, c = y_\nu \oplus y_{\nu-1}$, we can express $i^{y_\mu \oplus y_{\mu-1} \oplus y_\nu \oplus y_{\nu-1}}$ as a product of $i^{y_\mu}, i^{y_{\mu-1}}, i^{y_\nu \oplus y_{\nu-1}}$ and $i^{y_\mu \oplus y_{\mu-1}}, i^{y_\mu \oplus y_\nu \oplus y_{\nu-1}}, i^{y_{\mu-1} \oplus y_\nu \oplus y_{\nu-1}}$. Again, in a similar manner, we can decompose $i^{y_\mu \oplus y_\nu \oplus y_{\nu-1}}$ and $i^{y_{\mu-1} \oplus y_\nu \oplus y_{\nu-1}}$ into a product of powers of i , each with an exponent not exceeding 3 variables. In conclusion, there exist *constant-sized* sets $A, B \subset [n]$ such that

$$(-1)^{x_\mu x_\nu} = i^{\sum_{a \in A} u'_a y_a + \sum_{a, b \in B} u'_{a,b} (y_a \oplus y_b)}, \quad (53)$$

where $u'_\mu, u'_{\mu,\nu} \in \mathbb{Z}_4$. Therefore, upon noting that a CZ circuit has at most $\frac{n^2-n}{2}$ CZ gates, we have the following scheme for implementing *any* (long-ranged) CZ circuit in an LNN architecture:

1. Prepare a $2n$ -depth NN CNOT circuit based on the prescriptions in Ref. [1].
2. For each unitary $CZ_{j,k}$ acting on the j -th and k -th qubits, find the sets $A_{j,k}$ and $B_{j,k}$ such that $(-1)^{x_a x_b} = i^{\sum_{a \in A_{j,k}} u'_a y_a + \sum_{a, b \in B_{j,k}} u'_{a,b} (y_a \oplus y_b)}$. Record all u'_a and $u'_{a,b}$ corresponding to $A_{j,k}$ and $B_{j,k}$.
3. Insert the phase gates $S^{u'_a}$ ($a \in A_{j,k}$) and $S^{u'_{a,b}}$ ($a, b \in B_{j,k}$) according to the insertion rules in Ref. [1].
4. Repeat steps 2 and 3 for all $j, k \in [n]$. If there is already some phase gate acting on the location, we multiply the existing one and the gate we put this time.

The Reader may consult Ref. [42] for the precise NN CNOT-circuit prescription and phase-gate insertion rule. For each $j, k \in [n]$, we note that steps 2 to 4 each takes constant time to execute. Since there is a total of $\mathcal{O}(n^2)$ steps to be repeated, the total time-complexity is $\mathcal{O}(n^2)$.

5.4 Average gate fidelity

Suppose a circuit described by a unitary operator U is subjected to noise. The resulting operation is a noisy quantum channel \mathcal{U} . One can then measure the averaged quality of this noisy channel with respect to U over a uniform distribution of pure states, namely with the *average gate fidelity* defined as [62]

$$F_{avg}(\mathcal{U}) \equiv \int (d\phi) \langle \phi | U^\dagger \mathcal{U}(|\phi\rangle \langle \phi|) U | \phi \rangle. \quad (54)$$

Here, the integration element $(d\phi)$ is the Haar measure. This function can be generalized to a circuit unitary ensemble G where each circuit with operation U has the probability measure (dU) to be sampled,

$$F_{avg}(G) \equiv \int_{U \in G} (dU) F_{avg}(\mathcal{U}) = \int (d\phi) \int_{U \in G} (dU) \langle \phi | U^\dagger \mathcal{U}(|\phi\rangle \langle \phi|) U | \phi \rangle. \quad (55)$$

Terminology-wise, we shall also call this the average gate fidelity of G . If noise is absent, then $F_{avg}(G) = 1$, as it should.

Now, we list our procedure to give a noise to each gates in the (R)ESPOVM circuit, hence explaining the set up of Fig. 5.

First, we consider when we endow each gate with depolarization noise. This is equivalent to enacting a Pauli operation that is uniformly chosen from the single-qubit (or two-qubit resp.) Pauli group to each single-qubit (two-qubit) gate of a given error rate. Therefore, we can estimate the average gate fidelity $F_{avg}(G)$ with the depolarization error rates (η_1, η_2) according to the following Monte Carlo procedure for an n -qubit system:

1. Set the sufficiently large $M, N \in \mathbb{N}$. The M is the number of the Haar random input pure states and N is that of randomly chosen circuit samples for each state input.
2. Choose a quantum state $|\phi\rangle$ according to the Haar measure: generate a 2^n -dimensional complex column with all entries i.i.d. standard Gaussian distribution and normalize it by its norm.
3. Randomly choose $U \in G$ according to the distribution measure dU (in Fig. 5, we take dU to be uniform and discrete).
4. For each single-qubit (two-qubit resp.) gate in U , we toss a coin with the biased rate $(1 - \eta_1, \eta_1)$ $[(1 - \eta_2, \eta_2)]$. If a ‘‘tail’’ is obtained, one uniformly chooses a Pauli operator from the single-qubit (two-qubit) Pauli group and enact it after the gate. Doing this for all gates in U , one gets the new circuit unitary U' .
5. Calculate $f_{U,\phi} \equiv \langle \phi | U^\dagger U' | \phi \rangle \langle \phi | U'^\dagger U | \phi \rangle = \left| \langle \phi | U^\dagger U' | \phi \rangle \right|^2$.
6. Repeat steps 3 to 5 with the same input state $|\phi\rangle$ to obtain such $f_{U_1,\phi}, f_{U_2,\phi}, \dots, f_{U_N,\phi}$. Define $g_{\phi,N} = \frac{1}{N} \sum_{j=1}^N f_{U_j,\phi}$.

Repeat step 6 with M Haar-distributed input pure states $|\phi_1\rangle, \dots, |\phi_M\rangle$ and obtain $g_{\phi_1,N}, \dots, g_{\phi_M,N}$. Then $\frac{1}{M} \sum_{j=1}^M g_{\phi_j,N} \rightarrow F_{avg}(G)$ in the limit of large M and N .

For the Z (ZZ resp.)-noise case to each single (two)-qubit gate, in step 4, we enact Z (ZZ) after the each gate in U with probability η_1 (η_2).

Step 5 is not an efficient method for large n . However, even then, we can estimate the fidelity by uniformly sampling $|\phi\rangle$ from the stabilizer set \mathcal{S}_n . To be specific, we note that the noisy operation \mathcal{U} derived from a given unitary $U \in G$ on $|\phi\rangle \langle \phi|$ can be rewritten as

$$\mathcal{U}(|\phi\rangle \langle \phi|) = \sum_{K_U \in \mathcal{K}_U} K_U |\phi\rangle \langle \phi| K_U^\dagger, \quad (56)$$

where \mathcal{K} is a set of Kraus operators contributing \mathcal{U} . Then, Eq. (55) is,

$$\begin{aligned}
F_{\text{avg}}(G) &\equiv \int_{U \in G} (dU) \sum_{K_U \in \mathcal{K}_U} \int (d\phi) \langle \phi | U^\dagger K_U | \phi \rangle \langle \phi | K_U^\dagger U | \phi \rangle \\
&= \int_{U \in G} (dU) \sum_{K_U \in \mathcal{K}_U} \text{tr} \left(\int (d\phi) | \phi \rangle \langle \phi |^{\otimes 2} U^\dagger K_U \otimes K_U^\dagger U \right) \\
&= \int_{U \in G} (dU) \sum_{K_U \in \mathcal{K}_U} \text{tr} \left(\frac{1}{|\mathcal{S}_n|} \sum_{|\phi\rangle \in \mathcal{S}_n} | \phi \rangle \langle \phi |^{\otimes 2} U^\dagger K_U \otimes K_U^\dagger U \right) \\
&= \int_{U \in G} (dU) \sum_{K_U \in \mathcal{K}_U} \frac{1}{|\mathcal{S}_n|} \sum_{|\phi\rangle \in \mathcal{S}_n} \langle \phi | U^\dagger K_U | \phi \rangle \langle \phi | K_U^\dagger U | \phi \rangle \\
&= \frac{1}{|\mathcal{S}_n|} \sum_{|\phi\rangle \in \mathcal{S}_n} \int_{U \in G} (dU) \langle \phi | U^\dagger \mathcal{U}(|\phi\rangle \langle \phi|) U | \phi \rangle .
\end{aligned} \tag{57}$$

The third equation is derived by the fact that the set of pure stabilizer states are complex projective 3-design [16]. Therefore, in step 5 of the above procedure, we can uniformly sample $|\phi\rangle$ from \mathcal{S}_n and $f_{U,\phi}$ is then efficiently calculated [31] given that U and U' are Clifford operations.

5.5 Survey of recent CZ-gate implementation schemes

We shall list all recent fidelity values sorted according to some of these platforms. In photonic quantum computing, a fidelity of over 81% has been reported on silicon-nitride photonic chips [70], and over 99% when Zeeman coupling with quantum dots and nitrogen-vacancy centers is exploited in simulations [71]. Spin-based quantum computation allows for more than 99.5% fidelity [60, 72]. On Rydberg-interacting platforms, Ref. [73], [74] and later [59] respectively reported gate fidelities of 89%, 97% and 99.5% using atomic-qubit-array entanglement. Using adiabatic pulses, simulations revealed fidelity values greater than 99.9% [75]. On superconducting platforms, adiabaticity-shortcut techniques allows for over 96% fidelity [76], 97.6% with fluxonium qubits [77] and 99.1% through interfering superconducting qubits with weak anharmonicity [78]. Nonadiabatic CZ gates were also realized with 99.54% fidelity [79]. Furthermore, gmon qubits employed by Google AI Quantum demonstrated gate fidelities as high as 99.81% [80]. The more recent fidelity of 99.93% is possible with intermediate leakage control [61].

6 Acknowledgements

This work was supported by the National Research Foundation of Korea (NRF) grants funded by the Korean government (Grant Nos. NRF-2023R1A2C1006115, NRF-2022M3K4 A1097117, NRF2022M3E4A1076099 and RS-2023-00237959) via the Institute of Applied Physics at Seoul National University, the Institute of Information & Communications Technology Planning & Evaluation (IITP) grant funded by the Korea government (MSIT) (IITP-2021-0-01059 and IITP-2023-2020-0-01606), and the Brain Korea 21 FOUR Project grant funded by the Korean Ministry of Education.

References

- [1] Dmitri Maslov and Martin Roetteler. “Shorter stabilizer circuits via Bruhat decomposition and quantum circuit transformations”. *IEEE Transactions on Information Theory* **64**, 4729–4738 (2018).
- [2] Peter W. Shor. “Polynomial-Time Algorithms for Prime Factorization and Discrete Logarithms on a Quantum Computer”. *SIAM J. Comput* **26**, 1484–1509 (1997).
- [3] David Deutsch and Richard Jozsa. “Rapid solution of problems by quantum computation”. *Proc. R. Soc. Lond. A: Math. Phys. Sci.* **439**, 553–558 (1992).
- [4] M. Roetteler D. Gavinsky and J. Roland. “Quantum algorithm for the Boolean hidden shift problem” (2011).
- [5] G Mauro D’Ariano, Martina De Laurentis, Matteo GA Paris, Alberto Porzio, and Salvatore Solimeno. “Quantum tomography as a tool for the characterization of optical devices”. *J. opt., B Quantum semiclass. opt.* **4**, S127 (2002).
- [6] M. G. A. Paris and J. Řeháček, editors. “Quantum State Estimation”. Volume 649 of *Lect. Not. Phys.* Springer. Berlin (2004). url: www.biblio.com/book/quantum-state-estimation-lecture-notes-physics/d/1533004714.
- [7] Ryan O’Donnell and John Wright. “Efficient quantum tomography”. In *Proc. Annu. ACM Symp. Theory Comput.* Pages 899–912. (2016).
- [8] Erik Nielsen, John King Gamble, Kenneth Rudinger, Travis Scholten, Kevin Young, and Robin Blume-Kohout. “Gate set tomography”. *Quantum* **5**, 557 (2021).
- [9] Scott Aaronson. “Shadow tomography of quantum states”. In *Proc. Annu. ACM Symp. Theory Comput.* Pages 325–338. (2018).
- [10] Hsin-Yuan Huang, Richard Kueng, and John Preskill. “Predicting many properties of a quantum system from very few measurements”. *Nat. Phys* **16**, 1050–1057 (2020).
- [11] Atithi Acharya, Siddhartha Saha, and Anirvan M Sengupta. “Shadow tomography based on informationally complete positive operator-valued measure”. *Phys. Rev. A* **104**, 052418 (2021).
- [12] Hsin-Yuan Huang, Sitan Chen, and John Preskill. “Learning to predict arbitrary quantum processes” (2023).
- [13] Lorenzo Leone, Salvatore FE Oliviero, and Alioscia Hamma. “Stabilizer Rényi entropy”. *Phys. Rev. Lett.* **128**, 050402 (2022).
- [14] Salvatore FE Oliviero, Lorenzo Leone, Alioscia Hamma, and Seth Lloyd. “Measuring magic on a quantum processor”. *npj Quantum Inf.* **8**, 148 (2022).
- [15] Zak Webb. “The Clifford group forms a unitary 3-design”. *Quantum Inf. Comput.* **16**, 1379–1400 (2016).
- [16] Huangjun Zhu. “Multiqubit Clifford groups are unitary 3-designs”. *Phys. Rev. A* **96**, 062336 (2017).
- [17] Richard Kueng and David Gross. “Qubit stabilizer states are complex projective 3-designs” (2015).
- [18] Z. Puchała and J.A. Miszczyk. “Symbolic integration with respect to the Haar measure on the unitary groups”. *B POL ACAD SCI-TECH* **65**, 21–27 (2017).
- [19] Dmitri Maslov and Willers Yang. “CNOT circuits need little help to implement arbitrary Hadamard-free Clifford transformations they generate”. *npj Quantum Inf.* **9**, 96 (2023).
- [20] Sergey Bravyi and Dmitri Maslov. “Hadamard-Free Circuits Expose the Structure of the Clifford Group”. *IEEE Trans. Inf. Theory* **67**, 4546–4563 (2021).
- [21] Christian Bertoni, Jonas Haferkamp, Marcel Hinsche, Marios Ioannou, Jens Eisert,

- and Hakop Pashayan. “Shallow shadows: Expectation estimation using low-depth random Clifford circuits” (2022).
- [22] Hong-Ye Hu A. A. Akhtar and Yi-Zhuang You. “Scalable and Flexible Classical Shadow Tomography with Tensor Networks”. *Quantum* **7**, 1026 (2023).
- [23] Hong-Ye Hu, Soonwon Choi, and Yi-Zhuang You. “Classical shadow tomography with locally scrambled quantum dynamics”. *Phys. Rev. Res.* **5**, 023027 (2023).
- [24] Daniel Grier, Hakop Pashayan, and Luke Schaeffer. “Sample-optimal classical shadows for pure states” (2022).
- [25] H. Chau Nguyen, Jan Lennart Bönsel, Jonathan Steinberg, and Otfried Gühne. “Optimizing Shadow Tomography with Generalized Measurements”. *Phys. Rev. Lett.* **129**, 220502 (2022).
- [26] Sergey Bravyi and Alexei Kitaev. “Universal quantum computation with ideal Clifford gates and noisy ancillas”. *Phys. Rev. A* **71**, 022316 (2005).
- [27] Xiaowei Wang, Xiang Zhan, Yulin Li, Lei Xiao, Gaoyan Zhu, Dengke Qu, Quan Lin, Yue Yu, and Peng Xue. “Generalized Quantum Measurements on a Higher-Dimensional System via Quantum Walks”. *Phys. Rev. Lett.* **131**, 150803 (2023).
- [28] Sergey Bravyi and Jeongwan Haah. “Magic-state distillation with low overhead”. *Phys. Rev. A* **86**, 052329 (2012).
- [29] Steven T. Flammia and Yi-Kai Liu. “Direct Fidelity Estimation from Few Pauli Measurements”. *Phys. Rev. Lett.* **106**, 230501 (2011).
- [30] Marcus P. da Silva, Olivier Landon-Cardinal, and David Poulin. “Practical Characterization of Quantum Devices without Tomography”. *Phys. Rev. Lett.* **107**, 210404 (2011).
- [31] Scott Aaronson and Daniel Gottesman. “Improved simulation of stabilizer circuits”. *Phys. Rev. A* **70**, 052328 (2004).
- [32] Sergey Bravyi and David Gosset. “Improved classical simulation of quantum circuits dominated by Clifford gates”. *Phys. Rev. Lett.* **116**, 250501 (2016).
- [33] Sergey Bravyi, Dan Browne, Padraic Calpin, Earl Campbell, David Gosset, and Mark Howard. “Simulation of quantum circuits by low-rank stabilizer decompositions”. *Quantum* **3**, 181 (2019).
- [34] Qingyue Zhang, Qing Liu, and You Zhou. “Minimal Clifford Shadow Estimation by Mutually Unbiased Bases” (2023).
- [35] THOMAS DURT, BERTHOLD-GEORG ENGLERT, INGEMAR BENGTTSSON, and KAROL ŻYCZKOWSKI. “On mutually unbiased bases”. *International Journal of Quantum Information* **08**, 535–640 (2010).
- [36] Minoru Takahashi and Masuo Suzuki. “One-dimensional anisotropic Heisenberg model at finite temperatures”. *Prog. Theor. Phys* **48**, 2187–2209 (1972).
- [37] B. Bertini, F. Heidrich-Meisner, C. Karrasch, T. Prosen, R. Steinigeweg, and M. Žnidarič. “Finite-temperature transport in one-dimensional quantum lattice models”. *Rev. Mod. Phys.* **93**, 025003 (2021).
- [38] Daniel M. Greenberger, Michael A. Horne, and Anton Zeilinger. “Going Beyond Bell’s Theorem” (2007).
- [39] W. Dür, G. Vidal, and J. I. Cirac. “Three qubits can be entangled in two inequivalent ways”. *Phys. Rev. A* **62**, 062314 (2000).
- [40] Dax Enshan Koh and Sabee Grewal. “Classical Shadows With Noise”. *Quantum* **6**, 776 (2022).
- [41] Daniel Gottesman. “The Heisenberg Representation of Quantum Computers” (1998).
- [42] Y. S. Teo G. Park and H Jeong. “Appendix”. See Appendix for additional detailed explanations and proofs of this paper.

- [43] Dmitri Maslov and Ben Zindorf. “Depth Optimization of CZ, CNOT, and Clifford Circuits”. *IEEE Trans. Quantum Eng.* **3**, 1–8 (2022).
- [44] Andrew J Scott. “Tight informationally complete quantum measurements”. *J. Phys. A Math. Theor.* **39**, 13507 (2006).
- [45] Matthieu Lerasle. “Lecture Notes: Selected topics on robust statistical learning theory” (2019).
- [46] Charles Blair. “Problem complexity and method efficiency in optimization (a. s. nemirovsky and d. b. yudin)”. *SIAM Rev.* **27**, 264–265 (1985).
- [47] Mark R. Jerrum, Leslie G. Valiant, and Vijay V. Vazirani. “Random generation of combinatorial structures from a uniform distribution”. *Theor. Comput. Sci.* **43**, 169–188 (1986).
- [48] Hans J. Briegel and Robert Raussendorf. “Persistent Entanglement in Arrays of Interacting Particles”. *Phys. Rev. Lett.* **86**, 910–913 (2001).
- [49] Simon Anders and Hans J. Briegel. “Fast simulation of stabilizer circuits using a graph-state representation”. *Phys. Rev. A* **73**, 022334 (2006).
- [50] Andreas Bärttschi and Stephan Eidenbenz. “Deterministic Preparation of Dicke States”. *Pages 126–139*. Springer International Publishing. Denmark (2019).
- [51] Claude Berge and Jean Claude Fournier. “A short proof for a generalization of Vizing’s theorem”. *J. Graph Theory* **15**, 333–336 (1991).
- [52] Jayadev Misra and David Gries. “A constructive proof of Vizing’s theorem”. *Inf. Process. Lett* **41**, 131–133 (1992).
- [53] Dmitri Maslov and Martin Roetteler. “Shorter Stabilizer Circuits via Bruhat Decomposition and Quantum Circuit Transformations”. *IEEE Trans. Inf. Theory* **64**, 4729–4738 (2018).
- [54] Sergey Bravyi, Joseph A Latone, and Dmitri Maslov. “6-qubit optimal Clifford circuits”. *npj Quantum. Inf.* **8**, 79 (2022).
- [55] Ketan N Patel, Igor L Markov, and John P Hayes. “Optimal synthesis of linear reversible circuits.” (2008).
- [56] Kento Tsubouchi, Takahiro Sagawa, and Nobuyuki Yoshioka. “Universal cost bound of quantum error mitigation based on quantum estimation theory” (2023).
- [57] E. O’Neill-Judy R. Larose, A. Tikku. “6-qubit optimal Clifford circuits”. *npj Quantum. Inf.* **5**, 57 (2019).
- [58] Richard Cleve, Debbie Leung, Li Liu, and Chunhao Wang. “Near-linear constructions of exact unitary 2-designs” (2016).
- [59] Simon J. Evered, Dolev Bluvstein, Marcin Kalinowski, Sepehr Ebadi, Tom Manovitz, Hengyun Zhou, Sophie H. Li, Alexandra A. Geim, Tout T. Wang, Nishad Maskara, Harry Levine, Giulia Semeghini, Markus Greiner, Vladan Vuletić, and Mikhail D. Lukin. “High-fidelity parallel entangling gates on a neutral-atom quantum computer”. *Nature* **622**, 268–272 (2023).
- [60] Xiao Xue, Maximilian Russ, Nodar Samkharadze, Brennan Undseth, Amir Sammak, Giordano Scappucci, and Lieven M. K. Vandersypen. “Quantum logic with spin qubits crossing the surface code threshold”. *Nature* **601**, 343–347 (2022).
- [61] V. Negîrnea, H. Ali, N. Muthusubramanian, F. Battistel, R. Sagastizabal, M. S. Moreira, J. F. Marques, W. J. Vlothuizen, M. Beekman, C. Zachariadis, N. Haider, A. Bruno, and L. DiCarlo. “High-fidelity controlled- z gate with maximal intermediate leakage operating at the speed limit in a superconducting quantum processor”. *Phys. Rev. Lett.* **126**, 220502 (2021).
- [62] Lorenzo Leone, Salvatore F. E. Oliviero, and Alioscia Hamma. “Nonstabilizerness determining the hardness of direct fidelity estimation”. *Phys. Rev. A* **107**, 022429 (2023).

- [63] Shuai Shi, Biao Xu, Kuan Zhang, Gen-Sheng Ye, De-Sheng Xiang, Yubao Liu, Jingzhi Wang, Daiqin Su, and Lin Li. “High-fidelity photonic quantum logic gate based on near-optimal Rydberg single-photon source”. *Nat. Commun.* **13**, 4454 (2022).
- [64] Tianyu Xie, Zhiyuan Zhao, Shaoyi Xu, Xi Kong, Zhiping Yang, Mengqi Wang, Ya Wang, Fazhan Shi, and Jiangfeng Du. “99.92%-Fidelity CNOT Gates in Solids by Noise Filtering”. *Phys. Rev. Lett.* **130**, 030601 (2023).
- [65] Marco Cerezo, Andrew Arrasmith, Ryan Babbush, Simon C Benjamin, Suguru Endo, Keisuke Fujii, Jarrod R McClean, Kosuke Mitarai, Xiao Yuan, Lukasz Cincio, et al. “Variational quantum algorithms”. *Nat. Rev. Phys.* **3**, 625–644 (2021).
- [66] M Cerezo, Kunal Sharma, Andrew Arrasmith, and Patrick J Coles. “Variational quantum state eigensolver”. *npj Quantum Inf.* **8**, 113 (2022).
- [67] Timothée Goubault de Brugière, Marc Baboulin, Benoît Valiron, Simon Martiel, and Cyril Allouche. “Reducing the Depth of Linear Reversible Quantum Circuits”. *IEEE Trans. Quantum Eng.* **2**, 1–22 (2021).
- [68] Jiaqing Jiang, Xiaoming Sun, Shang-Hua Teng, Bujiao Wu, Kewen Wu, and Jialin Zhang. “Optimal space-depth trade-off of CNOT circuits in quantum logic synthesis”. In Proc. Annu. ACM-SIAM Symp. Discrete Algorithms. Pages 213–229. (2020).
- [69] Samuel A. Kutin, David Petrie Moulton, and Lawren M. Smithline. “Computation at a distance” (2007).
- [70] Jong-Moo Lee, Wook-Jae Lee, Min-Su Kim, SungWan Cho, Jung Jin Ju, Gabriele Navickaite, and Juan Fernandez. “Controlled-not operation of sin-photonic circuit using photon pairs from silicon-photonic circuit”. *Opt. Commun.* **509**, 127863 (2022).
- [71] Antonio Russo, Edwin Barnes, and Sophia E. Economou. “Photonic graph state generation from quantum dots and color centers for quantum communications”. *Phys. Rev. B* **98**, 085303 (2018).
- [72] Maximilian Rimbach-Russ, Stephan G J Philips, Xiao Xue, and Lieven M K Vandersypen. “Simple framework for systematic high-fidelity gate operations”. *Quantum Sci. Technol.* **8**, 045025 (2023).
- [73] T. M. Graham, M. Kwon, B. Grinkemeyer, Z. Marra, X. Jiang, M. T. Lichtman, Y. Sun, M. Ebert, and M. Saffman. “Rydberg-mediated entanglement in a two-dimensional neutral atom qubit array”. *Phys. Rev. Lett.* **123**, 230501 (2019).
- [74] Harry Levine, Alexander Keesling, Giulia Semeghini, Ahmed Omran, Tout T. Wang, Sepehr Ebadi, Hannes Bernien, Markus Greiner, Vladan Vuletić, Hannes Pichler, and Mikhail D. Lukin. “Parallel implementation of high-fidelity multiqubit gates with neutral atoms”. *Phys. Rev. Lett.* **123**, 170503 (2019).
- [75] M. Saffman, I. I. Beterov, A. Dalal, E. J. Pérez, and B. C. Sanders. “Symmetric rydberg controlled- z gates with adiabatic pulses”. *Phys. Rev. A* **101**, 062309 (2020).
- [76] Tenghui Wang, Zhenxing Zhang, Liang Xiang, Zhilong Jia, Peng Duan, Zhiwen Zong, Zhenhai Sun, Zhangjingzi Dong, Jianlan Wu, Yi Yin, and Guoping Guo. “Experimental realization of a fast controlled- z gate via a shortcut to adiabaticity”. *Phys. Rev. Appl.* **11**, 034030 (2018).
- [77] Ilya A. Simakov, Grigoriy S. Mazhorin, Ilya N. Moskalenko, Nikolay N. Abramov, Alexander A. Grigorev, Dmitry O. Moskalev, Anastasiya A. Pishchimova, Nikita S. Smirnov, Evgeniy V. Zikiy, Ilya A. Rodionov, and Ilya S. Besedin. “Coupler microwave-activated controlled phase gate on fluxonium qubits” (2023).
- [78] M. A. Rol, F. Battistel, F. K. Malinowski, C. C. Bultink, B. M. Tarasinski, R. Vollmer, N. Haider, N. Muthusubramanian, A. Bruno, B. M. Terhal, and L. DiCarlo. “Fast, high-fidelity conditional-phase gate exploiting leakage interference in weakly anharmonic superconducting qubits”. *Phys. Rev. Lett.* **123**, 120502 (2019).

- [79] Shaowei Li, Anthony D. Castellano, Shiyu Wang, Yulin Wu, Ming Gong, Zhiguang Yan, Hao Rong, Hui Deng, Chen Zha, Cheng Guo, Lihua Sun, Chengzhi Peng, Xiaobo Zhu, and Jian-Wei Pan. “Realisation of high-fidelity nonadiabatic cz gates with superconducting qubits”. *npj Quantum Inf.* **5**, 84 (2019).
- [80] B. Foxen, C. Neill, A. Dunsworth, P. Roushan, B. Chiaro, A. Megrant, J. Kelly, Zijun Chen, K. Satzinger, R. Barends, F. Arute, K. Arya, R. Babbush, D. Bacon, J. C. Bardin, S. Boixo, D. Buell, B. Burkett, Yu Chen, R. Collins, E. Farhi, A. Fowler, C. Gidney, M. Giustina, R. Graff, M. Harrigan, T. Huang, S. V. Isakov, E. Jeffrey, Z. Jiang, D. Kafri, K. Kechedzhi, P. Klimov, A. Korotkov, F. Kostritsa, D. Landhuis, E. Lucero, J. McClean, M. McEwen, X. Mi, M. Mohseni, J. Y. Mutus, O. Naaman, M. Neeley, M. Niu, A. Petukhov, C. Quintana, N. Rubin, D. Sank, V. Smelyanskiy, A. Vainsencher, T. C. White, Z. Yao, P. Yeh, A. Zalcman, H. Neven, and J. M. Martinis. “Demonstrating a continuous set of two-qubit gates for near-term quantum algorithms”. *Phys. Rev. Lett.* **125**, 120504 (2020).

Appendix

A Variance of sum of independent estimators

Here, we prove Eq. (21) in the main text by considering a more general case. Suppose $p(\mathbf{x})$ and $q(\mathbf{y})$ are independent probability distributions for the data bit strings \mathbf{x} and \mathbf{y} over domains A and B respectively, and that the estimators are $\hat{a}(\mathbf{x})$ and $\hat{b}(\mathbf{y})$ respectively. Now, let us define a new estimator $\hat{a}(\mathbf{x}) + \hat{b}(\mathbf{y})$. We calculate its variance, which is expressed as

$$\begin{aligned}
& \text{Var}(\hat{a}(\mathbf{x}) + \hat{b}(\mathbf{y})) \\
&= \sum_{\mathbf{x} \in A, \mathbf{y} \in B} p(\mathbf{x})q(\mathbf{y}) \left\{ \left((\hat{a}(\mathbf{x}) + \hat{b}(\mathbf{y})) - \sum_{\mathbf{x}' \in A, \mathbf{y}' \in B} \{p(\mathbf{x}')q(\mathbf{y}')(\hat{a}(\mathbf{x}') + \hat{b}(\mathbf{y}'))\} \right)^2 \right\} \\
&= \sum_{\mathbf{x} \in A, \mathbf{y} \in B} p(\mathbf{x})q(\mathbf{y}) \left[\hat{a}(\mathbf{x})^2 + \hat{b}(\mathbf{y})^2 + 2\hat{a}(\mathbf{x})\hat{b}(\mathbf{y}) \right. \\
&\quad \left. - 2(\hat{a}(\mathbf{x}) + \hat{b}(\mathbf{y})) \sum_{\mathbf{x}' \in A, \mathbf{y}' \in B} \{p(\mathbf{x}')q(\mathbf{y}')(\hat{a}(\mathbf{x}') + \hat{b}(\mathbf{y}'))\} \right] \\
&\quad + \left\{ \sum_{\mathbf{x}' \in A, \mathbf{y}' \in B} \{p(\mathbf{x}')q(\mathbf{y}')(\hat{a}(\mathbf{x}') + \hat{b}(\mathbf{y}'))\} \right\}^2 \\
&= \sum_{\mathbf{x} \in A, \mathbf{y} \in B} p(\mathbf{x})q(\mathbf{y}) \left[\hat{a}(\mathbf{x})^2 + \hat{b}(\mathbf{y})^2 + 2\hat{a}(\mathbf{x})\hat{b}(\mathbf{y}) \right. \\
&\quad \left. - 2(\hat{a}(\mathbf{x}) + \hat{b}(\mathbf{y})) \sum_{\mathbf{x}' \in A, \mathbf{y}' \in B} \{p(\mathbf{x}')q(\mathbf{y}')(\hat{a}(\mathbf{x}') + \hat{b}(\mathbf{y}'))\} \right] + \\
&\quad \left\{ \sum_{\mathbf{x} \in A, \mathbf{y} \in B} \{p(\mathbf{x})q(\mathbf{y})(\hat{a}(\mathbf{x}) + \hat{b}(\mathbf{y}))\} \right\} \left\{ \sum_{\mathbf{x}' \in A, \mathbf{y}' \in B} \{p(\mathbf{x}')q(\mathbf{y}')(\hat{a}(\mathbf{x}') + \hat{b}(\mathbf{y}'))\} \right\} \\
&= \sum_{\mathbf{x} \in A} p(\mathbf{x}) \left\{ \hat{a}(\mathbf{x})^2 - \left\{ \sum_{\mathbf{x}' \in A} p(\mathbf{x}')\hat{a}(\mathbf{x}') \right\}^2 \right\} + \sum_{\mathbf{y} \in A} q(\mathbf{y}) \left\{ \hat{b}(\mathbf{y})^2 - \left\{ \sum_{\mathbf{y}' \in A} q(\mathbf{y}')\hat{b}(\mathbf{y}') \right\}^2 \right\}, \tag{58}
\end{aligned}$$

where the last expression is the sum of variances of each independent estimator \hat{a} and \hat{b} . (R)ESPOVM and computational basis measurement are done independently and we take the estimator $\hat{O}_{\mathbf{A}, \mathbf{x}} \equiv \hat{O}_{\mathbf{A}}^{(\text{r})\text{eq}} + \hat{O}_{\mathbf{x}}^{\text{bin}} - \text{tr}(O)$. By ignoring the constant $\text{tr}(O)$ that does not contribute to the variance analysis, we easily note that Eq. (21) is just a special case of the above general argument. More explicitly, A is a (R)ESPOVM, B is the computational basis, a is $O_{\mathbf{A}}^{(\text{r})\text{eq}}$, and b is $\hat{O}_{\mathbf{x}}^{\text{bin}}$.

B Proofs of Lemmas

B.1 Proof of Lemma 1

The first and second moments of the equatorial-stabilizer set are shown in Ref. [33]. So, we only consider the RESPOVM case and adopt similar strategies for ESPOVMs. All bold-faced italicized symbols refer to columns (synonymous with ‘‘bit strings’’) and non-italicized

uppercase ones that are also bold-faced refer to matrices. Note that for $\forall \mathbf{p} \in \mathbb{Z}_2^n$,

$$\begin{aligned}
& Z^{\mathbf{p}} \mathbb{E}_{|\phi_{\mathbf{A}}^{\text{req}}\rangle \sim \mathcal{D}(\mathcal{S}_n^{\text{req}})} |\phi_{\mathbf{A}}^{\text{req}}\rangle \langle \phi_{\mathbf{A}}^{\text{req}}| Z^{\mathbf{p}} \\
&= \mathbb{E}_{|\phi_{\mathbf{A}}^{\text{req}}\rangle \sim \mathcal{D}(\mathcal{S}_n^{\text{req}})} \frac{1}{2^n} \sum_{\mathbf{x}, \mathbf{y} \in \mathbb{Z}_2^n} (-1)^{\mathbf{x}^\top \mathbf{A} \mathbf{x} + \mathbf{y}^\top \mathbf{A} \mathbf{y} + \mathbf{p} \cdot (\mathbf{x} + \mathbf{y})} |\mathbf{x}\rangle \langle \mathbf{y}|, \\
&= \mathbb{E}_{|\phi_{\mathbf{A}}^{\text{req}}\rangle \sim \mathcal{D}(\mathcal{S}_n^{\text{req}})} \frac{1}{2^n} \sum_{\mathbf{x}, \mathbf{y} \in \mathbb{Z}_2^n} (-1)^{\mathbf{x}^\top \mathbf{A}' \mathbf{x} + \mathbf{y}^\top \mathbf{A}' \mathbf{y}} |\mathbf{x}\rangle \langle \mathbf{y}|, \\
&= \mathbb{E}_{|\phi_{\mathbf{A}}^{\text{req}}\rangle \sim \mathcal{D}(\mathcal{S}_n^{\text{req}})} |\phi_{\mathbf{A}'}\rangle \langle \phi_{\mathbf{A}'}|, \\
&= \mathbb{E}_{|\phi_{\mathbf{A}}^{\text{req}}\rangle \sim \mathcal{D}(\mathcal{S}_n^{\text{req}})} |\phi_{\mathbf{A}}\rangle \langle \phi_{\mathbf{A}}|, \tag{59}
\end{aligned}$$

where for $\forall i, j \in [n]$, $A'_{ii} = A_{ii} + p_i \pmod{2}$ otherwise $A'_{ij} = A_{ij}$. The third equality holds because the reparametrization of \mathbf{A} does not affect its uniform-distribution first moment. Thus $\mathbb{E}_{|\phi_{\mathbf{A}}^{\text{req}}\rangle \sim \mathcal{D}(\mathcal{S}_n^{\text{req}})} |\phi_{\mathbf{A}}^{\text{req}}\rangle \langle \phi_{\mathbf{A}}^{\text{req}}|$ commutes with all Pauli Z -operators and is diagonal in the computational basis. Notice that all diagonal elements are $\frac{1}{2^n}$. Therefore, $\mathbb{E}_{|\phi_{\mathbf{A}}^{\text{req}}\rangle \sim \mathcal{D}(\mathcal{S}_n^{\text{req}})} |\phi_{\mathbf{A}}\rangle \langle \phi_{\mathbf{A}}| = \frac{I}{2^n}$, which is Lem. 1 (i).

Next, note that

$$\begin{aligned}
& \mathbb{E}_{|\phi_{\mathbf{A}}^{\text{req}}\rangle \sim \mathcal{D}(\mathcal{S}_n^{\text{req}})} |\phi_{\mathbf{A}}^{\text{req}}\rangle \langle \phi_{\mathbf{A}}^{\text{req}}|^{\otimes 2} \\
&= \mathbb{E}_{|\phi_{\mathbf{A}}^{\text{req}}\rangle \sim \mathcal{D}(\mathcal{S}_n^{\text{req}})} \frac{1}{4^n} \sum_{\mathbf{x}, \mathbf{y}, \mathbf{z}, \mathbf{w} \in \mathbb{Z}_2^n} (-1)^{\mathbf{x}^\top \mathbf{A} \mathbf{x} + \mathbf{y}^\top \mathbf{A} \mathbf{y} + \mathbf{z}^\top \mathbf{A} \mathbf{z} + \mathbf{w}^\top \mathbf{A} \mathbf{w}} |\mathbf{x}\mathbf{y}\rangle \langle \mathbf{z}\mathbf{w}|, \\
&= \frac{1}{4^n} \sum_{\mathbf{x}, \mathbf{y}, \mathbf{z}, \mathbf{w} \in \mathbb{Z}_2^n} \mathbb{E}_{|\phi_{\mathbf{A}}^{\text{req}}\rangle \sim \mathcal{D}(\mathcal{S}_n^{\text{req}})} \left\{ (-1)^{\mathbf{x}^\top \mathbf{A} \mathbf{x} + \mathbf{y}^\top \mathbf{A} \mathbf{y} + \mathbf{z}^\top \mathbf{A} \mathbf{z} + \mathbf{w}^\top \mathbf{A} \mathbf{w}} \right\} |\mathbf{x}\mathbf{y}\rangle \langle \mathbf{z}\mathbf{w}|. \tag{60}
\end{aligned}$$

Now, we focus on terms in the curly brackets. Since the elements of \mathbf{A} oscillate between 0 and 1, the nonzero coefficients of $|\mathbf{x}\mathbf{y}\rangle \langle \mathbf{z}\mathbf{w}|$ must satisfy the following equations for all $p, q \in [n] (p < q)$,

$$\begin{cases} x_p + y_p + z_p = w_p, \\ x_p x_q + y_p y_q + z_p z_q + w_p w_q = 0. \end{cases} \tag{61}$$

Now, substitute the upper equation to lower one. We obtain that

$$x_p(y_q + z_q) + y_p(z_q + x_q) + z_p(x_q + y_q) = 0. \tag{62}$$

If $\mathbf{x} = \mathbf{y} = \mathbf{z}$, the above equation must hold. Suppose $\mathbf{x}, \mathbf{y}, \mathbf{z}$ are not all the same. Then there exists $p' \in [n]$ such that two of $x_{p'}, y_{p'}, z_{p'}$ are equal but the rest are not. Also, $x_i = y_i = z_i$ for $i \leq p'$. WLOG, we may assume $x_{p'} = y_{p'} \neq z_{p'}$, then for $\forall q > p'$,

$$(x_q + y_q)(x_{p'} + z_{p'}) = 0 \rightarrow x_q = y_q \because x_{p'} \neq z_{p'}. \tag{63}$$

It follows that nonzero coefficients of $|\mathbf{x}\mathbf{y}\rangle \langle \mathbf{z}\mathbf{w}|$ must be such that two of $\mathbf{x}, \mathbf{y}, \mathbf{z}$ are equal. Based on this observation, (61) implies several cases: (i) $\mathbf{x} = \mathbf{y}, \mathbf{z} = \mathbf{w}$, (ii) $\mathbf{x} = \mathbf{z}, \mathbf{y} = \mathbf{w}$, and (iii) $\mathbf{x} = \mathbf{w}, \mathbf{y} = \mathbf{z}$. In all these cases $\mathbb{E}_{|\phi_{\mathbf{A}}^{\text{req}}\rangle \sim \mathcal{D}(\mathcal{S}_n^{\text{req}})} \left\{ (-1)^{\mathbf{x}^\top \mathbf{A} \mathbf{x} + \mathbf{y}^\top \mathbf{A} \mathbf{y} + \mathbf{z}^\top \mathbf{A} \mathbf{z} + \mathbf{w}^\top \mathbf{A} \mathbf{w}} \right\} = 1$.

Hence, we obtain the following results.

$$\begin{aligned}
& \mathbb{E}_{|\phi_{\mathbf{A}}^{\text{req}}\rangle \sim \mathcal{D}(\mathcal{S}_n^{\text{req}})} |\phi_{\mathbf{A}}^{\text{req}}\rangle \langle \phi_{\mathbf{A}}^{\text{req}}|^{\otimes 2} \\
&= \frac{1}{4^n} \left(I + \sum_{\mathbf{x}, \mathbf{y} \in \mathbb{Z}_2^N} |\mathbf{x}\mathbf{y}\rangle \langle \mathbf{y}\mathbf{x}| + \sum_{\mathbf{x}\mathbf{y} \in \mathbb{Z}_2^N} |\mathbf{x}\mathbf{x}\rangle \langle \mathbf{y}\mathbf{y}| - 2 \sum_{\mathbf{x} \in \mathbb{Z}_2^N} |\mathbf{x}\mathbf{x}\rangle \langle \mathbf{x}\mathbf{x}| \right), \tag{64}
\end{aligned}$$

which is the result of Lem. 1 (iii) and completes the proof.

B.2 Proof of Lemma 2

First, we consider ESPOVMs. By Lem. 1,

$$\begin{aligned}
& \mathbb{E}_{|\phi_{\mathbf{A}}^{\text{eq}}\rangle \sim \mathcal{D}(\mathcal{S}_n^{\text{eq}})} (\langle \phi_{\mathbf{A}}^{\text{eq}} | \sigma | \phi_{\mathbf{A}}^{\text{eq}} \rangle \langle \phi_{\mathbf{A}}^{\text{eq}} | O | \phi_{\mathbf{A}}^{\text{eq}} \rangle) \\
&= \text{tr} \left\{ \left(\mathbb{E}_{|\phi_{\mathbf{A}}^{\text{eq}}\rangle \sim \mathcal{D}(\mathcal{S}_n^{\text{eq}})} |\phi_{\mathbf{A}}^{\text{eq}}\rangle \langle \phi_{\mathbf{A}}^{\text{eq}}|^{\otimes 2} \right) (\sigma \otimes O) \right\} \\
&= \frac{1}{4^n} \text{tr} \left\{ \left(I + \sum_{\mathbf{x}, \mathbf{y} \in \mathbb{Z}_2^n} |\mathbf{x}\mathbf{y}\rangle \langle \mathbf{y}\mathbf{x}| - \sum_{\mathbf{x} \in \mathbb{Z}_2^n} |\mathbf{x}\mathbf{x}\rangle \langle \mathbf{x}\mathbf{x}| \right) (\sigma \otimes O) \right\}, \\
&= \frac{1}{4^n} \left\{ \text{tr}(O) + \sum_{\mathbf{x}, \mathbf{y} \in \mathbb{Z}_2^n} \langle \mathbf{y} | \sigma | \mathbf{x} \rangle \langle \mathbf{x} | O | \mathbf{y} \rangle - \sum_{\mathbf{x} \in \mathbb{Z}_2^n} \langle \mathbf{x} | \sigma | \mathbf{x} \rangle \langle \mathbf{x} | O | \mathbf{x} \rangle \right\}, \\
&= \frac{1}{4^n} \left\{ \text{tr}(O) + \text{tr}(O\sigma) - \sum_{\mathbf{x} \in \mathbb{Z}_2^n} \langle \mathbf{x} | \sigma | \mathbf{x} \rangle \langle \mathbf{x} | O | \mathbf{x} \rangle \right\}. \tag{65}
\end{aligned}$$

Hence, we obtain the following result,

$$\sum_{|\phi_{\mathbf{A}}^{\text{eq}}\rangle \in \mathcal{S}_n^{\text{eq}}} \frac{2^{2n}}{|\mathcal{S}_n^{\text{eq}}|} \langle \phi_{\mathbf{A}}^{\text{eq}} | \rho | \phi_{\mathbf{A}}^{\text{eq}} \rangle \langle \phi_{\mathbf{A}}^{\text{eq}} | O | \phi_{\mathbf{A}}^{\text{eq}} \rangle + \sum_{\mathbf{x} \in \mathbb{Z}_2^n} \langle \mathbf{x} | \rho | \mathbf{x} \rangle \langle \mathbf{x} | O | \mathbf{x} \rangle - \text{tr}(O) = \text{tr}(O\rho). \tag{66}$$

Next, we consider RESPOVMs and also assume O to be a real observable, that is $\langle \mathbf{a} | O | \mathbf{b} \rangle \in \mathbb{R}$ for $\forall \mathbf{a}, \mathbf{b} \in \mathbb{Z}_2^n$. Then,

$$\begin{aligned}
& \mathbb{E}_{|\phi_{\mathbf{A}}^{\text{req}}\rangle \sim \mathcal{D}(\mathcal{S}_n^{\text{req}})} (\langle \phi_{\mathbf{A}}^{\text{req}} | \sigma | \phi_{\mathbf{A}}^{\text{req}} \rangle \langle \phi_{\mathbf{A}}^{\text{req}} | O | \phi_{\mathbf{A}}^{\text{req}} \rangle) = \text{tr} \left\{ \left(\mathbb{E}_{|\phi_{\mathbf{A}}^{\text{eq}}\rangle \sim \mathcal{D}(\mathcal{S}_n^{\text{eq}})} |\phi_{\mathbf{A}}^{\text{eq}}\rangle \langle \phi_{\mathbf{A}}^{\text{eq}}|^{\otimes 2} \right) (\sigma \otimes O) \right\} \\
&= \frac{1}{4^n} \text{tr} \left\{ \left(I + \sum_{\mathbf{x}, \mathbf{y} \in \mathbb{Z}_2^n} |\mathbf{x}\mathbf{y}\rangle \langle \mathbf{y}\mathbf{x}| + \sum_{\mathbf{x}, \mathbf{y} \in \mathbb{Z}_2^n} |\mathbf{x}\mathbf{x}\rangle \langle \mathbf{y}\mathbf{y}| - 2 \sum_{\mathbf{x} \in \mathbb{Z}_2^n} |\mathbf{x}\mathbf{x}\rangle \langle \mathbf{x}\mathbf{x}| \right) (\sigma \otimes O) \right\} \\
&= \frac{1}{4^n} \left\{ \text{tr}(O) + \sum_{\mathbf{x}, \mathbf{y} \in \mathbb{Z}_2^n} \langle \mathbf{y} | \sigma | \mathbf{x} \rangle \langle \mathbf{x} | O | \mathbf{y} \rangle + \sum_{\mathbf{x}, \mathbf{y} \in \mathbb{Z}_2^n} \langle \mathbf{y} | \sigma | \mathbf{x} \rangle \langle \mathbf{y} | O | \mathbf{x} \rangle \right. \\
&\quad \left. - 2 \sum_{\mathbf{x} \in \mathbb{Z}_2^n} \langle \mathbf{x} | \sigma | \mathbf{x} \rangle \langle \mathbf{x} | O | \mathbf{x} \rangle \right\} \\
&= \frac{1}{4^n} \left\{ \text{tr}(O) + 2 \sum_{\mathbf{x}, \mathbf{y} \in \mathbb{Z}_2^n} \langle \mathbf{y} | \sigma | \mathbf{x} \rangle \langle \mathbf{x} | O | \mathbf{y} \rangle - 2 \sum_{\mathbf{x} \in \mathbb{Z}_2^n} \langle \mathbf{x} | \sigma | \mathbf{x} \rangle \langle \mathbf{x} | O | \mathbf{x} \rangle \right\} \tag{67}
\end{aligned}$$

$$= \frac{1}{4^n} \left\{ \text{tr}(O) + 2\text{tr}(O\sigma) - 2 \sum_{\mathbf{x} \in \mathbb{Z}_2^n} \langle \mathbf{x} | \sigma | \mathbf{x} \rangle \langle \mathbf{x} | O | \mathbf{x} \rangle \right\}. \tag{68}$$

This is equivalent to,

$$\sum_{|\phi_{\mathbf{A}}^{\text{req}}\rangle \in \mathcal{S}_n^{\text{req}}} \frac{2^{2n-1}}{|\mathcal{S}_n^{\text{req}}|} \langle \phi_{\mathbf{A}}^{\text{req}} | \rho | \phi_{\mathbf{A}}^{\text{req}} \rangle \langle \phi_{\mathbf{A}}^{\text{req}} | O | \phi_{\mathbf{A}}^{\text{req}} \rangle + \sum_{\mathbf{x} \in \mathbb{Z}_2^n} \langle \mathbf{x} | \rho | \mathbf{x} \rangle \langle \mathbf{x} | O | \mathbf{x} \rangle - \frac{1}{2} \text{tr}(O) = \text{tr}(O\rho). \tag{69}$$

Equation (67) is valid when O is real. This proves Lem. 2. In Eq. (21) of the main text, we ignore the $\text{tr}(O)$ term since it is constant and, hence, does not affect the variance.

B.3 Proof of Lemma 3

We start with $\mathcal{S}_n^{\text{req}}$. Similar to Eq. (60),

$$\begin{aligned}
& \mathbb{E}_{|\phi_{\mathbf{A}}^{\text{req}}\rangle \sim \mathcal{D}(\mathcal{S}_n^{\text{req}})} |\phi_{\mathbf{A}}^{\text{req}}\rangle \langle \phi_{\mathbf{A}}^{\text{req}}|^{\otimes 3} \\
&= \mathbb{E}_{|\phi_{\mathbf{A}}^{\text{req}}\rangle \sim \mathcal{D}(\mathcal{S}_n^{\text{req}})} \frac{1}{8^n} \sum_{\mathbf{x}, \mathbf{y}, \mathbf{z}, \mathbf{w}, \mathbf{s}, \mathbf{t} \in \mathbb{Z}_2^n} (-1)^{\mathbf{x}^\top \mathbf{A} \mathbf{x} + \mathbf{y}^\top \mathbf{A} \mathbf{y} + \mathbf{z}^\top \mathbf{A} \mathbf{z} + \mathbf{w}^\top \mathbf{A} \mathbf{w} + \mathbf{s}^\top \mathbf{A} \mathbf{s} + \mathbf{t}^\top \mathbf{A} \mathbf{t}} |\mathbf{x} \mathbf{y} \mathbf{z}\rangle \langle \mathbf{w} \mathbf{s} \mathbf{t}| \\
&= \frac{1}{8^n} \sum_{\mathbf{x}, \mathbf{y}, \mathbf{z}, \mathbf{w}, \mathbf{s}, \mathbf{t} \in \mathbb{Z}_2^n} \mathbb{E}_{|\phi_{\mathbf{A}}^{\text{req}}\rangle \sim \mathcal{D}(\mathcal{S}_n^{\text{req}})} \left\{ (-1)^{\mathbf{x}^\top \mathbf{A} \mathbf{x} + \mathbf{y}^\top \mathbf{A} \mathbf{y} + \mathbf{z}^\top \mathbf{A} \mathbf{z} + \mathbf{w}^\top \mathbf{A} \mathbf{w} + \mathbf{s}^\top \mathbf{A} \mathbf{s} + \mathbf{t}^\top \mathbf{A} \mathbf{t}} \right\} |\mathbf{x} \mathbf{y} \mathbf{z}\rangle \langle \mathbf{w} \mathbf{s} \mathbf{t}|.
\end{aligned} \tag{70}$$

By the same token, for nonzero coefficients in the summand, the following equations must hold for all $p, q \in [n]$:

$$\begin{cases} x_p + y_p + z_p + w_p + s_p = t_p \pmod{2}, \\ x_p x_q + y_p y_q + z_p z_q + w_p w_q + s_p s_q + t_p t_q = 0 \pmod{2}. \end{cases} \tag{71}$$

Substituting the upper equation into the lower one, we obtain,

$$\begin{aligned}
& x_p(y_q + z_q + w_q + s_q) + y_p(z_q + x_q + w_q + s_q) + z_p(x_q + y_q + w_q + s_q) + \\
& \quad w_p(x_q + y_q + z_q + s_q) + s_p(x_q + y_q + z_q + w_q) = 0.
\end{aligned} \tag{72}$$

If $\mathbf{x} = \mathbf{y} = \mathbf{z} = \mathbf{w} = \mathbf{s}$, the above equation clearly holds. Otherwise, we have two cases:

(i) There exists $p' \in [N]$ such that two of $x_{p'}, y_{p'}, z_{p'}, w_{p'}, s_{p'}$ are 0 (1 resp.) and the rest are 1 (0), and $x_i = y_i = z_i = w_i = s_i$ for $i < p'$.

(ii) There exists $p' \in [N]$ such that four of $x_{p'}, y_{p'}, z_{p'}, w_{p'}, s_{p'}$ are 0 (1 resp.) and the other is 1 (0), and $x_i = y_i = z_i = w_i = s_i$ for $i < p'$.

First, suppose case (i). WLOG, when $x_{p'} = y_{p'}$ (*), then $z_{p'} = w_{p'} = s_{p'} = x_{p'} + 1$, which together with Eq. (72), implies that

$$x_{p'} y_q + x_q y_{p'} + (x_{p'} + 1)(x_q + y_q) = x_q + y_q = 0 \pmod{2} \quad \because x_{p'} = y_{p'}. \tag{73}$$

So, we obtain $\mathbf{x} = \mathbf{y}$. Substituting this back to Eq. (71),

$$\begin{cases} z_p + w_p + s_p = t_p \pmod{2}, \\ z_p z_q + w_p w_q + s_p s_q + t_p t_q = 0 \pmod{2}. \end{cases} \tag{74}$$

This is exactly what we have obtained during the calculation of the second moment. Hence we conclude the same statement, two of $\mathbf{z}, \mathbf{w}, \mathbf{s}$ are equal. By the first equation of Eq. (74), the remaining one equals \mathbf{t} . Therefore, we conclude that each two of $\mathbf{x}, \mathbf{y}, \mathbf{z}, \mathbf{w}, \mathbf{s}, \mathbf{t}$ must be equal. Note that even if we chose two other variables, not \mathbf{x} and \mathbf{y} in assumption(*), we arrive at the same conclusion.

Next, let us suppose case (ii). By the first equation of Eq. (71), $x_i = y_i = z_i = w_i = s_i = t_i$ for $i < p'$. WLOG, assume that $x_{p'} = y_{p'} = z_{p'} = w_{p'} \neq s_{p'}$. Then, we obtain $s_{p'} = t_{p'}$ from Eq. (71). Next, we rewrite the problem as

$$\begin{cases} y_p + z_p + w_p + s_p + t_p = x_p \pmod{2}, \\ x_p x_q + y_p y_q + z_p z_q + w_p w_q + s_p s_q + t_p t_q = 0 \pmod{2} \end{cases} \tag{75}$$

Similarly, substituting the first equation into the second,

$$\begin{aligned}
& t_p(y_q + z_q + w_q + s_q) + y_p(z_q + x_q + w_q + s_q) + z_p(t_q + y_q + w_q + s_q) + \\
& w_p(t_q + y_q + z_q + s_q) + s_p(t_q + y_q + z_q + w_q) = 0. \tag{76}
\end{aligned}$$

Remember we assumed that $t_{p'} = s_{p'}$, $t_{p'} \neq w_{p'}$, $y_{p'} = z_{p'} = w_{p'}$, and $y_i = z_i = w_i = s_i = t_i$ for $i < p'$. This is exactly the case of solving under the assumption (i). So we conclude the same statement that $\mathbf{t} = \mathbf{s}$, two of $\mathbf{y}, \mathbf{z}, \mathbf{w}$ are equal and hence remaining one equals \mathbf{x} .

Throughout cases (i) and (ii), we finally conclude that the coefficient of $|\mathbf{x}\mathbf{y}\mathbf{z}\rangle\langle\mathbf{w}\mathbf{s}\mathbf{t}|$ is nonzero only when each 3-couples in variable set $\{\mathbf{x}, \mathbf{y}, \mathbf{z}, \mathbf{w}, \mathbf{s}, \mathbf{t}\}$ must be equal and in such all cases, coefficients $\mathbb{E}_{|\phi_{\mathbf{A}}^{\text{req}}\rangle\sim\mathcal{D}(\mathcal{S}_n^{\text{req}})}\left\{(-1)^{\mathbf{x}^\top\mathbf{A}\mathbf{x}+\mathbf{y}^\top\mathbf{A}\mathbf{y}+\mathbf{z}^\top\mathbf{A}\mathbf{z}+\mathbf{w}^\top\mathbf{A}\mathbf{w}+\mathbf{s}^\top\mathbf{A}\mathbf{s}+\mathbf{t}^\top\mathbf{A}\mathbf{t}}\right\} = 1$. The proof for RESPOVM is now completed.

Now, we move on to $\mathcal{S}_n^{\text{eq}}$, whence

$$\begin{aligned}
& \mathbb{E}_{|\phi_{\mathbf{A}}^{\text{eq}}\rangle\sim\mathcal{D}(\mathcal{S}_n^{\text{eq}})}|\phi_{\mathbf{A}}^{\text{eq}}\rangle\langle\phi_{\mathbf{A}}^{\text{eq}}|^{\otimes 3} \\
& = \mathbb{E}_{|\phi_{\mathbf{A}}^{\text{eq}}\rangle\sim\mathcal{D}(\mathcal{S}_n^{\text{eq}})}\frac{1}{8^n}\sum_{\mathbf{x},\mathbf{y},\mathbf{z},\mathbf{w},\mathbf{s},\mathbf{t}\in\mathbb{Z}_2^n}i^{\mathbf{x}^\top\mathbf{A}\mathbf{x}+\mathbf{y}^\top\mathbf{A}\mathbf{y}+\mathbf{z}^\top\mathbf{A}\mathbf{z}-\mathbf{w}^\top\mathbf{A}\mathbf{w}-\mathbf{s}^\top\mathbf{A}\mathbf{s}-\mathbf{t}^\top\mathbf{A}\mathbf{t}}|\mathbf{x}\mathbf{y}\mathbf{z}\rangle\langle\mathbf{w}\mathbf{s}\mathbf{t}| \\
& = \frac{1}{8^n}\sum_{\mathbf{x},\mathbf{y},\mathbf{z},\mathbf{w},\mathbf{s},\mathbf{t}\in\mathbb{Z}_2^n}\mathbb{E}_{|\phi_{\mathbf{A}}^{\text{eq}}\rangle\sim\mathcal{D}(\mathcal{S}_n^{\text{eq}})}\left\{i^{\mathbf{x}^\top\mathbf{A}\mathbf{x}+\mathbf{y}^\top\mathbf{A}\mathbf{y}+\mathbf{z}^\top\mathbf{A}\mathbf{z}-\mathbf{w}^\top\mathbf{A}\mathbf{w}-\mathbf{s}^\top\mathbf{A}\mathbf{s}-\mathbf{t}^\top\mathbf{A}\mathbf{t}}\right\}|\mathbf{x}\mathbf{y}\mathbf{z}\rangle\langle\mathbf{w}\mathbf{s}\mathbf{t}|. \tag{77}
\end{aligned}$$

By the same argument, for the coefficient not to be 0, the following equation must hold. For all $p, q \in \mathbb{Z}_2^n$ ($p < q$),

$$\begin{cases} x_p + y_p + z_p = w_p + s_p + t_p \pmod{4} \\ x_px_q + y_py_q + z_pz_q + w_pw_q + s_ps_q + t_pt_q = 0 \pmod{2}. \end{cases} \tag{78}$$

We add $w_p + s_p$ for both sides of the first equation of (78), we obtain that

$$\begin{cases} x_p + y_p + z_p + w_p + s_p = t_p \pmod{2} \\ x_px_q + y_py_q + z_pz_q + w_pw_q + s_ps_q + t_pt_q = 0 \pmod{2}. \end{cases} \tag{79}$$

This is equation for $\mathcal{S}_n^{\text{req}}$ -case. Hence we obtain the same statement, each 3-couples in variable set $\{\mathbf{x}, \mathbf{y}, \mathbf{z}, \mathbf{w}, \mathbf{s}, \mathbf{t}\}$ must be equal. However, in this case, we have a stricter condition, the first equation of Eq. (78). WLOG, we only consider two cases.

(i) $\mathbf{x} = \mathbf{y}$: $2x_p + z_p = w_p + s_p + t_p \pmod{4} \rightarrow z_p = w_p + s_p + t_p \pmod{2}$. Hence two variables in $\{\mathbf{z}, \mathbf{w}, \mathbf{s}, \mathbf{t}\}$ are equal each other.

(ii) $\mathbf{x} = \mathbf{w}$: $y_p + z_p = s_p + t_p \pmod{4}$. If $\mathbf{y} = \mathbf{z}$, $2y_p = s_p + t_p \rightarrow \mathbf{y} = \mathbf{z} = \mathbf{s} = \mathbf{t}$. If $\mathbf{y} = \mathbf{s}, \mathbf{z} = \mathbf{t}$. If $\mathbf{y} = \mathbf{w}$, all cases are equivalent to previous cases. Therefore for the coefficients to be non-zero, if $|\mathbf{x}\mathbf{y}\mathbf{z}\rangle\langle\mathbf{w}\mathbf{s}\mathbf{t}|$ has 2 same variables where each do not locate in the same position(bra and ket) and the other 2 variables in bra (or ket) are equal, remaining variables in ket (or bra) must be equal to previous 2 variables. Finally, in those cases, the coefficient cannot be other values but 1.

Other cases can be managed similarly and are known to have similar effects of (i) or (ii). We thus proved Lem. 3.

B.4 Proof of Lemma 4

First, we note that

$$\begin{aligned} \sum_{\mathbf{x} \in \mathbb{Z}_2^N} \text{tr}(|\mathbf{x}\mathbf{x}\mathbf{x}\rangle \langle \mathbf{x}\mathbf{x}\mathbf{x}| (\sigma \otimes O_0 \otimes O_0)) &= \sum_{\mathbf{x} \in \mathbb{Z}_2^N} \langle \mathbf{x} | \sigma | \mathbf{x} \rangle \langle \mathbf{x} | O_0 | \mathbf{x} \rangle \langle \mathbf{x} | O_0 | \mathbf{x} \rangle \\ &\leq \sum_{\mathbf{x}, \mathbf{y} \in \mathbb{Z}_2^N} \langle \mathbf{x} | \sigma | \mathbf{x} \rangle \langle \mathbf{x} | O_0 | \mathbf{y} \rangle \langle \mathbf{y} | O_0 | \mathbf{x} \rangle \leq \text{tr}(O_0^2). \end{aligned} \quad (80)$$

Here, we used the fact that $\langle \mathbf{x} | O_0 | \mathbf{y} \rangle \langle \mathbf{y} | O_0 | \mathbf{x} \rangle \geq 0$ for $\forall \mathbf{x}, \mathbf{y} \in \mathbb{Z}_2^n$. This proves the Eq. (41).

Also, we easily note that

$$\sum_{\mathbf{x}, \mathbf{y}, \mathbf{z} \in \mathbb{Z}_2^N} \text{tr}(|\mathbf{x}\mathbf{y}\mathbf{z}\rangle \langle \mathbf{x}\mathbf{y}\mathbf{z}| + |\mathbf{x}\mathbf{y}\mathbf{z}\rangle \langle \mathbf{x}\mathbf{z}\mathbf{y}| + |\mathbf{x}\mathbf{y}\mathbf{z}\rangle \langle \mathbf{y}\mathbf{x}\mathbf{z}| + |\mathbf{x}\mathbf{y}\mathbf{z}\rangle \langle \mathbf{z}\mathbf{x}\mathbf{y}| + |\mathbf{x}\mathbf{y}\mathbf{z}\rangle \langle \mathbf{z}\mathbf{y}\mathbf{x}| +$$

$$|\mathbf{x}\mathbf{y}\mathbf{z}\rangle \langle \mathbf{y}\mathbf{z}\mathbf{x}| (\sigma \otimes O_0 \otimes O_0)) = (\text{tr}(O_0))^2 + \text{tr}(O_0^2) + 2\text{tr}(O_0)\text{tr}(\sigma O_0) + 2\text{tr}(\sigma O_0^2) \quad (81)$$

$$\begin{aligned} &\leq (\text{tr}(O_0))^2 + \text{tr}(O_0^2) + 2\text{tr}(O_0)\|O_0\|_\infty + 2\|O_0^2\|_\infty \leq (\text{tr}(O_0))^2 + 3\text{tr}(O_0^2) + 2\text{tr}(O_0)\|O_0\|_\infty \\ &\leq 3\text{tr}(O_0^2), \end{aligned} \quad (82)$$

where $\|O\|_\infty \equiv \max_{|\psi\rangle} \{|\langle \psi | O | \psi \rangle|\}$. Furthermore, we can consider another case when two variables are the same in ket. Let $\sigma = \sum_\lambda \lambda |\lambda\rangle \langle \lambda|$ be spectral decomposition of σ , hence $\forall \lambda \geq 0$ and $\sum_\lambda \lambda = 1$. Then we obtain that

$$\begin{aligned} \left| \sum_{\mathbf{x}, \mathbf{y}, \mathbf{z} \in \mathbb{Z}_2^N} \text{tr}(|\mathbf{x}\mathbf{x}\mathbf{y}\rangle \langle \mathbf{z}\mathbf{z}\mathbf{y}| (\sigma \otimes O_0 \otimes O_0)) \right| &= \left| \sum_{\mathbf{x}, \mathbf{y}, \mathbf{z} \in \mathbb{Z}_2^N} \langle \mathbf{z} | \sigma | \mathbf{x} \rangle \langle \mathbf{z} | O_0 | \mathbf{x} \rangle \langle \mathbf{y} | O_0 | \mathbf{y} \rangle \right| \\ &= \left| \text{tr}(O_0)\text{tr}(\sigma O_0^\top) \right| \leq \left| \text{tr}(O_0)\text{tr}(O_0^\top) \right| = 0 \end{aligned} \quad (83)$$

$$\begin{aligned} \left| \sum_{\mathbf{x}, \mathbf{y}, \mathbf{z} \in \mathbb{Z}_2^N} \text{tr}(|\mathbf{x}\mathbf{x}\mathbf{y}\rangle \langle \mathbf{z}\mathbf{y}\mathbf{z}| (\sigma \otimes O_0 \otimes O_0)) \right| &= \left| \sum_{\mathbf{x}, \mathbf{y}, \mathbf{z} \in \mathbb{Z}_2^N} \langle \mathbf{z} | \sigma | \mathbf{x} \rangle \langle \mathbf{y} | O_0 | \mathbf{x} \rangle \langle \mathbf{z} | O_0 | \mathbf{y} \rangle \right| \\ &= \left| \text{tr}(\sigma (O_0^\top)^2) \right| \leq \|(O_0^\top)^2\|_\infty \leq \text{tr}((O_0^\top)^2) \\ &= \text{tr}(O_0^2) \end{aligned} \quad (84)$$

$$\begin{aligned} \left| \sum_{\mathbf{x}, \mathbf{y}, \mathbf{z} \in \mathbb{Z}_2^N} \text{tr}(|\mathbf{x}\mathbf{x}\mathbf{y}\rangle \langle \mathbf{y}\mathbf{z}\mathbf{z}| (\sigma \otimes O_0 \otimes O_0)) \right| &= \left| \sum_{\mathbf{x}, \mathbf{y}, \mathbf{z} \in \mathbb{Z}_2^N} \langle \mathbf{y} | \sigma | \mathbf{x} \rangle \langle \mathbf{z} | O_0 | \mathbf{x} \rangle \langle \mathbf{z} | O_0 | \mathbf{y} \rangle \right| \\ &= \left| \text{tr}(\sigma O_0^\top O_0) \right| \leq \|O_0^\top O_0\|_\infty \end{aligned} \quad (85)$$

$$\begin{aligned} \left| \sum_{\mathbf{x}, \mathbf{y}, \mathbf{z} \in \mathbb{Z}_2^N} \text{tr}(|\mathbf{y}\mathbf{x}\mathbf{x}\rangle \langle \mathbf{z}\mathbf{z}\mathbf{y}| (\sigma \otimes O_0 \otimes O_0)) \right| &= \left| \sum_{\mathbf{x}, \mathbf{y}, \mathbf{z} \in \mathbb{Z}_2^N} \langle \mathbf{z} | \sigma | \mathbf{y} \rangle \langle \mathbf{z} | O_0 | \mathbf{x} \rangle \langle \mathbf{y} | O_0 | \mathbf{x} \rangle \right| \\ &= \left| \text{tr}(\sigma O_0 O_0^\top) \right| \leq \|O_0 O_0^\top\|_\infty \end{aligned} \quad (86)$$

$$\begin{aligned}
\left| \sum_{\mathbf{x}, \mathbf{y}, \mathbf{z} \in \mathbb{Z}_2^N} \text{tr}(|\mathbf{y}\mathbf{x}\mathbf{x}\rangle \langle \mathbf{z}\mathbf{y}\mathbf{z}| (\sigma \otimes O_0 \otimes O_0)) \right| &= \left| \sum_{\mathbf{x}, \mathbf{y}, \mathbf{z} \in \mathbb{Z}_2^N} \langle \mathbf{z} | \sigma | \mathbf{x} \rangle \langle \mathbf{y} | O_0 | \mathbf{x} \rangle \langle \mathbf{z} | O_0 | \mathbf{y} \rangle \right| \\
&= \text{tr}(\sigma (O_0^\top)^2) \leq \|(O_0^\top)^2\|_\infty \leq \text{tr}((O_0^\top)^2) \\
&= \text{tr}(O_0^2) \tag{87}
\end{aligned}$$

$$\begin{aligned}
\left| \sum_{\mathbf{x}, \mathbf{y}, \mathbf{z} \in \mathbb{Z}_2^N} \text{tr}(|\mathbf{y}\mathbf{x}\mathbf{x}\rangle \langle \mathbf{y}\mathbf{z}\mathbf{z}| (\sigma \otimes O_0 \otimes O_0)) \right| &= \left| \sum_{\mathbf{x}, \mathbf{y}, \mathbf{z} \in \mathbb{Z}_2^N} \langle \mathbf{y} | \sigma | \mathbf{y} \rangle \langle \mathbf{z} | O_0 | \mathbf{x} \rangle \langle \mathbf{z} | O_0 | \mathbf{x} \rangle \right| \\
&= \left| \text{tr}(O_0 O_0^\top) \right| \tag{88}
\end{aligned}$$

$$\begin{aligned}
\left| \sum_{\mathbf{x}, \mathbf{y}, \mathbf{z} \in \mathbb{Z}_2^N} \text{tr}(|\mathbf{x}\mathbf{y}\mathbf{x}\rangle \langle \mathbf{z}\mathbf{z}\mathbf{y}| (\sigma \otimes O_0 \otimes O_0)) \right| &= \left| \sum_{\mathbf{x}, \mathbf{y}, \mathbf{z} \in \mathbb{Z}_2^N} \langle \mathbf{z} | \sigma | \mathbf{x} \rangle \langle \mathbf{z} | O_0 | \mathbf{y} \rangle \langle \mathbf{y} | O_0 | \mathbf{x} \rangle \right| \\
&\leq \text{tr}(O_0^2) \tag{89}
\end{aligned}$$

$$\begin{aligned}
\left| \sum_{\mathbf{x}, \mathbf{y}, \mathbf{z} \in \mathbb{Z}_2^N} \text{tr}(|\mathbf{x}\mathbf{y}\mathbf{x}\rangle \langle \mathbf{z}\mathbf{y}\mathbf{z}| (\sigma \otimes O_0 \otimes O_0)) \right| &= \left| \sum_{\mathbf{x}, \mathbf{y}, \mathbf{z} \in \mathbb{Z}_2^N} \langle \mathbf{z} | \sigma | \mathbf{x} \rangle \langle \mathbf{y} | O_0 | \mathbf{y} \rangle \langle \mathbf{z} | O_0 | \mathbf{x} \rangle \right| \\
&\leq (\text{tr}(O_0))^2 = 0 \tag{90}
\end{aligned}$$

$$\begin{aligned}
\left| \sum_{\mathbf{x}, \mathbf{y}, \mathbf{z} \in \mathbb{Z}_2^N} \text{tr}(|\mathbf{x}\mathbf{y}\mathbf{x}\rangle \langle \mathbf{y}\mathbf{z}\mathbf{z}| (\sigma \otimes O_0 \otimes O_0)) \right| &= \left| \sum_{\mathbf{x}, \mathbf{y}, \mathbf{z} \in \mathbb{Z}_2^N} \langle \mathbf{y} | \sigma | \mathbf{x} \rangle \langle \mathbf{z} | O_0 | \mathbf{y} \rangle \langle \mathbf{z} | O_0 | \mathbf{x} \rangle \right| \\
&\leq \|O_0 O_0^\top\|_\infty \tag{91}
\end{aligned}$$

$$\begin{aligned}
&\left| \sum_{\mathbf{x}, \mathbf{y} \in \mathbb{Z}_2^N} \text{tr}(|\mathbf{x}\mathbf{x}\mathbf{y}\rangle \langle \mathbf{y}\mathbf{y}\mathbf{y}| (\sigma \otimes O_0 \otimes O_0)) \right| = \left| \sum_{\mathbf{x}, \mathbf{y} \in \mathbb{Z}_2^N} \langle \mathbf{y} | \sigma | \mathbf{x} \rangle \langle \mathbf{y} | O_0 | \mathbf{x} \rangle \langle \mathbf{y} | O_0 | \mathbf{y} \rangle \right| \\
&\leq \sum_{\mathbf{y} \in \mathbb{Z}_2^N} \left| \langle \mathbf{y} | \sigma O_0^\top | \mathbf{y} \rangle \langle \mathbf{y} | O_0 | \mathbf{y} \rangle \right| \leq \sqrt{\sum_{\mathbf{y} \in \mathbb{Z}_2^N} |\langle \mathbf{y} | \sigma O_0^\top | \mathbf{y} \rangle|^2 \sum_{\mathbf{z} \in \mathbb{Z}_2^N} \langle \mathbf{z} | O_0 | \mathbf{z} \rangle \langle \mathbf{z} | O_0 | \mathbf{z} \rangle} \\
&\leq \sqrt{\sum_{\mathbf{y} \in \mathbb{Z}_2^N} \left| \sum_{\lambda} \lambda \langle \mathbf{y} | \lambda \rangle \langle \lambda | O_0^\top | \mathbf{y} \rangle \right|^2 \sum_{\mathbf{z}, \mathbf{k} \in \mathbb{Z}_2^N} \langle \mathbf{z} | O_0 | \mathbf{k} \rangle \langle \mathbf{k} | O_0 | \mathbf{z} \rangle} \\
&\leq \sqrt{\sum_{\mathbf{y} \in \mathbb{Z}_2^N} |\langle \lambda_{\mathbf{y}} | O_0^\top | \mathbf{y} \rangle|^2 |\langle \mathbf{y} | \lambda_{\mathbf{y}} \rangle|^2 \text{tr}(O_0^2)} \left(\lambda_{\mathbf{y}} \equiv \text{argmax}_{\lambda} \left\{ |\langle \lambda | O_0^\top | \mathbf{y} \rangle \langle \mathbf{y} | \lambda \rangle| \right\} \right) \\
&\leq \sqrt{\sum_{\mathbf{y} \in \mathbb{Z}_2^N} \sum_{\lambda} |\langle \mathbf{y} | \lambda \rangle|^2 \langle \lambda | O_0^\top | \mathbf{y} \rangle \langle \mathbf{y} | O_0^\top | \lambda \rangle \text{tr}(O_0^2)} \\
&\leq \sqrt{\sum_{\lambda} \langle \lambda | O_0^\top | \mathbf{y}_{\lambda} \rangle \langle \mathbf{y}_{\lambda} | O_0^\top | \lambda \rangle \text{tr}(O_0^2)} \left(\mathbf{y}_{\lambda} \equiv \text{argmax}_{\mathbf{y} \in \mathbb{Z}_2^N} \left\{ |\langle \lambda | O_0^\top | \mathbf{y} \rangle|^2 \right\} \right) \\
&\leq \sqrt{\sum_{\lambda} \sum_{\mathbf{z} \in \mathbb{Z}_2^N} \langle \lambda | O_0^\top | \mathbf{z} \rangle \langle \mathbf{z} | O_0^\top | \lambda \rangle \text{tr}(O_0^2)} = \sqrt{\sum_{\lambda} \langle \lambda | (O_0^\top)^2 | \lambda \rangle \text{tr}(O_0^2)} \\
&= \sqrt{\text{tr}((O_0^\top)^2)} \sqrt{\text{tr}(O_0^2)} = \text{tr}(O_0^2), \tag{92}
\end{aligned}$$

$$\begin{aligned}
\left| \sum_{\mathbf{x}, \mathbf{y} \in \mathbb{Z}_2^N} \text{tr}(|\mathbf{x}\mathbf{x}\mathbf{y}\rangle \langle \mathbf{x}\mathbf{y}\mathbf{x}| (\sigma \otimes O_0 \otimes O_0)) \right| &= \left| \sum_{\mathbf{x}, \mathbf{y} \in \mathbb{Z}_2^N} \langle \mathbf{x} | \sigma | \mathbf{x} \rangle \langle \mathbf{y} | O_0 | \mathbf{x} \rangle \langle \mathbf{x} | O_0 | \mathbf{y} \rangle \right| \\
&\leq \sum_{\mathbf{x}, \mathbf{y} \in \mathbb{Z}_2^N} \langle \mathbf{y} | O_0 | \mathbf{x} \rangle \langle \mathbf{x} | O_0 | \mathbf{y} \rangle = \text{tr}(O_0^2) \quad (93)
\end{aligned}$$

$$\begin{aligned}
\left| \sum_{\mathbf{x}, \mathbf{y} \in \mathbb{Z}_2^N} \text{tr}(|\mathbf{x}\mathbf{x}\mathbf{y}\rangle \langle \mathbf{x}\mathbf{y}\mathbf{x}| (\sigma \otimes O_0 \otimes O_0)) \right| &= \left| \sum_{\mathbf{x}, \mathbf{y} \in \mathbb{Z}_2^N} \langle \mathbf{x} | \sigma | \mathbf{x} \rangle \langle \mathbf{x} | O_0 | \mathbf{x} \rangle \langle \mathbf{y} | O_0 | \mathbf{y} \rangle \right| \\
&\leq \sum_{\mathbf{x} \in \mathbb{Z}_2^N} |\langle \mathbf{x} | \sigma | \mathbf{x} \rangle \langle \mathbf{x} | O_0 | \mathbf{x} \rangle \text{tr}(O_0)| \\
&= |\text{tr}(O_0)| \|O_0\|_\infty = 0 \quad (94)
\end{aligned}$$

$$\begin{aligned}
\left| \sum_{\mathbf{x}, \mathbf{y} \in \mathbb{Z}_2^N} \text{tr}(|\mathbf{x}\mathbf{x}\mathbf{y}\rangle \langle \mathbf{y}\mathbf{x}\mathbf{x}| (\sigma \otimes O_0 \otimes O_0)) \right| &= \left| \sum_{\mathbf{x}, \mathbf{y} \in \mathbb{Z}_2^N} \langle \mathbf{x} | \sigma^\top | \mathbf{y} \rangle \langle \mathbf{x} | O_0 | \mathbf{x} \rangle \langle \mathbf{x} | O_0 | \mathbf{y} \rangle \right| \\
&= \left| \sum_{\mathbf{x}, \mathbf{y} \in \mathbb{Z}_2^N} \langle \mathbf{y} | \sigma^\top | \mathbf{x} \rangle \langle \mathbf{y} | O_0 | \mathbf{y} \rangle \langle \mathbf{y} | O_0 | \mathbf{x} \rangle \right| \\
&\leq \text{tr}(O_0^2) (\because \text{Eq. (92)}) \quad (95)
\end{aligned}$$

$$\begin{aligned}
\left| \sum_{\mathbf{x}, \mathbf{y} \in \mathbb{Z}_2^N} \text{tr}(|\mathbf{y}\mathbf{x}\mathbf{x}\rangle \langle \mathbf{y}\mathbf{y}\mathbf{y}| (\sigma \otimes O_0 \otimes O_0)) \right| &= \left| \sum_{\mathbf{x}, \mathbf{y} \in \mathbb{Z}_2^N} \langle \mathbf{y} | \sigma | \mathbf{y} \rangle \langle \mathbf{y} | O_0 | \mathbf{x} \rangle \langle \mathbf{x} | O_0^\top | \mathbf{y} \rangle \right| \\
&\leq \sum_{\mathbf{y} \in \mathbb{Z}_2^N} \langle \mathbf{y} | \sigma | \mathbf{y} \rangle |\langle \mathbf{y} | O_0 O_0^\top | \mathbf{y} \rangle| \leq \|O_0 O_0^\top\|_\infty \quad (96)
\end{aligned}$$

$$\begin{aligned}
\left| \sum_{\mathbf{x}, \mathbf{y} \in \mathbb{Z}_2^N} \text{tr}(|\mathbf{x}\mathbf{y}\mathbf{x}\rangle \langle \mathbf{y}\mathbf{y}\mathbf{y}| (\sigma \otimes O_0 \otimes O_0)) \right| &= \left| \sum_{\mathbf{x}, \mathbf{y} \in \mathbb{Z}_2^N} \langle \mathbf{y} | \sigma | \mathbf{x} \rangle \langle \mathbf{y} | O_0 | \mathbf{y} \rangle \langle \mathbf{y} | O_0 | \mathbf{x} \rangle \right| \\
&\leq \text{tr}(O_0^2) (\because \text{Eq. (92)}) \quad (97)
\end{aligned}$$

$$\begin{aligned}
\left| \sum_{\mathbf{x}, \mathbf{y} \in \mathbb{Z}_2^N} \text{tr}(|\mathbf{y}\mathbf{x}\mathbf{x}\rangle \langle \mathbf{x}\mathbf{y}\mathbf{x}| (\sigma \otimes O_0 \otimes O_0)) \right| &= \left| \sum_{\mathbf{x}, \mathbf{y} \in \mathbb{Z}_2^N} \langle \mathbf{x} | \sigma | \mathbf{y} \rangle \langle \mathbf{x} | O_0 | \mathbf{x} \rangle \langle \mathbf{y} | O_0 | \mathbf{x} \rangle \right| \\
&\leq \text{tr}(O_0^2) (\because \text{Eq. (92)}) \quad (98)
\end{aligned}$$

$$\begin{aligned}
\left| \sum_{\mathbf{x}, \mathbf{y} \in \mathbb{Z}_2^N} \text{tr}(|\mathbf{y}\mathbf{x}\mathbf{x}\rangle \langle \mathbf{y}\mathbf{x}\mathbf{x}| (\sigma \otimes O_0 \otimes O_0)) \right| &= \left| \sum_{\mathbf{x}, \mathbf{y} \in \mathbb{Z}_2^N} \langle \mathbf{y} | \sigma | \mathbf{y} \rangle \langle \mathbf{x} | O_0 | \mathbf{x} \rangle \langle \mathbf{x} | O_0 | \mathbf{x} \rangle \right| \\
&\leq \sum_{\mathbf{x}, \mathbf{z} \in \mathbb{Z}_2^N} \langle \mathbf{x} | O_0 | \mathbf{z} \rangle \langle \mathbf{z} | O_0 | \mathbf{x} \rangle \leq \text{tr}(O_0^2). \quad (99)
\end{aligned}$$

$$\begin{aligned}
\left| \sum_{\mathbf{x}, \mathbf{y} \in \mathbb{Z}_2^N} \text{tr}(|\mathbf{y}\mathbf{x}\mathbf{x}\rangle \langle \mathbf{x}\mathbf{y}\mathbf{x}| (\sigma \otimes O_0 \otimes O_0)) \right| &= \left| \sum_{\mathbf{x}, \mathbf{y} \in \mathbb{Z}_2^N} \langle \mathbf{x} | \sigma | \mathbf{y} \rangle \langle \mathbf{y} | O_0 | \mathbf{x} \rangle \langle \mathbf{x} | O_0 | \mathbf{x} \rangle \right| \\
&\leq \text{tr}(O_0^2) (\because \text{Eq. (92)}) \quad (100)
\end{aligned}$$

$$\left| \sum_{\mathbf{x}, \mathbf{y} \in \mathbb{Z}_2^N} \text{tr}(|\mathbf{x}\mathbf{y}\mathbf{x}\rangle \langle \mathbf{x}\mathbf{y}\mathbf{x}| (\sigma \otimes O_0 \otimes O_0)) \right| = \left| \sum_{\mathbf{x}, \mathbf{y} \in \mathbb{Z}_2^N} \langle \mathbf{x} | \sigma | \mathbf{x} \rangle \langle \mathbf{x} | O_0 | \mathbf{y} \rangle \langle \mathbf{y} | O_0 | \mathbf{x} \rangle \right| \leq \text{tr}(O_0^2) \quad (101)$$

$$\left| \sum_{\mathbf{x}, \mathbf{y} \in \mathbb{Z}_2^N} \text{tr}(|\mathbf{x}\mathbf{y}\mathbf{x}\rangle \langle \mathbf{x}\mathbf{y}\mathbf{x}| (\sigma \otimes O_0 \otimes O_0)) \right| = \left| \sum_{\mathbf{x}, \mathbf{y} \in \mathbb{Z}_2^N} \langle \mathbf{x} | \sigma | \mathbf{x} \rangle \langle \mathbf{y} | O_0 | \mathbf{y} \rangle \langle \mathbf{x} | O_0 | \mathbf{x} \rangle \right| \leq (\text{tr}(O_0))^2 = 0 \quad (102)$$

$$\left| \sum_{\mathbf{x}, \mathbf{y} \in \mathbb{Z}_2^N} \text{tr}(|\mathbf{x}\mathbf{y}\mathbf{x}\rangle \langle \mathbf{y}\mathbf{x}\mathbf{x}| (\sigma \otimes O_0 \otimes O_0)) \right| = \left| \sum_{\mathbf{x}, \mathbf{y} \in \mathbb{Z}_2^N} \langle \mathbf{y} | \sigma | \mathbf{x} \rangle \langle \mathbf{x} | O_0 | \mathbf{y} \rangle \langle \mathbf{x} | O_0 | \mathbf{x} \rangle \right| \leq \text{tr}(O_0^2) (\because \text{Eq. (92)}). \quad (103)$$

Throughout the above equations, we used the fact that $\text{tr}(O_0) = 0$. Also, Eqs. (85), (86), (88), (91), and (96) do not contribute to $\mathcal{C}^{(\text{i,ii,iv})}$, and are thus of no consequence to the ESPOVM analysis, for which we can assume O_0 is real and $O_0^\top = O_0$. So we can easily note that these can be also upper bounded by $\text{tr}(O_0^2)$. Note that values of other cases can be calculated from the above-known cases, by re-parametrizing or transpose-conjugating both sides for example. After realizing that other cases are 0 or upper bounded by $\text{tr}(O_0^2)$, based on simple trigonometric inequalities, the remaining equations of Lem. 4 other than Eq. (41) may also be proven.

B.5 Proof of Lemma 5

If the averaged variance $\overline{\text{Var}^{(\text{r})\text{eq}}(\hat{\sigma}_{\mathbf{A}, \mathbf{x}})^{\rho, \sigma}}$ over uniformly chosen input and target state is proved to be 1 (1/2 resp.) for (R)ESPOVM when $2^n \gg 1$, by the result of Ref. [45–47, 10], Thm. 2 (ii),(iii) will be proved.

Moreover, we recall that the mean squared error (MSE) is defined by the sample mean value of the squares of the additive error between estimation and target value. If an estimation variance is $\text{Var}(\hat{\sigma})$, then for a large sampling-copy number N , the averaged MSE $\overline{\epsilon^2}$ over many experiments of different input and target state becomes $\frac{2\overline{\text{Var}^{(\text{r})\text{eq}}(\hat{\sigma}_{\mathbf{A}, \mathbf{x}})^{\rho, \sigma}}}{N}$ (Note that sampling trial-number is $N/2$ that is why we have the factor 2). Therefore, the asymptotic lines of Fig. 2 (a–c) are explained.

Now, let us assume that $2^n \gg 1$. We take the RESPOVM first. Recall the Eq. (69).

$$\sum_{|\phi_{\mathbf{A}}^{\text{req}}\rangle \in \mathcal{S}_N^{\text{req}}} \frac{2^{2n-1}}{|\mathcal{S}_n^{\text{req}}|} \langle \phi_{\mathbf{A}}^{\text{req}} | \rho | \phi_{\mathbf{A}}^{\text{req}} \rangle \langle \phi_{\mathbf{A}}^{\text{req}} | O | \phi_{\mathbf{A}}^{\text{req}} \rangle = \sum_{\mathbf{x} \in \mathbb{Z}_2^N} \langle \mathbf{x} | \rho | \mathbf{x} \rangle \langle \mathbf{x} | O | \mathbf{x} \rangle + \frac{1}{2} \text{tr}(O) + \text{tr}(O\rho). \quad (104)$$

Then we obtain that

$$\begin{aligned} \mathbb{E}(\hat{\sigma}_{\mathbf{A}}^{\text{req}})^2 &= \left(\text{tr}(\rho\sigma) + \frac{1}{2} \text{tr}(\sigma) - \sum_{\mathbf{x} \in \mathbb{Z}_2^N} \langle \mathbf{x} | \rho | \mathbf{x} \rangle \langle \mathbf{x} | \sigma | \mathbf{x} \rangle \right)^2 \\ &= \frac{1}{4} + \text{tr}((\sigma \otimes \sigma)(\rho \otimes \rho)) + \sum_{\mathbf{x}, \mathbf{y} \in \mathbb{Z}_2^N} \text{tr}((\rho^{\otimes 2} \sigma^{\otimes 2})(|\mathbf{x}\mathbf{y}\rangle \langle \mathbf{y}\mathbf{x}|^{\otimes 2})) + \text{tr}(\sigma\hat{\sigma}) \\ &\quad - 2\text{tr}(\sigma\rho) \sum_{\mathbf{x} \in \mathbb{Z}_2^N} \text{tr}((\rho \otimes \sigma)(|\mathbf{x}\mathbf{x}\rangle \langle \mathbf{x}\mathbf{x}|)). \end{aligned} \quad (105)$$

Now, we use the following famous results:

Lemma 6 ([18]). *For a general N -qubit pure state $\rho = |\phi\rangle\langle\phi|$, the following identity holds:*

$$\int (d\phi) |\phi\rangle\langle\phi| = \frac{I}{2^n}, \quad (106)$$

$$\int (d\phi) |\phi\rangle\langle\phi|^{\otimes 2} = \frac{1}{2^n(2^n+1)} (I + \tau), \quad (107)$$

where I is identity operator and τ is the swap operator between two tensor product parties. The volume measure $(d\phi)$ refers to the uniform distribution (Haar-measure) of all single-qubit pure states.

From this, when we averaged over all pure input states ρ , all terms except $\frac{1}{4}$ are at most the order of $\frac{1}{2^n}$ for all σ . Hence, when $2^n \gg 1$,

$$\overline{\mathbb{E}((\hat{\sigma}_{\mathbf{A}}^{\text{req}})^2)^{\rho, \sigma}} \simeq \frac{1}{4}. \quad (108)$$

Next,

$$\mathbb{E}((\hat{\sigma}_{\mathbf{A}}^{\text{req}})^2) = 2^{3n-2} \text{tr} \left(\mathbb{E}_{|\phi_{\mathbf{A}}^{\text{req}}\rangle \sim \mathcal{D}(\mathcal{S}_n^{\text{req}})} |\phi_{\mathbf{A}}^{\text{req}}\rangle\langle\phi_{\mathbf{A}}^{\text{req}}|^{\otimes 3} \rho \otimes \sigma^{\otimes 2} \right) \quad (109)$$

$$\rightarrow \overline{\mathbb{E}((\hat{\sigma}_{\mathbf{A}}^{\text{req}})^2)^{\rho, \sigma}} = 2^{2n-2} \text{tr} \left(\mathbb{E}_{|\phi_{\mathbf{A}}^{\text{req}}\rangle \sim \mathcal{D}(\mathcal{S}_n^{\text{req}})} |\phi_{\mathbf{A}}^{\text{req}}\rangle\langle\phi_{\mathbf{A}}^{\text{req}}|^{\otimes 2} \sigma^{\otimes 2} \right) \quad (\because \text{Lem. 6}). \quad (110)$$

Now, since σ is pure and real, let us rewrite $\sigma = |\phi\rangle\langle\phi|$ where $|\phi\rangle = \sum_{\mathbf{i} \in \mathbb{Z}_2^n} c_{\mathbf{i}} |\mathbf{i}\rangle$ ($c_{\mathbf{i}} \in \mathbb{R}$). Then $|\phi\rangle\langle\phi|^{\otimes 2} = \sum_{\mathbf{i}, \mathbf{j}, \mathbf{k}, \mathbf{l} \in \mathbb{Z}_2^n} c_{\mathbf{i}} c_{\mathbf{j}} c_{\mathbf{k}} c_{\mathbf{l}} |\mathbf{i}\mathbf{j}\rangle\langle\mathbf{k}\mathbf{l}|$. Since \mathbf{c} lies on hypersphere S^{2^n-1} , we obtain that from Lem. 1,

$$\begin{aligned} & \overline{\mathbb{E}((\hat{\sigma}_{\mathbf{A}}^{\text{req}})^2)^{\rho, \sigma}} \\ &= \frac{1}{4A} \int_{S^{2^n-1}} d^{2^n-1} \Omega \cdot \sum_{\mathbf{x}, \mathbf{y} \in \mathbb{Z}_2^n} (|\mathbf{x}\mathbf{y}\rangle\langle\mathbf{x}\mathbf{y}| + |\mathbf{x}\mathbf{y}\rangle\langle\mathbf{y}\mathbf{x}| + |\mathbf{x}\mathbf{x}\rangle\langle\mathbf{y}\mathbf{y}| - 2|\mathbf{x}\mathbf{x}\rangle\langle\mathbf{x}\mathbf{x}|) \\ & \cdot \sum_{\mathbf{i}, \mathbf{j}, \mathbf{k}, \mathbf{l}} c_{\mathbf{i}} c_{\mathbf{j}} c_{\mathbf{k}} c_{\mathbf{l}} |\mathbf{i}\mathbf{j}\rangle\langle\mathbf{k}\mathbf{l}| = \frac{1}{4A} \sum_{\mathbf{x}, \mathbf{y}} \int_{S^{2^n-1}} 3c_{\mathbf{x}}^2 c_{\mathbf{y}}^2 - 2c_{\mathbf{x}}^4 d^{2^n-1} \Omega, \end{aligned} \quad (111)$$

where A is area of surface of S^{2^n-1} . Note that the sphere is invariant under permutation hence,

$$\overline{\mathbb{E}((\hat{\rho}_{\mathbf{A}}^{\text{req}})^2)^{\rho, \sigma}} = \frac{1}{4A} \left\{ 2^n \int_{S^{2^n-1}} c_1^4 d^{2^n-1} \Omega + 3 \cdot 2^n (2^n - 1) \int_{S^{2^n-1}} c_1^2 c_2^2 d^{2^n-1} \Omega \right\}. \quad (112)$$

We will separately calculate the first and second terms of the right-hand side. First,

$$\begin{aligned} & \int_{S^{2^n-1}} c_1^4 d^{2^n-1} \Omega \\ &= \oint \cos^4(\phi_1) \sin^{2^n-2}(\phi_1) \sin^{2^n-3}(\phi_2) \cdots \sin(\phi_{2^n-2}) d\phi_1 d\phi_2 d\phi_3 \cdots d\phi_{2^n-1} \\ & \text{(where } 0 \leq \phi_1, \phi_2 \dots, \phi_{2^n-2} \leq \pi, 0 \leq \phi_{2^n-1} \leq 2\pi) \\ &= \oint d^{2^n-1} \Omega \cdot \frac{\int_0^\pi \cos^4(\phi_1) \sin^{2^n-2}(\phi_1) d\phi_1}{\int_0^\pi \sin^{2^n-2}(\phi_1) d\phi_1} = \frac{A \int_0^{\frac{\pi}{2}} \cos^4(\phi_1) \sin^{2^n-2}(\phi_1) d\phi_1}{\int_0^{\frac{\pi}{2}} \sin^{2^n-2}(\phi_1) d\phi_1}. \end{aligned} \quad (113)$$

now we use the formula,

$$\int_0^{\frac{\pi}{2}} \sin^m(\phi) d\phi = \begin{cases} \frac{\pi}{2} \left(\frac{m!}{2^m \left(\left(\frac{m}{2} \right)! \right)^2} \right) & \text{if } m \text{ is even} \\ \frac{2^{m-1} \left(\left(\frac{m-1}{2} \right)! \right)^2}{m!} & \text{if } m \text{ is odd,} \end{cases} \quad (114)$$

and the beta function $\frac{1}{2}B(p, q) = \frac{\Gamma(p)\Gamma(q)}{2\Gamma(p+q)} = \int_0^{\frac{\pi}{2}} \sin^{2p-1}(\phi) \cos^{2q-1}(\phi) d\phi$, where $\Gamma(p)$ is gamma function. Then we obtain that with Stirling's formula,

$$\begin{aligned} \int_{S^{2^n-1}} c_1^4 d^{2^n-1}\Omega &= \frac{A}{\pi} \cdot \frac{B\left(\frac{5}{2}, 2^{n-1} - \frac{1}{2}\right)}{\left(\frac{(2^n-2)!}{2^{(2^n-2)((2^{n-1}-1)!)^2}\right)} \\ &\simeq \frac{A}{\pi} \Gamma\left(\frac{5}{2}\right) \frac{2^{2^n-2}}{(2^{n-1}+1)2^{n-1}} \cdot \sqrt{2\pi e} \cdot \sqrt{\frac{(2^{n-1}-\frac{3}{2})(2^{n-1}-1)}{2^n-2}} \\ &\quad \cdot \frac{(2^{n-1}-\frac{3}{2})^{2^{n-1}-\frac{3}{2}}(2^{n-1}-1)^{2^{n-1}-1}}{(2^n-2)^{2^n-2}} \\ &\simeq \frac{A}{\pi} \Gamma\left(\frac{5}{2}\right) \underbrace{\sqrt{2\pi e} \cdot 2^{2^n-\frac{5n}{2}-1} \cdot \frac{(2^{n-1}-\frac{3}{2})^{2^{n-1}-\frac{3}{2}}(2^{n-1}-1)^{2^{n-1}-1}}{(2^n-2)^{2^n-2}}}_{\equiv C}. \end{aligned} \quad (115)$$

Note that

$$\begin{aligned} \log_2(C) &\simeq \left(2^n - \frac{5n}{2} - 1\right) + \left(2^{n-1} - \frac{3}{2}\right)(n-1) + (2^{n-1}-1)(n-1) - (2^n-2)n \\ &= \left(-3n + \frac{3}{2}\right) \end{aligned} \quad (116)$$

$$\rightarrow \therefore \frac{1}{A} \int_{S^{2^n-1}} c_1^4 d^{2^n-1}\Omega \simeq \frac{1}{\pi} \Gamma\left(\frac{5}{2}\right) \sqrt{2\pi e} \cdot 2^{-3n+\frac{3}{2}}. \quad (117)$$

Let us go to the second term.

$$\int_{S^{2^n-1}} c_1^2 c_2^2 d^{2^n-1}\Omega \quad (118)$$

$$= \oint \cos^2(\phi_1) \cos^2(\phi_2) \sin^2(\phi_2) \sin^{2^n-2}(\phi_1) \sin^{2^n-3}(\phi_2) \cdots \sin(\phi_{2^n-2}) d\phi_1 d\phi_2 d\phi_3 \cdots d\phi_{2^n-1}$$

(where $0 \leq \phi_1, \phi_2, \dots, \phi_{2^n-2} \leq \pi$, $0 \leq \phi_{2^n-1} \leq 2\pi$)

$$\begin{aligned} &= \oint d^{2^n-1}\Omega \cdot \frac{\int_0^\pi \cos^2(\phi_1) \sin^{2^n-2}(\phi_1) d\phi_1}{\int_0^\pi \sin^{2^n-2}(\phi_1) d\phi_1} \cdot \frac{\int_0^\pi \cos^2(\phi_2) \sin^{2^n-1}(\phi_2) d\phi_2}{\int_0^\pi \sin^{2^n-3}(\phi_2) d\phi_2} \\ &= \frac{A}{2\pi} \cdot \frac{B\left(\frac{3}{2}, 2^{n-1} - \frac{1}{2}\right) B\left(\frac{3}{2}, 2^{n-1}\right)}{\left(\frac{(2^n-2)!}{2^{2^n-2}((2^{n-1}-1)!)^2}\right) \left(\frac{2^{2^n-4}((2^{n-1}-2)!)^2}{(2^n-3)!}\right)} \\ &= \frac{2A}{\pi} \cdot \frac{\Gamma\left(\frac{3}{2}\right)^2 (2^{n-1} - \frac{3}{2})! (2^{n-1} - 1)! (2^{n-1} - 1)^2}{(2^n - 2)(2^{n-1})! (2^{n-1} + \frac{1}{2})} \\ &= \frac{2A}{\pi} \Gamma\left(\frac{3}{2}\right)^2 \frac{(2^{n-1})^2}{(2^n - 2)2^{n-1}(2^{n-1} + \frac{1}{2})(2^{n-1} - \frac{1}{2})} \simeq A \cdot 2^{-2n} \left[\therefore \Gamma\left(\frac{3}{2}\right) = \frac{\sqrt{\pi}}{2} \right]. \end{aligned} \quad (119)$$

Therefore, substituting the Eq. (115), (116), (108), and (118) into Eq. (112) leads to

$$\overline{\text{Var}(\hat{\sigma}_{\mathbf{A}}^{\text{req}})^{\rho, \sigma}} = \overline{\mathbb{E}((\hat{\sigma}_{\mathbf{A}}^{\text{req}})^2)^{\rho, \sigma}} - \overline{\mathbb{E}(\hat{\sigma}_{\mathbf{A}}^{\text{req}})^2}^{\rho, \sigma} \simeq \frac{1}{2}. \quad (120)$$

Next, let us direct our attention to ESPOVM. As we proceed in a similar manner, we may skip most of the steps but note that

$$\sum_{|\phi_{\mathbf{A}}^{\text{req}}\rangle \in \mathcal{S}_N^{\text{eq}}} \frac{2^{2n}}{|\mathcal{S}_n^{\text{req}}|} \langle \phi_{\mathbf{A}}^{\text{req}} | \rho | \phi_{\mathbf{A}}^{\text{req}} \rangle \langle \phi_{\mathbf{A}}^{\text{req}} | O | \phi_{\mathbf{A}}^{\text{req}} \rangle = \sum_{\mathbf{x} \in \mathbb{Z}_2^N} \langle \mathbf{x} | \rho | \mathbf{x} \rangle \langle \mathbf{x} | O | \mathbf{x} \rangle + \text{tr}(O) + \text{tr}(O\rho), \quad (121)$$

and

$$\begin{aligned} \overline{\mathbb{E}((\hat{\sigma}_{\mathbf{A}}^{\text{eq}})^2)^{\rho, \sigma}} &= \frac{1}{A} \int_{\mathbf{c} \in S^{2^n-1}} d^{2^n-1} \Omega \cdot \sum_{\mathbf{x}, \mathbf{y} \in \mathbb{Z}_2^n} (|\mathbf{x}\mathbf{y}\rangle \langle \mathbf{x}\mathbf{y}| + |\mathbf{x}\mathbf{y}\rangle \langle \mathbf{y}\mathbf{x}| - |\mathbf{x}\mathbf{x}\rangle \langle \mathbf{x}\mathbf{x}|) \\ &\quad \cdot \sum_{i,j,k,l} c_i c_j c_k c_l |ij\rangle \langle kl| \\ &= \frac{1}{A} \sum_{\mathbf{x}, \mathbf{y}} \int_{\mathbf{c} \in S^{2^n-1}} 2c_{\mathbf{x}}^2 c_{\mathbf{y}}^2 - c_{\mathbf{x}}^4 d^{2^n-1} \Omega, \end{aligned} \quad (122)$$

By the same method with RESPOVM, we can find that

$$\overline{\mathbb{E}((\hat{\sigma}_{\mathbf{A}}^{\text{eq}})^2)^{\rho, \sigma}} \simeq 2, \text{ and } \overline{\mathbb{E}(\hat{\sigma}_{\mathbf{A}}^{\text{eq}})^{2\rho, \sigma}} \simeq 1, \rightarrow \overline{\text{Var}(\hat{O}_{\mathbf{A}}^{\text{eq}})^{\rho, \sigma}} = \overline{\mathbb{E}((\hat{\sigma}_{\mathbf{A}}^{\text{eq}})^2)^{\rho, \sigma}} - \overline{\mathbb{E}(\hat{\sigma}_{\mathbf{A}}^{\text{eq}})^{2\rho, \sigma}} \simeq 1. \quad (123)$$

Lastly, for both ESPOVM and RESPOVM,

$$\mathbb{E}((\hat{\sigma}^{\text{bin}})^2) = \sum_{\mathbf{x}} \langle \mathbf{x} | \rho | \mathbf{x} \rangle |\langle \mathbf{x} | \sigma | \mathbf{x} \rangle|^2 = \sum_{\mathbf{x}} \text{tr}((\rho \otimes \sigma \otimes \sigma) |\mathbf{x}\mathbf{x}\mathbf{x}\rangle \langle \mathbf{x}\mathbf{x}\mathbf{x}|) \quad (124)$$

$$\rightarrow \overline{\mathbb{E}((\hat{\sigma}^{\text{bin}})^2)^{\rho}} = \frac{1}{2^n} \sum_{\mathbf{x}} (\langle \mathbf{x} | \sigma | \mathbf{x} \rangle)^2 \simeq 0. \quad (125)$$

Hence, even if we average over real pure states σ , the result will be nearly 0. Lastly, let us consider randomized-Clifford tomography. Then, we can refer to Eq. (S43) of Ref. [10] stating that the estimation variance is equal to the *shadow norm* without maximizing over ρ and it is,

$$\text{Var}(\hat{\sigma}^{\text{s}}) = \frac{2^n + 1}{2^n + 2} \left(\text{tr}(\rho) \text{tr} \left(\left(\sigma - \frac{I}{2^n} \right)^2 \right) + 2 \text{tr} \left(\rho \left(\sigma - \frac{I}{2^n} \right)^2 \right) \right) - \left(\text{tr} \left(\rho \left(\sigma - \frac{I}{2^n} \right) \right) \right)^2. \quad (126)$$

After we average over pure ρ , by Lem. 6, we the second and last terms are ignored and

$$\overline{\text{Var}(\hat{\sigma}^{\text{s}})^{\rho, \sigma}} \simeq \overline{\text{tr} \left(\sigma^2 - \frac{2\sigma}{2^n} + \frac{I}{4^n} \right)^{\sigma}} \simeq 1, \quad (127)$$

which settles the proof for Lem. 5 (i). Note that RESPOVM gives half the average variance than even randomized-Clifford. Since we need two input states for a single sampling trial, the number of states is not improved but we can reduce the total gate count for the whole estimation process. This is because in RESPOVM, half of the input-state copies are used for direct Z -basis measurement.

The proof of Lem. 5 (ii) is much simpler. We start with

$$\overline{\mathbb{E}((\hat{\sigma}_{\mathbf{A}}^{\text{eq}})^2)^{\rho}} = 2^{2n} \text{tr} \left(\mathbb{E}_{|\phi_{\mathbf{A}}^{\text{eq}}\rangle \sim \mathcal{D}(\mathcal{S}_n^{\text{eq}})} |\phi_{\mathbf{A}}^{\text{eq}}\rangle \langle \phi_{\mathbf{A}}^{\text{eq}}|^{\otimes 2} \sigma^{\otimes 2} \right). \quad (128)$$

By averaging over Haar-random pure state σ , by Lem. 6 and using the fact that $\text{tr}((\rho \otimes \sigma)\tau) = \text{tr}(\rho\sigma)$, we conclude that $\overline{\mathbb{E}((\hat{\sigma}_{\mathbf{A}}^{\text{eq}})^2)^{\rho, \sigma}} = 2$. Also, $\overline{\mathbb{E}(\hat{\sigma}_{\mathbf{A}}^{\text{eq}})^{2\rho, \sigma}} \simeq 1$, in exactly the same way as with Eq. (121). Hence $\overline{\text{Var}(\hat{\sigma}_{\mathbf{A}}^{\text{eq}})^{\rho, \sigma}} = \overline{\mathbb{E}((\hat{\sigma}_{\mathbf{A}}^{\text{eq}})^2)^{\rho, \sigma}} - \overline{\mathbb{E}(\hat{\sigma}_{\mathbf{A}}^{\text{eq}})^{2\rho, \sigma}} \simeq 1$. Furthermore, similar to Eq. (127), the average variance of random Clifford tomography is also 1. The proof is thus completed.

C Informational completeness of ESPOVM+computational basis

In this section, we prove that the ESPOVM+computational basis is informationally complete (IC) so that this POVM can fully extract all density-matrix information of any given input state. Explicitly, the condition for informational completeness of the POVM $\{\Pi_j\}_{j \in J}$, where J is an index set and $\Pi_j > 0$ for all $j \in J$, necessitates that any quantum state be expressible as a linear combination of the elements Π_j .

We now prove the following lemmas:

Lemma 7. *For a d -dimensional Hilbert space, a POVM, comprising a set of $M \geq d^2$ positive-operator elements Π_j that sum to the identity, is IC if the matrix*

$$\mathbf{V} = (|\Pi_1\rangle\rangle \ |\Pi_2\rangle\rangle \ \cdots \ |\Pi_M\rangle\rangle) \quad (129)$$

has rank d^2 , and only then. Here $|\Pi_j\rangle\rangle$ is a basis-dependent superket (vectorization) of Π_j .

Proof. Since \mathbf{V} has rank $d^2 = \dim(\mathbb{C}^d \otimes \mathbb{C}^d)$ if and only if it spans a set of vectorized quantum states. By reversing the vectorization (which is an injective map), we note that all quantum state can be expressed as a linear combination of $\{\Pi_j\}$. \square

Lemma 8. *A POVM $\{\Pi_j\}$ is IC if the frame operator [44]*

$$\mathcal{F} \equiv \sum_{j=1}^M \frac{|\Pi_j\rangle\rangle \langle\langle \Pi_j|}{\text{tr}(\Pi_j)} \quad (130)$$

is invertible, and only then.

Proof. Suppose we have the IC POVM. Clearly from Lem. 7, $\text{rank}\{\mathbf{V}\} = d^2$. Note that $\mathcal{F} \equiv \mathbf{V}\mathbf{V}^{-1}\mathbf{V}^\dagger$, where

$$\mathbf{\Pi} = \begin{pmatrix} \text{tr}(\Pi_1) & 0 & \cdots & 0 \\ 0 & \text{tr}(\Pi_2) & \cdots & 0 \\ \vdots & \vdots & \ddots & \vdots \\ 0 & 0 & \cdots & \text{tr}(\Pi_M) \end{pmatrix}. \quad (131)$$

Also, if $\mathbf{x} \in \text{Ker}(\mathbf{V})$, it is easy to see that $\mathbf{x} \in \text{Ker}(\mathcal{F})$, or $\mathbf{x}^\top \mathcal{F} \mathbf{x} = \mathbf{x}^\top \mathbf{V}^\dagger \mathbf{\Pi}^{-1} \mathbf{V} \mathbf{x} = 0 \rightarrow \|\mathbf{V} \mathbf{x}\|^2 = 0$ (the inner product is defined by the Euclidean product with the weights $1/\text{tr}(\Pi_j) > 0$ ($j \in [M]$)). Hence $\mathbf{V} \mathbf{x} = 0 \rightarrow \mathbf{x} \in \text{Ker}(\mathbf{V})$. So, $\text{rank}(\mathcal{F}) = M - \dim(\text{Ker}(\mathcal{F})) = M - \dim(\text{Ker}(\mathbf{V})) = \text{rank}(\mathbf{V})$. Since $\text{rank}(\mathbf{V}) = d^2$, $\text{rank}(\mathcal{F}) = d^2$. As \mathcal{F} is also a $d^2 \times d^2$ matrix, \mathcal{F}^{-1} exists.

Conversely, suppose that \mathcal{F}^{-1} exists. Then $\text{rank}\{\mathcal{F}\} = d^2$. Since $\text{rank}\{\mathcal{F}\} \leq \text{rank}\{\mathbf{V}\} \leq d^2$, we conclude that $\text{rank}\{\mathbf{V}\} = d^2$. By Lem. 7, $\{\Pi_j\}_{j \in J}$ is IC. \square

Setting $d = 2^n$ therefore yields the desirable result.

Proposition 4. *The collection of ESPOVM and computational basis forms an IC measurement. However, ESPOVM itself is not an IC POVM.*

Proof. First, we calculate the frame operator of the ESPOVM.

$$\mathcal{F}_{\text{es}} = \sum_{|\phi_{\mathbf{A}}^{\text{eq}}\rangle \in \mathcal{S}_n^{\text{eq}}} \frac{2^n}{|\mathcal{S}_n^{\text{eq}}|} |\phi_{\mathbf{A}}^{\text{eq}}\rangle \langle\langle \phi_{\mathbf{A}}^{\text{eq}}| \rangle\langle \phi_{\mathbf{A}}^{\text{eq}}| \rangle\langle \phi_{\mathbf{A}}^{\text{eq}}|^* = 2^n \left(\mathbb{E}_{|\phi_{\mathbf{A}}^{\text{eq}}\rangle \sim \mathcal{D}(\mathcal{S}_n^{\text{eq}})} |\phi_{\mathbf{A}}^{\text{eq}}\rangle \langle\langle \phi_{\mathbf{A}}^{\text{eq}}|^{\otimes 2} \rangle\langle \rangle \right)^{\top_2}, \quad (132)$$

where \top_2 means partial transpose for the second part. From Lem. 1, we note that

$$\mathcal{F}_{\text{es}} = \frac{1}{2^n} \left(1 + \sum_{\mathbf{x}, \mathbf{y} \in \mathbb{Z}_2^n} |\mathbf{x}\mathbf{x}\rangle \langle \mathbf{y}\mathbf{y}| - \sum_{\mathbf{x} \in \mathbb{Z}_2^n} |\mathbf{x}\mathbf{x}\rangle \langle \mathbf{x}\mathbf{x}| \right) = \frac{1}{2^n} \left(1 + \sum_{\mathbf{x} \in \mathbb{Z}_2^n} \sum_{\mathbf{y} \neq \mathbf{x} \in \mathbb{Z}_2^n} |\mathbf{x}\mathbf{x}\rangle \langle \mathbf{y}\mathbf{y}| \right). \quad (133)$$

One can show that the operator $W = \sum_{\mathbf{x} \in \mathbb{Z}_2^n} \sum_{\mathbf{y} \neq \mathbf{x} \in \mathbb{Z}_2^n} |\mathbf{x}\mathbf{x}\rangle \langle \mathbf{y}\mathbf{y}|$ has at least one eigenvalue equal to -1 by inspecting its action on $|\mathbf{z}\mathbf{z}\rangle$ for any $\mathbf{z} \in \mathbb{Z}_2^n$,

$$W|\mathbf{z}\mathbf{z}\rangle = \sum_{\mathbf{x} \neq \mathbf{z} \in \mathbb{Z}_2^n} |\mathbf{x}\mathbf{x}\rangle = \sum_{\mathbf{x} \in \mathbb{Z}_2^n} |\mathbf{x}\mathbf{x}\rangle - |\mathbf{z}\mathbf{z}\rangle. \quad (134)$$

It follows that any ket $(|z_1, z_1\rangle - |z_2, z_2\rangle)/\sqrt{2}$ with $z_1, z_2 \in \mathbb{Z}_2^n$ is an eigenket in the “ -1 ”-eigenvalue subspace. As a side note, it is easy to check that the superposition $|\phi\rangle \equiv \sum_{\mathbf{z} \in \mathbb{Z}_2^n} |\mathbf{z}, \mathbf{z}\rangle 2^{-n/2}$ is an eigenket that gives a positive eigenvalue of $2^n - 1$,

$$W \sum_{\mathbf{z} \in \mathbb{Z}_2^n} |\mathbf{z}\mathbf{z}\rangle 2^{-n/2} = \sum_{\mathbf{x} \in \mathbb{Z}_2^n} |\mathbf{x}\mathbf{x}\rangle \sum_{\mathbf{z} \neq \mathbf{x} \in \mathbb{Z}_2^n} 2^{-n/2} = \sum_{\mathbf{x} \in \mathbb{Z}_2^n} |\mathbf{x}\mathbf{x}\rangle 2^{-n/2} (2^n - 1). \quad (135)$$

We may then conclude that \mathcal{F}_{es} has at least one null eigenvalue. Based on Lem. 8, it follows that the ESPOVM is non-IC.

Upon recognizing that $\sum_{\mathbf{x} \in \mathbb{Z}_2^n} |\mathbf{x}\mathbf{x}\rangle \langle \mathbf{x}\mathbf{x}|$ is the frame operator $\mathcal{F}_{\text{comp}}$ for the computational basis, the total frame operator may be written as

$$\mathcal{F} = \mathcal{F}_{\text{es}} + \mathcal{F}_{\text{comp}} = \frac{1}{2^n} + |\phi\rangle \langle \phi| + \left(1 - \frac{1}{2^n}\right) \sum_{\mathbf{x} \in \mathbb{Z}_2^n} |\mathbf{x}\mathbf{x}\rangle \langle \mathbf{x}\mathbf{x}| > 0. \quad (136)$$

Therefore, \mathcal{F} has full rank (with all eigenvalues positive) and is invertible. By Lem. 8, ESPOVM+computational basis is IC POVM. \square

D CNOT—CZ—CNOT decomposition of a CZ circuit

Here, we show the method to transform any CZ circuit into the form CNOT—CZ—CNOT so that we may then ignore the last CNOT section for (R)ESPOVM. This will further improve the gate reduction via the Patel-Markov-Hayes (PMH) construction [55]. Note that a CZ circuit can be defined by a binary-valued quadratic function $Q(\mathbf{x})$ and the mapping

$$CZ : |\mathbf{x}\rangle \mapsto (-1)^{Q(\mathbf{x})} |\mathbf{x}\rangle \quad (137)$$

on the computational basis. Now, we rewrite $Q_{\{1,2,\dots,k\}}$ as a quadratic function not having x_1 or x_2 or \dots or x_k . We can then express $Q(\mathbf{x})$ as $c_1 x_1 L_{\{1\}}(\mathbf{x}) + Q_{\{1\}}(\mathbf{x})$, where $c_1 \in \{0, 1\}$ and $L_{\{1,2,\dots,k\}}$ is a linear function not having variables x_1 or x_2 or \dots or x_k . Next, we find the linear transformation S_1 such that maps x_{i_1} to $L_{\{1\}}(\mathbf{x})$ where x_{i_1} is a single term contained in $L_{\{1\}}(\mathbf{x})$, and makes other variables intact. This is invertible transformation and maps $Q(\mathbf{x})$ to $Q_1(\mathbf{x}) = c_1 x_1 x_{i_1} + Q'_{\{1\}}(\mathbf{x})$, where $Q'_{\{1\}}(\mathbf{x})$ is some quadratic polynomial.

The same procedure may then be repeated for $Q_{\{1\}}^{(1)}(\mathbf{x})$ to become $Q_1(\mathbf{x}) = c_1 x_1 x_{i_1} + c_2 x_2 x_{i_2} + Q'_{\{1,2\}}(\mathbf{x})$. After $n-1$ repetitions, we obtain the transformations S_1, S_2, \dots, S_{n-1} to map the function $Q_L(\mathbf{x}) \equiv c_1 x_1 x_{i_1} + c_2 x_2 x_{i_2} + \dots + c_{n-1} x_{n-1} x_{i_{n-1}} + L^{(1,2,\dots,n-1)}(\mathbf{x})$, where $L^{(1,2,\dots,n-1)}(\mathbf{x})$ is some linear function.

From these elements, we can implement the original CZ circuit in a different yet equivalent way. We first implement CNOT-gate mapping $|\mathbf{x}\rangle \mapsto |(S_1 S_2 \dots S_{n-1})^{-1}(\mathbf{x})\rangle$ and then we utilize the CZ+Z mapping $|\mathbf{x}\rangle \mapsto (-1)^{Q_L(\mathbf{x})} |\mathbf{x}\rangle$, and finally take CNOT gates for $S_1 S_2 \dots S_{n-1}$ to send $|(S_1 S_2 \dots S_{n-1})^{-1}(\mathbf{x})\rangle$ back to $|\mathbf{x}\rangle$. If an X-basis measurement is performed after that, there is no need to physically enact the last CNOT section and just, instead, treat it as linear post-processing of the measurement outcome.

E Linear nearest-neighboring (LNN) architecture of CZ circuits [1]

In this section, we explain how to transform the arbitrary CZ circuit to the $2n + 2$ -depth LNN form, which has only neighboring CNOT gates. We encourage readers who are interested in Clifford circuit synthesis to read Ref. [1], from which some techniques were borrowed. This section briefly discusses some relevant background content in Ref. [1].

The actual circuit we transform is the so-called $\widehat{\text{CZ}}$ circuit. This is defined by CZ circuit followed by *qubit-reversal* layers, $\text{REV} : |x_1, x_2, \dots, x_n\rangle \mapsto |x_n, x_{n-1}, \dots, x_1\rangle$. However, the CZ section is equal to CZ-REV-REV and the last REV can be ignored by reversing the measurement outcome if we only do the non-adaptive measurement. Hence, if $\widehat{\text{CZ}}$ can be transformed to a $(2n + 2)$ -depth LNN architecture, the proof is complete.

Now, consider some arbitrary $\widehat{\text{CZ}}$ circuit. We will prove this only when n is odd, since that for even n follows similarly. Suppose we take $|x_1, x_2, \dots, x_n\rangle$ as the input and define the two unitaries

$$C_1 \equiv \text{CNOT}_{1 \rightarrow 2} \text{CNOT}_{3 \rightarrow 4} \dots \text{CNOT}_{n-2 \rightarrow n-1} \text{CNOT}_{3 \rightarrow 2} \text{CNOT}_{5 \rightarrow 4} \dots \text{CNOT}_{n \rightarrow n-1}, \quad (138)$$

$$C_2 \equiv \text{CNOT}_{2 \rightarrow 1} \text{CNOT}_{4 \rightarrow 3} \dots \text{CNOT}_{n-1 \rightarrow n-2} \text{CNOT}_{2 \rightarrow 3} \text{CNOT}_{4 \rightarrow 5} \dots \text{CNOT}_{n-1 \rightarrow n} \quad (139)$$

and $C \equiv C_1 C_2$. Now, let $n = 2m + 1$. If we operate C on the input $t \leq m$ times, the output state becomes

$$C^t |x_1, x_2, \dots, x_n\rangle = \left| \bigoplus_{i=1}^n [Pj(n-3-2(t-1)+i), Pk(2(t-1)+i)] \right\rangle, \quad (140)$$

where $[x_j, x_k] (x_j \neq x_k) \equiv x_j \oplus x_{j+1} \oplus \dots \oplus x_k$, $[x_j, x_j] \equiv x_j$ and the *patterns*

$$Pj \equiv (n-1, n-3, n-3, \dots, 4, 4, 2, 2, 1, 1, 3, 3, \dots, n-2, n-2), \quad (141)$$

$$Pk \equiv (3, 3, 5, 5, \dots, n, n, n-1, n-1, n-3, n-3, \dots, 6, 6, 4, 4, 2). \quad (142)$$

Note that both are of length $2n - 3$. Also, $P(j \text{ or } k)(a)$ where $a \in [2n - 3]$ means the a -th element of such patterns. We note that given $t \leq m$ and $i \in [n]$, there is no case when $[Pj(n-3-2(t-1)+i), Pk(2(t-1)+i)]$ is equal with $[Pj(n-3-2(t'-1)+i'), Pk(2(t'-1)+i')]$ for the other $t' \leq m$ and $i' \in [n]$. This is schematically seen in Ref. [1]. Also, the number of tuples obtained during $t = 0, 1, \dots, m$ is $(m+1)n = \frac{n(n+1)}{2} = {}_n C_2 + n$. These mean that after we recorded all elements of output ket at each step we operate S , for m times, we can see all $[j, k]$ ($j, k \in [n]$). Note that $[j, j]$ can be seen at the starting point ($t = 0$).

Now, we show that C^{m+1} is a qubit-reversal operation. After the m -th operation, we operate C once more and calculate the p -th qubit output of the output state for an even p . By the neighboring property, we just need to sum the $\{p-1, p, p+1\}$ -th inputs, resulting in $[n - (2\lfloor \frac{p-1}{2} \rfloor + 1), n - (2\lfloor \frac{p-2}{2} \rfloor - 1)] \oplus [n - (2\lfloor \frac{p}{2} \rfloor + 1), n - (2\lfloor \frac{p-1}{2} \rfloor + 1)] \oplus [n - (2\lfloor \frac{p+1}{2} \rfloor + 1), n - (2\lfloor \frac{p}{2} \rfloor + 1)] = n - p + 1$, which is a reversal of p . We can also note that the result for an odd p is also a reversal. Similarly, we conclude that S^{m+1} is a qubit reversal.

Next, we recall Eq. (50), that is $y_i = x_1 \oplus x_2 \oplus \dots \oplus x_i$, in the main text. In this context, $y_i = [1, i]$ and $y_j \oplus y_k = [j + 1, k]$. Hence, one can achieve $i^{u_j y_j}$ and $i^{u_{j,k}(y_j \oplus y_k)}$ ($u_j, u_{j,k} \in \mathbb{Z}_4$) by inserting phase gates in each section of the C -operated output, or at the starting point. Also, the depth of the LNN architecture is $4(m + 1) = 2n + 2$. The 1-to-1 mapping $(t, i) \leftrightarrow [Pj(n - 3 - 2(t - 1) + i), Pk(2(t - 1) + i)]$ must be recorded in $\mathcal{O}(n^2)$ -memory before the circuit sampling so that we do not need to be bothered with the time to find the right location for phase-gate insertion. A similar consideration applies when n is even but with slightly different C_1, C_2 , and patterns [1]. In conclusion, we can realize the $\widehat{\text{CZ}}$ operation with only nearest-neighboring CNOT and phase gates of depth $2n + 2$. Lastly, we note that Y -basis measurements can be carried with X -basis measurements after phase gates. If these phase operations are performed before the CZ action to transform the CZ circuit into an LNN architecture, the double-layered rightmost CNOT gates can simply be regarded as classical post-processing of the X -basis outcome of the equatorial-stabilizer measurement. Therefore, only $2n$ -depth circuits are needed.